Collective Quantum Effects in Field Theory and Gravity

Daniel Flassig

München 2016

Collective Quantum Effects in Field Theory and Gravity

Daniel Flassig

Dissertation
an der Fakultät für Physik
der Ludwig-Maximilians-Universität
München

vorgelegt von
Daniel Flassig
geboren in Würzburg

München, 30. Juni 2016

Erstgutachter: Prof. Dr. Georgi Dvali
Zweitgutachter: Prof. Dr. Stefan Hofmann
Tag der mündlichen Prüfung: 26. Juli 2016

Zusammenfassung

Kollektive Quanteneffekte haben traditionell keine große Aufmerksamkeit in der Hochenergiephysik erfahren. Vor kurzem ist jedoch ein Modell für die Physik schwarzer Löcher vorgeschlagen worden, in dem diese als Bose-Kondensate von Gravitonen nahe an einem kritischen Punkt beschrieben werden. In einer anderen Forschungsrichtung haben Abschätzungen der Hochenergiekollisionen in der elektroschwachen Theorie Hinweise darauf geliefert, dass Streuprozesse mit mehreren Higgs- oder Vektorbosonen im Endzustand in Reichweite künftiger Teilchenbeschleuniger sein könnten. In beiden Fällen dürften kollektive Quanteneffekte zentral für das Verständnis der Physik sein.

Im ersten Teil dieser Arbeit behandeln wir das Gravitonkondensat-Bild für schwarze Löcher von Dvali und Gomez. Wir untersuchen ein Bosonisches Vielteilchensystem (attraktives Lieb-Liniger), das einen Quantenphasenübergang zeigt und als Modell für Gravitonkondensate vorgeschlagen worden ist. Wir zeigen, dass - selbst für makroskopische Teilchenzahlen - Quanteneffekte am kritischen Punkt wichtig sind. Das wird an der Verschränkung unterschiedlicher Impulsmoden und dem Quantenmissklang zwischen zwei aufeinanderfolgenden Dichtemessungen besonders klar. Wir heben hervor, dass der führende Beitrag zu diesen Phänomenen aus langwelligen Moden hervorgeht und daher von der ultravioletten Physik unabhängig ist. Diese Ergebnisse implizieren für schwarze Löcher im Gravitonkondensat-Bild, dass die semiklassische Beschreibung zusammenbricht, und sie könnten der Schlüssel dazu sein, das lange bestehende Informationsproblem zu lösen.

Dann wenden wir uns der Frage der Informationsverarbeitung in schwarzen Löchern zu. Inspiriert von den Eigenschaften dreidimensionaler attraktiver Bose-Kondensate schlagen wir einen konkreten Mechanismus für das schnelle Scrambling in Gravitonkondensat-schwarzen-Löchern vor. Um diese Behauptung zu stützen führen wir Simulationen am Lieb-Liniger Modell in einem geeigneten Regime durch, die Verschränkungs-Erzeugung in logarithmischer Zeit offenbaren. Wir weisen auch darauf hin, dass die Idee, Instabilität und gegebenenfalls Chaos als Ursache für schnelles Quantenbrechen und Scrambling zu betrachten, relevant für andere Modelle von schwarzen

Löchern sein kann.

Im zweiten Teil dieser Arbeit verwenden wir Integrabilitäts-Techniken (Bethe-Ansatz) um den Phasenübergang des attraktiven Lieb-Liniger Modells analytisch zu analysieren. Wir leiten den Kontinuumslimes der Bethe-Gleichungen her und lösen ihn für den Grundzustand bei beliebiger Kopplungsstärke. Wir stellen eine genaue Äquivalenz zwischen der Bethe-Ansatz Beschreibung im Vielteilchen-Limes und dem groß-N Sattelpunkt von Euklidischer zweidimensionaler $U(N)$ Yang-Mills Theorie, auf der Sphäre quantisiert, her. Der Übergang zwischen der homogenen und solitonischen Phase des Lieb-Liniger Modells ist dadurch dual zum Douglas-Kazakov Übergang zwischen Confinement und Deconfinement.

Im letzten Teil widmen wir uns Streuamplituden von vielen Teilchen. In einem einfachen Integralmodell untersuchen wir im Detail den Zusammenbruch der Störungstheorie und betonen, dass reine Baum-Näherungen parametrisch noch früher versagen. Wir demonstrieren dann, dass sich die Streuamplituden hoher Multiplizität, in drei verschiedenen (Integral- und quantenmechanischen) Modellsystemen, auf Basis der führenden Ordnung von (nicht-perturbativen) Sattelpunkten, vorhersagen lassen. In den nicht Borel-summierbaren Fällen dominiert allein der Beitrag eines nicht-perturbativen Sattelpunkts. Wir zeigen auf, dass die Amplituden hoher Multiplizität daher wohl eine lohnenswerte Anwendung für die Techniken der Resurgenztheorie sind.

Abstract

Collective quantum effects have traditionally not received much attention in high energy physics. Recently, however, a model for black hole physics was put forward, in which black holes are described as Bose-condensates of gravitons close to a critical point. In a different line of research, estimates of high-energy collisions in the electro-weak theory have hinted that scattering processes with multiple Higgs or vector Bosons in the final state might be in reach for future particle colliders. In both scenarios, collective quantum effects may be crucial for understanding the physics.

In the first part of this thesis, we address the black hole condensate picture of Dvali and Gomez. We study a Bosonic many-body system (attractive Lieb-Liniger) which exhibits a quantum phase transition and was proposed as a model for the graviton condensate. We demonstrate that, even for macroscopic particle number, quantum effects are prominent at the critical point. This becomes especially clear in the entanglement of different momentum modes and in the quantum discord between two successive density measurements. We point out that the leading contribution to these phenomena arises from long-wavelength modes and is therefore insensitive to ultra-violet physics. For black holes in the graviton condensate picture, these findings imply a breakdown of the semiclassical description and may be the key to resolving the long-standing information problem.

We then turn our attention to the question of information processing in black holes. Inspired by the properties of three-dimensional attractive Bose condensates, we propose a concrete mechanism for fast scrambling in graviton-condensate black holes. To bolster our claims, we perform simulations of the Lieb-Liniger model in an appropriate regime that reveal entanglement-generation in logarithmic time. We also point out that the idea of instability and possibly chaos as the origin of fast quantum breaking and scrambling may also be relevant for other models of black holes.

In the second part of this thesis, we use techniques of integrability (Bethe ansatz) to address the phase transition of the attractive Lieb-Liniger model analytically. We derive the continuum limit of the Bethe equations and solve

it for the ground state at arbitrary coupling. We establish an exact equivalence between the Bethe-ansatz description in the large-particle-number limit and the large-N saddle point of Euclidean two dimensional $U(N)$ Yang-Mills theory quantized on a sphere. The transition between the homogeneous and solitonic phases of the Lieb-Liniger model is thus dual to the Douglas-Kazakov confinement-deconfinement transition.

In the last part, we consider scattering amplitudes involving many particles. In a simple integral-model, we study in detail the breakdown of perturbation theory and emphasize that the pure tree-level approximation fails earlier, parametrically. We then demonstrate, in three different (integral and quantum mechanical) model systems, that the physical high multiplicity amplitudes can be predicted on the basis of leading-order information from (non-perturbative) saddle points. In the non-Borel summable cases, one non-perturbative saddle contribution alone dominates the amplitudes. We highlight that high-multiplicity amplitudes may thus be a fruitful application for the methods of resurgence theory.

Contents

List of Figures

List of Tables

Chapter 1

Introduction

1.1 Invitation

This world is a curious place. The physics that governs humans' everyday lives, and also most of the stuff that we can build, is extremely well described by the quantum theory of electrons and nuclei interacting through Maxwell's laws. In spite of the simplicity of this theory, the world displays a stunning variety of different phenomena. Among these are some that initially surprise even students of physics, not to mention their initial discoverers. One example is superconductivity, the phenomenon in which rather simple materials like mercury or lead, at low temperatures, lose any resistivity [Onn11] and gain the ability to sustain currents when no external voltage is applied [Onn14], while expelling magnetic fields [MO33]. A satisfactory theoretical explanation was only given much later [GL50; BCS57]. Another example is the fractional quantum Hall effect [TSG82], in which a material acts as if it contained particles with a fraction of an electron charge, even though no such elementary particles are actually there [Lau83]. In these examples, the effective theory of electrons is still completely valid. The key reason that such striking phenomena may occur is the conspiration of many particles in conjunction with the laws of quantum mechanics - they are collective quantum effects.

We are more interested in the high energy frontier of physics, the field that occupies itself with the description of the interactions of particles when they are forced to approach each other to tiny distances. But also with extreme conditions of gravity - for example in the vicinity of the densest astronomical objects - black holes. Rest assured that the world is not any less curious in the high energy realm. Collective quantum effects, however, have traditionally not played a very prominent role in this field of study for different reasons.

One is that the way we set up particle collisions in experiments can only ever bring two of them close to each other in any collision and our energies are insufficient to produce a very large number of them in the process[1]. Others reasons are just historical.

Over the last decade, high energy physicists had the privilege to witness experimentalists and observers confirm our basic theories to unprecedented levels of accuracy. To pick just a few examples, the discovery of a new light particle [AA+12; Cha+12], identified as the long sought Higgs Boson [Hig64], has completed the electroweak sector of our standard model of particle physics [Wei67]. The discovery [SB+92] and ever more precise measurement [KS+11; AA+15] of temperature anisotropies in the cosmic microwave background radiation has forcefully confirmed our understanding of the interplay between inflating gravitational backgrounds and quantum fluctuations [MC81]. And lastly, the direct detection of gravitational waves [AA+16c] created in the collision of two black holes has once again vindicated Einstein [Ein16] and our rudimentary understanding of black holes.

Even though no direct experimental evidence of any new heavy particles is in sight[2] (see, e.g., [KS+16]), important conceptual problems still remain in high energy physics. One example is our lack of detailed understanding of the interplay between quantum mechanics and black hole physics. Following a recent proposal by Dvali and Gomez [DG13b; DG14], we have pursued the idea that black hole physics may, after all, be a manifestation of collective quantum effects in high energy physics. In this work, we present some of the results obtained for simplified model systems and the conclusion we draw for black holes. From this point, we were intrigued to further explore the relevance of quantum collective effects. During our efforts to unravel the phenomena using techniques of integrability, we discovered a surprising equivalence between our model system (Lieb-Liniger) and an otherwise seemingly unrelated theory in two dimensions (Yang-Mills). Finally, we turned to particle collisions, in which many particles are produced. These may only be accessible at future experiments, but until then, we need to dramatically improve upon our capabilities to calculate such processes, where quantum collective effects are dominant. In this domain, the present work contains some formal developments that aim to further our understanding of the required mathematical tools.

This work on collective quantum effects in areas of high energy physics, as diverse as gravity and scattering in field theory, has lead us to recognize their

[1] Those who study collisions of heavy nuclei at high energies might take issue with this oversimplified account. Collective quantum effects may indeed be relevant for them, but in a different manner than the high multiplicity scattering studied in one part of this work.

[2] Barring 2σ deviations like the current diphoton excess at 750 GeV [AA+16a].

potential impact on both areas. With this work, we hope to draw further attention to the present ideas that may be vital to finally understanding the inner workings of black holes as well as collisions at future particle colliders.

1.2 Results

As one part of this thesis, we have studied the phase transition in the Lieb-Liniger model [LL63], a system of heavy attractive Bosons in one spatial dimension, as a proxy for black hole graviton condensates. We have explored further indicators for the phase transition and present the spectrum of excitations, entanglement of few-particle subsystems, and the so-called ground state fidelity as examples. With a peak in the entanglement of fluctuations and the quantum discord as well, we have clear evidence that the system behaves most quantum-mechanical near its critical point. The quantumness is due to long-wavelength modes in this example. We interpret these phenomena as clues for black holes in the graviton condensate picture.

We then turn to time-dependent phenomena in order to address the question of fast scrambling that has been conjectured to take place in actual black holes. With intuition from laboratory atomic condensates and some insights from quantum chaos, we conjure an appealing picture for the origin of scrambling in the black hole portrait of Dvali and Gomez. We back the claims with simulations in the Lieb-Liniger model in an appropriate regime, where we observe entanglement generation in logarithmic time. We believe that these insights about scrambling are more widely applicable than the graviton condensate model and comment on their broader relevance.

We stick to the attractive Lieb-Liniger model some longer, now rather for its own sake. We extend the techniques of integrability to the infinite particle number limit in order to tackle the phase transition and derive continuum Bethe description. We find the ground state explicitly for arbitrary coupling. We then reveal a surprising equivalence with two dimensional $U(N)$ Yang-Mills theory quantized on a sphere [DK93]. The phase transition of the Lieb-Liniger model thus maps to the Douglas-Kazakov confinement-deconfinement transition of the latter system.

Finally, we consider high multiplicity scattering amplitudes in Bosonic theories. We study in more detail the manner of the expected breakdown of perturbation theory. This yields some cautionary conclusions for naive reasoning about its limit of applicability and a nice parallel to our previous observations from the Lieb-Liniger model. We then put forward some new results about the analog of scattering amplitudes in zero and one dimensions. In these models, high multiplicity amplitudes may be dominated by one

non-perturbative saddle points and can be determined on the basis of the leading-order saddle point approximation.

This thesis thus covers a wide range of aspects regarding collective quantum effects in high energy physics, ranging from the question of black-hole-information to field theoretic studies. And from more speculative attempts to results with many digits of precision.

1.3 Outline

As our research has tackled collective quantum phenomena from three distinct angles, this whole thesis is divided in three parts.

Chapter 2, *Black Hole Condensate Model*, contains our work on the Dvali-Gomez black hole portrait. After a necessary, but brief, review of conventional black hole physics and the quantum portrait, 2.4–2.7 study the quantumness of condensates close to a critical point and draw conclusions for black holes as graviton condensates. These results have been published in [FPW13]. Sections 2.8–2.12 present a concrete proposal, how graviton condensate black holes manage to scramble information. This research has been published in [DF+13].

Our work on the integrable Lieb-Liniger model, that has uncovered an unexpected equivalence with two-dimensional Yang-Mills theory is contained in chapter 3, *Bethe Ansatz at Large-N*. The content of 3.3–3.5 has been published in [FFP15].

Chapter 4, *High-Multiplicity Scattering*, finally contains our work regarding scattering processes that produce many particles and the role of resurgence theory in their calculation. These results will be contained in an upcoming publication [Fla16].

Note that this work is not aimed to provide a review of collective quantum behavior in condensed matter systems. References are, of course, provided, where we invoke known examples.

For completeness, we have to point out that some of the results obtained and published together with our collaborators have subsequently been reported in the dissertations of some of the collaborators. Explicitly, results from [FPW13] and [DF+13] were reported by A. Pritzel [Pri14] and N. Wintergerst [Win14], while results of [FFP15] will also be reported by A. Franca (in preparation). In this thesis, however, we give an independent account of the jointly pursued research directions and even present some additional results in each chapter that have not appeared anywhere before.

Chapter 2

Black Hole Condensate Model

2.1 Motivation

Black holes have been a source of puzzle for physicists nearly ever since Schwarzschild wrote down his exact solution to the gravitational field equations [Sch16]. Luckily, however, at least the subject of our puzzlement has gradually evolved over time.

The main problems we currently face in the description of black holes have to do with Hawking radiation [Haw76]. More precisely, how to reconcile the apparently perfectly thermal properties[1] of the radiation that remains, when the black hole has completely evaporated, with the unitarity of time evolution in quantum physics. We may just as well ask where the standard semiclassical picture of black holes goes wrong and how one might improve it.

The graviton condensate portrait of black holes developed by Dvali and Gomez [DG13b; DG14] is one attempt in this direction. They posit that the rigid classical background should be replaced by a condensate of gravitons (quanta of the gravitational field). In spite of the extremely weak interaction of long wavelength gravitons (the condensate gravitons are supposed to have a wavelength comparable to the radius of the black hole horizon), their sheer number ensures that quantum effects are still important. This last fact is key in making the picture viable. Because collective quantum effects are thought to be important in the condensate, a classical (i.e., mean field) description can easily fail to capture relevant corrections.

In this chapter, we will explore the possible implications of this black

[1] Except for gray body factors due to the gravitational potential barrier and, of course, a UV cutoff; see, e.g., [Vis15] for a recent discussion.

hole portrait in some detail. Because a faithful mathematical description of a condensate of actual gravitons is elusive[2], we employ a toy model - already proposed by Dvali and Gomez - in order to attain a better understanding of the nature of the quantum collective effects that we might find in an actual graviton condensate.

After a brief review of some relevant black hole physics (section 2.2) and an introduction to the ideas of Dvali and Gomez (s. 2.3), we exhibit the toy model and relevant techniques in 2.4. We study the properties of the phase transition and find some new indicators of criticality (s. 2.5). Section 2.6 presents clear and novel evidence that quantumness is most important at the critical point - even at finite particle number, where the exact ground state is a superposition of solitons. We then (s. 2.7) speculate on the import of these findings for actual black hole graviton condensates. The novel results of sections 2.5–2.7 have been presented in our publication [DF+13].

The second half of the chapter is geared towards understanding fast scrambling in the black hole portrait. After introducing some known facts about attractive Bose condensates in three dimensions (s. 2.8) and some properties of quantum chaotic systems (s. 2.9), we assemble the pieces and present novel ideas about fast scrambling in section 2.10. In 2.11, we substantiate our ideas with additional, now real time, simulations in the toy model. Finally (s. 2.12) we also comment on which parts of this picture may also be relevant to other microscopic models of black holes. The new insights of sections 2.10 and 2.12 have been put forward in our publication [FFP15].

2.2 Short Review of Black Hole Physics

In this section, we will recapitulate some of the classic results of the semi-classical treatment of black holes. We will cherry-pick the directions that are relevant as background-material for our work and will not try to give a complete or historically faithful account of the subject (see, e.g., [Wal01] for a more thorough review).

When we talk about black holes, we usually imply Schwarzschild black holes. Just for definiteness, their classical metric in Schwarzschild coordinates is

$$ds^2 = \left(1 - \frac{R_\mathrm{S}}{r}\right)dt^2 - \frac{1}{1 - \frac{R_\mathrm{S}}{r}}\,dr^2 - r^2\,d\Omega^2 \tag{2.1}$$

where $R_\mathrm{S} = 2G_\mathrm{N}M$ is the Schwarzschild radius, which marks the position of the horizon, M is the ADM-mass of the object, and $d\Omega^2$ is the metric on

[2]Note, however, the approach of [HR16; GH+15] to develop a calculational formalism.

the two-sphere. It will be important to keep in mind that the Schwarzschild radius is the only classical length scale present in this problem and that the zone around the horizon therefore has low curvature for a large black hole.

The maximally extended Schwarzschild metric is that of an eternal black hole. We will, however, usually reason about black holes that are formed in gravitational collapse and, as we shall review momentarily, evaporate over long time scales. The region of interest is, nevertheless, described classically by the Schwarzschild metric.

Our ideas should be easily transferable to other black hole geometries. Only extremal black holes (those with maximum charges) probably require additional attention.

2.2.1 Semiclassical Black Holes

One of the most far-sighted observations in black hole physics was made by Bekenstein, who realized that some black hole properties behave like thermodynamic variables [Bek73]. Explicitly, the horizon area is associated with entropy and the surface gravity κ with temperature

$$S = \frac{A}{4L_{\mathrm{P}}^2} \qquad T = \frac{\kappa}{2\pi} \tag{2.2}$$

in natural units ($\hbar = c = k_{\mathrm{B}} = 1$).

Soon after, Hawking found out that the temperature is not only a crutch to make the laws of black hole thermodynamics work. By quantizing quantum fields on the background of a black hole (formed in collapse), he was able to show that radiation with a Planckian spectrum emanates from the horizon [Haw74; Haw75]. That is, the black hole behaves like a thermal black-body radiator[3]. As black holes give off radiation, they must naturally diminish in mass. Thus, the Stefan-Boltzmann law leads to a black hole lifetime that scales like $t_{\mathrm{BH}} \sim M^3/M_{\mathrm{Pl}}^3$ (barring further accretion of matter).

It took much longer, until concrete evidence was found that the black hole entropy is also statistically meaningful as the logarithm of the degeneracy of states. Strominger and Vafa conceived a string-theoretic setup in which the BPS-properties of an extremal black brane allowed them to make a connection with its weak-coupling description as a stack of D-branes [SV96]. The degeneracy of states obtained at weak coupling coincides with the expected black hole entropy. Their example confirms that there is a microscopic degeneracy of states associated with the thermodynamic black hole entropy.

[3]Only then could the constants of proportionality in (2.2) actually be fixed.

Given that the Hawking radiation looks thermal and originates in the near-horizon zone, which is self-cleaning[4], it is a short step to conclude that the evaporation does not reveal any information about the internal state of a black hole (this also pertains to global charges trapped in the black hole). This is at the heart of the black hole information problem (see [Pre92] for an early review). It is important to reiterate that this result is based on quantizing fluctuations on top of a rigid Schwarzschild background.

The assumption that Hawking radiation does not contain any information about the state from which a black hole was formed allows for two equally undesirable outcomes. Either, black hole evaporation stops when the remaining mass is of the order of the Planck-mass (then the semiclassical evaporation need not be trusted any more). The heavy "particle" that remains, a black hole remnant, then needs to have as much degeneracy as the evaporated black hole. Such an infinite density of states most likely spells trouble in the form of infinite decay rates and infinite contributions in loop calculations [Hoo85]. Or the information is lost in the black hole and the theory is non-unitary. This second possibility has severe problems of its own [BSP84]. It has finally fallen from grace [Haw05] when the AdS/CFT correspondence [Mal99] implied that a gravitational theory on anti-de-Sitter space (a rather specific one, though) should have a dual description as a certainly unitary conformal field theory in one fewer dimension[5,6].

Now, the information problem is one of understanding by which mechanism information is released in Hawking radiation. And which part of the argument for information loss needs to be reconsidered.

2.2.2 More about Black Hole Information

Given that black holes do lose information through Hawking radiation, one may ask at which point during their evaporation information can meaningfully be gathered by an outside observer. This question was first addressed by Page, who dared to treat the black hole just like any other evaporating quantum system [Pag93a; Pag93b]. He found out that the entanglement between the black hole "interior" and the emitted Hawking radiation is generically determined by the size of the smaller Hilbert space. Thus, the entanglement must, at the latest, cease to increase when the dimension of the internal

[4] I.e., which only supports decaying quasi-normal modes [RW57].

[5] Thus realizing the older dream of holography in quantum gravity [Hoo93; Sus95].

[6] An obvious idea is to calculate properties of black holes in AdS by using the CFT-description. Apart from the technical complication that this is a strongly-coupled CFT, it is not yet clear how bulk operators close to or inside the black hole should be implemented, although some progress has been made recently [PR14].

Hilbert space has shrunk to half its original value. The corresponding age of the black hole is denoted as Page-time and scales like $t_{\mathrm{P}} \sim M^3/M_{\mathrm{Pl}}^3$.

A related, but distinct, question is how long black holes retain newly inserted information. That is, assuming one has been gathering information about an old black hole for at least a Page-time, when a (unknown) qubit of information is thrown into the black hole, how quickly can one reconstruct this qubit from the Hawking radiation. Hayden and Preskill found that, after internal thermalization of the black hole state, information is released nearly immediately [HP07]. Black holes behave as information mirrors[7]. They were then able to give a lower bound for the thermalization time, based on the notion of black-hole-complementarity[8]. In order not to violate the quantum no-cloning theorem, thermalization cannot happen faster than

$$t_{\mathrm{sc}} \sim R_{\mathrm{S}} \log(R_{\mathrm{S}}/L_{\mathrm{P}}) \tag{2.3}$$

in Schwarzschild time. The conjecture that this lower bound actually represents the thermalization-time was reinforced and popularized by [SS08] under the name of fast-scrambling.

Ever since, it has been an intriguing task to give a microscopic explanation of the fast-scrambling time (see, e.g., [LS+13; BM11; BM12]) which is much shorter than time-scales expected for, e.g., diffusion.

2.3 Black Hole Quantum Portrait

This section reviews some parts of the proposal put forward by Dvali and Gomez in a series of publications [DG13b; DG12b; DG13a; DG12a; DG14] for a novel picture of black hole physics. They used insights from the study of quantum many-body systems to develop the framework and gave convincing arguments why similar physics may be at play in the realm of black holes. Our account of these matters will start from the black hole information paradox, but will subsequently reproduce their ideas in a way close to the account in [DG13b].

[7] Nonetheless, it might be much harder in practice to decipher the emitted information [HH13].

[8] Complementarity is the concept that both, an observer falling into the black hole and an outside observer, should each have a consistent, though not necessarily identical, quantum-mechanical description of physics within their respective past light-cones [STU93].

The black hole information paradox arises, when the result of thermal Hawking radiation is applied to the entirety of the evaporation process. One should therefore scrutinize the (implicit) assumptions made in the derivation of Hawking radiation.

On the one hand, Einstein gravity is treated as an effective, weakly coupled effective quantum field theory in the calculation. For large black holes this seems warranted, because the curvature radius is small around the horizon - the crucial region for the calculation. By standard effective field theory reasoning, higher order operators corresponding to effects from UV physics should be suppressed by powers of the cutoff scale (presumably Planck mass) and therefore be negligible [Don94]. Still, one may ask whether UV physics provides unexpected effects in the near horizon region. All stretched horizon models, e.g. 't Hooft's brickwall [Hoo85] rely on this. The story of long strings at the horizon [Sus93] also belongs in this category. Concrete fuzzball ideas like [Mat05] also leverage specific UV degrees of freedom to avoid introducing a horizon. While these investigations are interesting in their own right, they have not produced a persuasive coherent picture for Schwarzschild black holes.

On the other hand, the theory is treated in the semiclassical approximation. The field operator (e.g. for the metric) is split into a c-numbered classical part (the Schwarzschild metric) plus small fluctuations on top of it. Among the fluctuations, only the ones with wavelength sufficiently smaller than Schwarzschild radius are taken into account. As we will demonstrate in some detail in section 2.6, there is ample opportunity for these assumptions to go wrong, even in simple many-body systems. The proposal of Dvali and Gomez contains a concrete argument, why strong collective effects should be at play in Schwarzschild black holes and render semiclassical reasoning unreliable.

2.3.1 Graviton Condensates

Let us consider a situation where we confine N low energy gravitons with wavelength λ to a volume of size R. We can then wonder whether their interaction may suffice to create a self sustained bound state. We can obtain the following estimate from the virial theorem. For a bound state, the average kinetic and potential energy scale similarly

$$\langle E_{\text{kin}} \rangle \sim \langle V \rangle \tag{2.4}$$

Note that we are omitting factors of order one here and in the rest of this section. We will now make crude estimates for both quantities: the kinetic

energy approximated as N times the energy of a single graviton

$$\langle E \rangle \sim N \frac{\hbar}{\lambda} \tag{2.5}$$

and the total potential energy as roughly $N^2/2$ times the mutual Newtonian potential of a pair

$$\langle V \rangle \sim N^2 \frac{G_{\rm N}(\hbar/\lambda)^2}{R} \tag{2.6}$$

If we now assume that the gravitons have the maximum possible wavelength in the given volume $\lambda \sim R$, the self-sustainability condition (2.4) becomes

$$R \sim \sqrt{N} L_{\rm Pl} \tag{2.7}$$

Let us interpret this equation. The total mass of the gravitons turns out to be $M \sim \sqrt{N} M_{\rm Pl}$ and the expected size of the bound state scales exactly like the Schwarzschild radius associated with this mass. Of course the approximations used above were taken for gravitons on a Minkowski background. The mass, for example, did not take into account redshifts and the potential was just the Newtonian approximation. We will, nevertheless, take this hint seriously that a self sustained bound state of gravitons would look very much like a black hole. Let us therefore explore the possibility that Schwarzschild black holes should properly be thought of as self sustained bound states of gravitons.

Consider, now, the mutual attraction of low energy gravitons with wavelength $\lambda \sim R$. Their dimensionless scattering strength scales like $\alpha \sim L_{\rm Pl}^2/R^2$. We can define the collective interaction as the product of the two body interaction with the number of participating particles

$$g \sim \alpha N \sim 1 \tag{2.8}$$

and find that it is of order one for the kind of bound state discussed above. This is very noteworthy, because a collective coupling of order one often implies the onset of collective quantum effects as we will see in rich detail below. It is this observation that makes us optimistic that a black hole in a properly understood description as a graviton condensate may easily avoid the information paradox.

2.3.2 Hawking Radiation in the Condensate Picture

In [DG13b; DG13a] it has also been concluded that a self sustained graviton bound state would lose constituents at a rate commensurate with Hawking

radiation. The evaporation is due to re-scattering of condensate gravitons and can be estimated from the corresponding Feynman diagrams.

The corrections to thermality are thought to be suppressed by just a factor of $1/N$ [DG13b] (this might be related to a recent observation in string-black-holes [Ven13]). This is in stark contrast to the semiclassical reasoning, where corrections are exponentially suppressed by the black hole action $\exp(-S)$ (see, e.g., [Mal03]).

Another consequence, implicit in the black hole portrait, is the non-violation of global symmetries. As the only physics involved is that of long wavelength gravitons, and Hawking radiation merely a result of rescattering, there is no reason for global charges to be violated. As long as the deposited global charge is much smaller than the number of condensate gravitons, it should only lead to $1/N$-hair [DG13a]. See [DG16] for a discussion of a situation, where baryon charge comes to dominate.

2.3.3 Relevance of Toy Models

While this picture of graviton condensates may be an appealing possibility to explore for solving the long standing black hole puzzles, its major drawback is that detailed calculations of graviton condensates in the regimes envisioned are not currently possible.

The closest cousins to graviton condensates that have been studied may be gravitational geons [BH64]. These compact gravitational objects are, however, sourced by highly energetic classical gravitational waves and are therefore a long stretch from the long wavelength, highly quantum-mechanical condensates that we envision.

In this work, we will follow the proposal of [DG14] to study tractable Bosonic condensates as a proxy for graviton condensates. While we will have to be careful not to draw any definitive conclusions about black holes, insights from toy models will help to shape our understanding of real graviton condensates.

2.3.4 A Parallel with Black Holes in M-Theory

As a tangent, we will point out a parallel with string theoretically motivated ideas about black holes. This connection has not been commented upon in the literature yet, but we will come back to it again in section 2.12. To this end, we have to recall some facts about the BFFS matrix model as a formulation of M-theory [BF+97] and the description of black holes in this framework [BF+98a; BF+98b].

In the strong coupling limit, type IIA string theory obtains an additional spatial dimension. The resulting eleven-dimensional theory is known as M-theory [Wit95] and is closely interwoven with various other limits of string theory. While its low energy description is 11d supergravity, Banks, Fischler, Shenker, and Susskind used the IIA limit to argue that M-theory in the infinite-momentum-frame should coincide with the short distance description of a stack of D0-branes[9]. Thus they conjectured the theory to be supersymmetric $U(N)$ Yang-Mills matrix-quantum-mechanics, where N is the number of participating D0-branes and 9 matrix multiplets implement the transverse coordinates of the branes [BF+97].

Despite its simple appearance, the matrix theory has been shown to not only account for D0-branes, but to contain super-membranes [BF+97], as well, and even string excitations [Mot97].

Shortly after the conjecture, some of the original authors and Klebanov investigated how Schwarzschild black holes could be realized in the matrix theory [BF+98a]. With the spatial dimension corresponding to the infinite-momentum-frame compactified on a circled, a big Schwarzschild black hole needs to be boosted to actually fit. From this boost, they conjectured that the minimum dimension of the matrices N to faithfully describe the black hole without including redundant degrees of freedom is

$$N_{\min} \sim M R_{\mathrm{S}} \sim S \tag{2.9}$$

where M is the mass and R_{S} is the Schwarzschild radius. This value corresponds to the entropy of the black hole S.

Then they went on to confirm that the matrix model in the appropriate regime and with this N has the same scaling of the statistical entropy as an actual black hole. Furthermore, the expected transverse extent matches the Schwarzschild radius. In [BF+98a], these considerations were made in the context of $7+1$ dimensional black holes with the other three transverse dimensions compactified on a torus. In [BF+98b], the arguments were then generalized to other dimensions and the picture was simplified, consisting now of a gas of D0 branes in some matrix background. See [IM+98] for a different perspective on the matrix black hole, which is more aligned with the AdS/CFT reasoning.

We want to point out the following intriguing similarity between black holes in matrix theory and the black hole graviton condensate picture. The D0 branes in the IIA limit of M-theory correspond to the multiplet of the first

[9]The D0 branes are the only objects in the theory that carry the requisite charges.

Kaluza-Klein excitation of the eleven-dimensional supergraviton. Thus, a gas of N D0 branes, which supposedly is the matrix description of black holes, is very similar in spirit to the bound state of N gravitons of the black hole portrait. Even the conjectured numbers N match, although the considerations culminating in the respective pictures are quite unalike.

2.4 The Lieb-Liniger Model

In this section, we will introduce the Lieb-Liniger model [LL63]. It will be our workhorse not only in the rest of this chapter, where we treat it as a proxy of graviton bound state behavior, but also in chapter 3, where we study it further in its own right. It is a nonrelativistic quantum mechanical many-body system composed of N indistinguishable Bosons with mass m and mutual contact-interaction in one spatial dimension. It can be described by the following Hamiltonian acting on the Bose-symmetric wave-function $\Psi(x_1, \ldots, x_N)$ as a differential operator

$$H = -\frac{\hbar^2}{2m} \sum_{i=1}^{N} \partial_i^2 - c \sum_{i \neq j} \delta(x_i - x_j) \tag{2.10}$$

where a positive c parametrizes the strength of the delta attraction[10]. We will always consider the model to be quantized on a ring of radius R, i.e., with periodic boundary conditions

$$\Psi(\ldots, x_i + 2\pi R, \ldots) = \Psi(\ldots, x_i, \ldots) \tag{2.11}$$

It is easy to see that the system compactified at radius R is unitarily equivalent to a version with radius R' and a modified strength of the delta potential $c' = c\,R/R'$ as well as scaled energy levels. Thus, a thermodynamic limit, in which the radius is made large at fixed c and fixed particle density effectively renders the system strongly coupled (we will later observe the manifestation of this fact).

For the discussion in this chapter, it will be most convenient to use the second quantized form of the Lieb-Liniger Hamiltonian

$$H = \int dx \left[-\frac{\hbar^2}{2m} \psi^\dagger(x)\, \partial_x^2\, \psi(x) - \frac{\hbar^2}{2mR} \frac{\pi\alpha}{2}\, \psi^\dagger(x)\, \psi^\dagger(x)\, \psi(x)\, \psi(x) \right] \tag{2.12}$$

where $\psi(x)$ is the field operator obeying canonical commutation relations and a dimensionless α now parametrizes the mutual interaction of the bosons. The scaling of the interaction has been chosen to simplify notation below.

[10] The original study of Lieb and Liniger was mostly interested in repulsive interactions, but we will concentrate on the attractive case.

We can, furthermore, introduce canonical creation and annihilation operators $a_k^\dagger$ and a_k for the momentum modes indexed by k and expand the field operator

$$\psi(x) = \frac{1}{\sqrt{2\pi R}} \sum_{k=-\infty}^{\infty} a_k \, e^{ixk/R} \tag{2.13}$$

After choosing units in which $1 = \hbar = R = 2m$, the Hamiltonian can be rewritten as

$$H = \sum_{k=-\infty}^{\infty} k^2 \, a_k^\dagger a_k - \frac{\alpha}{4} \sum_{k,l,m=-\infty}^{\infty} a_k^\dagger a_l^\dagger a_{m+k} a_{l-m} \tag{2.14}$$

For the sake of completeness, it should be noted already that the Lieb-Liniger model is integrable. We will, however, postpone the discussion of this fact until chapter 3, where integrability takes center stage.

2.4.1 Gross-Pitaevskii Equation for the Dilute Bose Gas

In this section, we will review some well-known facts about Bose-Einstein condensate physics and results obtained by applying mean-field techniques to the Lieb-Liniger model. These analyses show that the Lieb-Liniger model, in an appropriate large particle number limit, undergoes a second order quantum phase transition[11] [KSU03]. It is this transition that we will be most interested in, for the rest of the chapter. A more thorough discussion of Bose-condensate physics may be found in [PS03].

Mean-field treatment applies to states that are close to Bose-Einstein condensates. That is, where one mode is macroscopically occupied

$$|\Psi\rangle = C \, P_d(a_1^\dagger a_0, \, a_2^\dagger a_0, \, \ldots) \left(a_0^\dagger\right)^N |0\rangle \tag{2.15}$$

where $a_0^\dagger$ is the creation operator of the normalized condensate mode $\Psi_0(x)$ (not to be confused with the Fourier modes above), P_d is a polynomial of degree d that takes particles out of the condensate (depletion), C is a normalization, and the maximal depletion d/N is much smaller than 1.

When the Hamiltonian (2.12) is evaluated between states of this form, it can be expanded in powers of the depletion d/N. To leading order, all creation and annihilation operators in the Hamiltonian act on the condensate mode and the time-independent Schrödinger equation implies the Gross-Pitaevskii equation (also known as nonlinear Schrödinger equation) for the

[11] A thermal, liquid-gas phase transition of first has also been found, recently [HOC14].

mode function

$$\left[\partial_\theta^2 + \pi\,\alpha N\,|\Psi_0(\theta)|^2\right]\Psi_0(\theta) = \mu\,\Psi_0(\theta) \tag{2.16}$$

where μ is the chemical potential and an angular variable $\theta = x/R$ is used. It is already clear now that the relevant effective coupling of the Lieb-Liniger system is αN, enhanced by the number of particles. That the state characterized by the Gross-Pitaevskii equation really corresponds to the quantum mechanical ground state in the large particle number limit has only been proven rigorously quite recently in [LSY00] for repulsive systems. The leading correction is obtained in the Bogoliubov approximation, as we will see later.

Exact solutions of the nonlinear Schrödinger equation are known [CCR00] (see also fig. 2.1)

$$\Psi_0(\theta) = \begin{cases} \sqrt{\frac{1}{2\pi}} & \text{for} \quad \alpha N \leq 1 \\ \sqrt{\frac{\mathrm{K}(m)}{2\pi\,\mathrm{E}(m)}}\ \mathrm{dn}\left[\frac{\mathrm{K}(m)}{\pi}(\theta-\theta_0)\middle|m\right] & \text{for} \quad \alpha N > 1 \end{cases} \tag{2.17}$$

where the conditions on the coupling indicate the lowest energy solution in the given range (the homogeneous solution is naturally still a valid solution for $\alpha N > 1$). The parameter m needs to be determined from the condition

$$4\,\mathrm{K}(m)\,\mathrm{E}(m) = \pi^2\alpha N \tag{2.18}$$

The respective chemical potential is

$$\mu = \begin{cases} \frac{\alpha N}{2} & \text{for} \quad \alpha N \leq 1 \\ \frac{(2-m)\,\mathrm{K}^2(m)}{\pi^2} & \text{for} \quad \alpha N > 1 \end{cases} \tag{2.19}$$

The energy per particle in the mean-field state is

$$E/N = \begin{cases} -\pi^2\alpha & \text{for} \quad \alpha N \leq 1 \\ -\frac{4}{3}\,\frac{\mathrm{K}^2(m)}{\mathrm{E}(m)}[(2-m)\,\mathrm{E}(m) + (1-m)\,\mathrm{K}(m)] & \text{for} \quad \alpha N > 1 \end{cases} \tag{2.20}$$

In [KSU03], it was realized that this implies a quantum phase transition between a homogeneous phase at low values of the effective coupling $\alpha N \leq 1$ and a solitonic phase, in which the Bosons lump together, at larger effective coupling. Based on the behavior of the energy per particle, the transition was judged to be of second order.

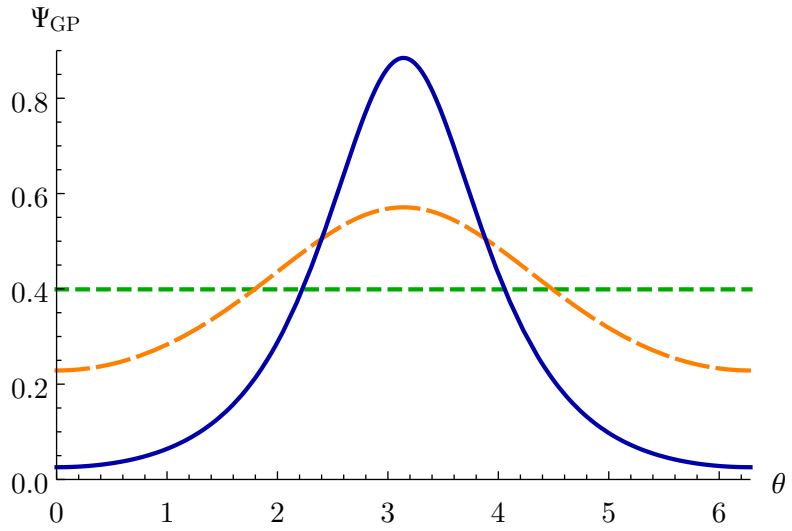

Figure 2.1: Mean-field solution of the Gross-Pitaevski equation in the homogeneous phase (green, short dashes) as well as in the solitonic phase for $\alpha N = 1.1$ (orange, long dashes) and $\alpha N = 2.0$ (blue, solid curve). Normalized to unit norm.

2.4.2 Bogoliubov Approximation

Here we will introduce the Bogoliubov approximation for the Lieb-Liniger model and report some results of Kanamoto, Saito and Ueda [KSU03] about the explicit modes.

Taking the condensate mode as determined by the Gross-Pitaevskii equation, we now turn to the next-to-leading order in the expansion of the Hamiltonian with respect to the depletion, while holding αN constant. The resulting Hamiltonian is quadratic in the non-condensate modes. To this order, the effect on the condensate is just a reduction in the effective number of particles through depletion.

Explicitly, on top of the homogeneous mean field $\Psi_0 = 1/\sqrt{2\pi}$, the Hamiltonian, in terms of Fourier modes, is approximately

$$H = \sum_{k\neq 0} (k^2 - \alpha N/2)\, a_k^\dagger a_k - \frac{\alpha N}{4} \sum_{k\neq 0} \left(a_k^\dagger a_{-k}^\dagger + a_k a_{-k} \right) \tag{2.21}$$

It can be diagonalized with a Bogoliubov transformation

$$a_k = u_k\, b_k + v_k^\star\, b_{-k}^\dagger \tag{2.22}$$

where the coefficients need to satisfy $u_k^2 - v_k^2 = 1$ in order for the $b_k, b_k^\dagger$ operators to fulfill the standard ladder-operator algebra. Here the diagonalization

is easy to obtain

$$u_k^2 = \frac{1}{2}\left(1 + \frac{k^2 - \alpha N/2}{\epsilon_k}\right), \qquad v_k^2 = \frac{1}{2}\left(-1 + \frac{k^2 - \alpha N/2}{\epsilon_k}\right) \tag{2.23}$$

such that

$$H = \sum_{k\neq 0} \epsilon_k \, b_k^\dagger b_k \quad \text{with} \quad \epsilon_k = \sqrt{k^2(k^2 - \alpha N)} \tag{2.24}$$

The ground state is obviously the b-vacuum, a squeezed state in terms of the original a-operators.

We should briefly pause and comment on the applicability of the approximation. The expected number of depleted particles is

$$\langle d \rangle = \sum_{k\neq 0} \langle a_k^\dagger a_k \rangle = \sum_{k\neq 0} |v_k|^2 \tag{2.25}$$

and is determined by the effective coupling only. The depletion in the $k = 1$ mode seems to diverge at the critical point $\alpha N = 1$, i.e., the approximation breaks down there. Nevertheless, for any fixed effective coupling $\alpha N < 1$, as we take the infinite particle number limit $N \to \infty$, the depleted fraction $\langle d \rangle / N$ diminishes. Thus, for any effective coupling away from criticality, the Bogoliubov approximation becomes good, eventually.

In the non-homogeneous condensate, the approximate Hamiltonian is still quadratic, but it mixes the modes in a more complicated fashion. Thus, the Bogoliubov transformation requires a direct decomposition into normal modes

$$\delta\psi(\theta) = \sum_k \left[u_k(\theta)\, b_k + v_k^\star(\theta)\, b_k^\dagger \right] \tag{2.26}$$

where the $b_k, b_k^\dagger$ operators still behave as ladder operators. The mode functions need to satisfy the Bogoliubov-de-Gennes equation to diagonalize the Hamiltonian

$$-\partial_\theta^2 u_j + 2\alpha N |\Psi_0|^2 \, u_j + \alpha N \Psi_0^2 \, v_j = (\mu + E_j) u_j \tag{2.27}$$

$$-\partial_\theta^2 v_j + 2\alpha N |\Psi_0|^2 \, v_j + \alpha N \Psi_0^{\star 2} \, u_j = (\mu - E_j) v_j \tag{2.28}$$

We cite an analytic expression for the first modes, here, because we will rely on them later.

$$u_1(\theta) = \quad C_1 \, \mathrm{sn}^2 \left[\tfrac{\mathrm{K}(m)}{\pi} (\theta - \theta_0) \middle| m \right] \tag{2.29}$$

$$v_1(\theta) = -C_1 \, \mathrm{cn}^2 \left[\tfrac{\mathrm{K}(m)}{\pi} (\theta - \theta_0) \middle| m \right] \tag{2.30}$$

with normalization

$$C_1^2 = \frac{m\,\mathrm{K}(m)}{2\pi[(2-m)\,\mathrm{K}(m) - 2\,\mathrm{E}(m)]} \tag{2.31}$$

Finally, let us introduce k-particle density matrices with matrix elements

$$\rho_{(ij\ldots)(mn\ldots)} = \langle a_i^\dagger a_j^\dagger \cdots\ a_m a_n \cdots \rangle \tag{2.32}$$

where there are k creation and k annihilation operators in the expectation value and the k-sequences in brackets represent the matrix-element-indices. It is obvious that the N-particle density matrix characterizes the state completely. Successively smaller density matrices, generically, contain ever less complete information about the quantum state. A pure condensate, however, is fully characterized by the one-particle density matrix, because all particles occupy the same mode. A macroscopic occupation of just one eigenvalue of the one-particle density matrix is often used to define a Bose-Einstein condensate.

2.4.3 Symmetry Breaking in Finite Volume

In the solitonic regime of the Lieb-Liniger model, the Bosons tend to lump. As the Hamiltonian is translationally invariant, however, the true ground state, will be an eigenstate of zero total momentum. This state can be regarded as a superposition of condensate states with different center of mass coordinates. It is, by the strict definition above, not a Bose-Einstein condensate, but a fragmented condensate, as discussed in, e.g., [KSU06]. As the particle number is increased, the overlap of condensate states with differing center of mass decreases exponentially, and so do matrix elements of operators between them (e.g. the Hamiltonian). In the infinite particle number limit, the states with different center of mass fall into different superselection sectors. This explains the appearance of spontaneous symmetry breaking - even though the system under consideration has finite spatial extent[12].

The center of mass motion of the soliton could be trapped with an external potential, but separation of scales is tricky if one does not want to deform the soliton condensate wave-function as well. We will make use of another technique in section 2.6.4, where we will come back to the issue.

With the above discussion in mind, we will sometimes be slightly sloppy and also refer to a soliton in a smeared state as a condensate.

[12]The well-known proof of the absence of spontaneous symmetry breaking in finite volume relies on the assumption that expectation values of composite operators remain finite (e.g. finite energy density).

2.4.4 Numerical Diagonalization

The Bogoliubov approximation only becomes exact in the $N \to \infty$ limit. This, however, is the semiclassical limit, which we argued, is responsible for most of the so called black hole paradoxa. Especially for our purposes, it is therefore necessary to have a complementary way to study the Bose condensate - one that can track $1/N$ effects. Here we will briefly describe the method we used.

We use direct numerical diagonalization of the Hamiltonian to simulate the system. Of course, even for a finite number of Bosons, the Hilbert space is infinite dimensional. A suitable truncation is required for numerical diagonalization to be feasible. One consideration played a significant role in selecting this specific numerical method. At the quantum critical point that we are most interested in, we suspect the system to possess large entanglement. Many numerical methods break down for strong long-range entanglement (compare, e.g., [PV+06] or [AV01]). Direct diagonalization, in contrast, has no such limitations.

We use the energy eigenstates of the free system as a basis for the Hilbert space, similar to the techniques reported in [KSU03]. These are states with well defined occupation number n_l in each free particle orbital with wavenumber l. We usually restrict the occupation to modes with momenta $|l| \leq 1$ and sometimes ≤ 2. All terms involving higher momentum modes are simply discarded from the Hamiltonian (2.14) preserving its hermiticity. In order to verify that this approximation still gives reasonably accurate results, we performed some simulations including momentum modes $|l| = 2, 3$ as well. Only for $\alpha N \gtrsim 1.5$ do these modes start to give relevant contributions. The simulations confirm that for $\alpha N \lesssim 2$, the restriction to the lowest excited free orbital gives qualitatively correct results. It is not unexpected that the truncation to the lowest momentum modes is good because the soliton (2.17) starts out with maximal width and only becomes narrower when αN is increased way past the phase transition.

A further simplification arises from the translation invariance of the system. As total momentum is conserved and we are interested in the ground state of total momentum zero, we can further restrict the Hilbert space to the states in the momentum zero sector

$$L = \sum_l l\, n_l = 0 \tag{2.33}$$

Finally, the matrix for the Hamiltonian in this basis is diagonalized using standard numerical techniques.

Our code allowed to simulate particle numbers up to roughly $N \lesssim 10000$ for $|l| \leq 1$. In order to guard against unexpected scaling properties, all cal-

culations were performed for various particle numbers. However, since the relevant effective coupling is αN, the analyses may be done for a fixed N by varying α.

We should note that the size of the Hilbert space grows much faster for Bosonic systems in two or three spatial dimensions. For an analogous truncation scheme, the size is enhanced by an additional power of the dimension. This places much stronger restrictions on the number of particles accessible in simulations and limits the utility of direct diagonalization in higher dimension.

As a final comment on our numerical techniques, we want to mention, again, that the ground state so obtained is a momentum eigenstate and does not correspond to a localized soliton (see the discussion in 2.4.3). It will instead represent a superposition of solitons centered around all possible positions x. There are several ways to overcome this problem. One is, by making successive measurements to first localize the soliton and measure the quantities of interest afterwards. This is what our discussion of the quantum discord is physically based on. Another possibility that we have explored is to introduce a weak, symmetry breaking potential to trap the soliton,

$$H' = H + \epsilon V \quad \text{with} \quad V = \frac{1}{N^2} \int d\theta \, \psi^\dagger(\theta) \cos\theta \, \psi(\theta) \tag{2.34}$$

As the parameter ϵ is increased, the potential becomes deeper and the soliton more localized. The symmetry breaking potential, however, comes with some problems of its own. As total momentum is no longer conserved, the Hilbert space cannot be restricted to $L = 0$ and simulations become significantly slower. Also, because a separation of scales between the compactification radius, the width of the potential well, and the size of the soliton is impossible, right after the phase transition, it becomes harder to interpret observed effects. This is, why the results presented in this work do not rely on such a localization potential.

2.4.5 Experimental Realization

Studies of the Lieb-Liniger model are not a purely theoretic exercise as the model has also been realized experimentally. This should not come as a big surprise, because the contact interaction is a good effective description in a regime where two-body scattering is dominated by the s-wave contribution.

It has long been known that light traveling through a self-focusing nonlinear optical fibre can form solitons and that the classical evolution is governed

by a nonlinear Schrödinger equation [HT73]. In this case, the interacting Bosons are dressed photons or polaritons. The quantum nature of these solitons has been studied [DC87] and observed in experiment [DS+93]. In this realization, however, it seems difficult to address the phase transition that we will be interested in.

The progress in controlling ultra-cold gases (see [BDZ08] for a broader review) has provided another way to produce attractive one-dimensional Bose condensates. In this case, a gas of cold atoms is prepared in an elongated axisymmetric trap that renders the physics effectively one-dimensional. Experiments have been conducted with atoms that naturally have a negative scattering length (explicitly ^{7}Li in certain spin states) [SP+02]. A more flexible alternative is to employ Feshbach-resonance techniques [KS+02; PW+04; HG+09]. By varying an external magnetic field, a Feshbach resonance (originally studied in nuclear physics [Fes58]) with other Zeeman-split states may be induced for certain species of atoms (like ^{85}Rb) [TVS93; VT+97]. Because the scattering length varies wildly around the resonance, this allows for experiments at virtually arbitrary interaction strength.

To compare experimental results, the Lieb-Liniger coupling c in (2.10) needs to be matched to the three-dimensional s-wave scattering length a by

$$c = -\frac{\hbar^2 a}{m r^2} \tag{2.35}$$

where r is the oscillator length of transverse trapping potential (see [Ols98] for a detailed treatment).

2.5 Indicators of Phase Transition

In this section we will study the known phase transition of the one-dimensional attractive Bose gas in some additional detail using both the Bogoliubov approximation and the numerical techniques outlined before. Of course, the number of particles is limited in our simulation and a true phase transition does not occur as discussed in 2.4.3. Nevertheless, precursors to the phase transition will be discernible. We will study three indicators and discuss their physical interpretation. This sets the stage for more insightful measures of quantumness that will be the focus of the next section.

The results presented below are new (except for 2.5.1). They were part of our publication [FPW13].

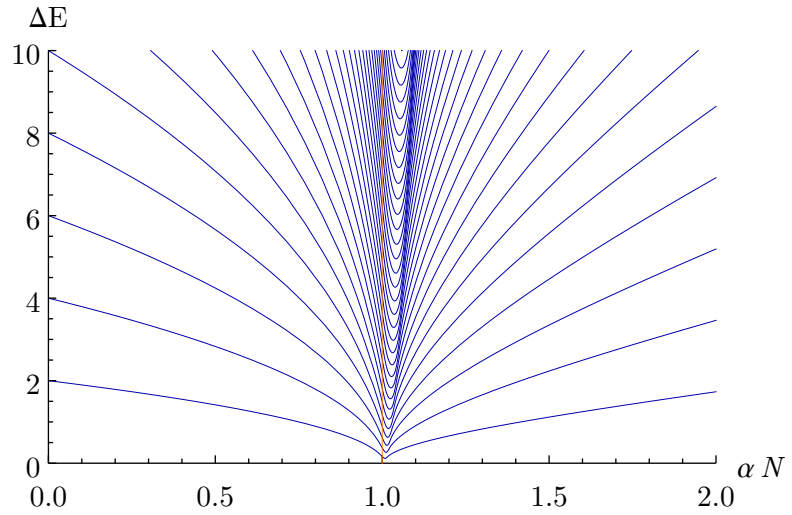

Figure 2.2: Energy spectrum of excitations above the ground state $E_n - E_0$ as a function of the effective coupling αN; calculated numerically for $N = 5000$ with modes truncated to $l = -1, 0, 1$. The orange line highlights the phase transition point $\alpha N = 1$. A version of this plot was included in [FPW13].

2.5.1 Spectrum of Excited States

The spectrum of excitations has already been calculated in the Bogoliubov approximation in section 2.4.2. It was clear that the excitations in the zero momentum sector around the homogeneous state and soliton both become gapless at the phase transition. This behavior is intimately related to the change in ground state. At the phase transition, the cost of forming a soliton out of the homogeneous state vanishes as the two solutions exchange their roles.

Another class of excitations, those with net momentum, need to be interpreted separately. Their gap also diminishes at the phase transition, it does, however, not grow again on the solitonic side. Instead, it stays small. Physically speaking, these excitations correspond to the translation modes of the soliton and their gap is expected to be the kinetic energy of the moving soliton $\hbar^2 k^2/(2m_{\text{sol}})$. Thus it also scales as $1/N$ on the strong coupling side, but this is rather a hint that there is a localized object than a characteristic of the transition point itself.

The excitation spectrum has already been investigated numerically by the authors of [KSU03] and our numerical calculations confirm their results. The spectrum of zero momentum excitation for $N = 5000$ particles is displayed in figure 2.2. It is clear that the energy gap shrinks at the critical point.

Yet, there is only one mode with small gap (not counting the translations of the soliton). Thus, one cannot attribute a large entropy to the system at the phase transition point ($S \ll N$), even though the density of states is significantly enhanced, there (see already fig. 2.13 which we need for different purposes later).

In the Bogoliubov approximation, the gap goes to zero at the phase transition point (even though the approximation itself ceases to be valid there). This result, however is only exact for infinite N. For finite N, Kanamoto et al. have conjectured that the minimal gap should behave like $1/\sqrt[3]{N}$. This scaling has only been proven quite recently by Panchenko [Pan15] using analytical methods to diagonalize the Hamiltonian matrix that we have treated numerically.

2.5.2 One-Particle Entanglement

In section 2.4.2, we have reviewed that the classical limit of our Bosonic many-body system - mean field - corresponds to a pure one-particle density matrix. I.e., a matrix with just one nonzero eigenvalue. The von Neumann entropy of this matrix

$$S_1 = -\operatorname{Tr}(\rho_1 \log \rho_1) \tag{2.36}$$

therefore measures deviations from a mean-field state. It is also referred to as one-particle entanglement because it can just as well be interpreted as quantifying, how well the knowledge of the mode occupied by any one particle characterizes the state of the whole system.

Explicitly, in the momentum eigenbasis (2.13) used for our numerical calculations with $|l| \leq 1$, the one-particle density matrix has a simple form

$$(\rho_1)_{ij} = \delta_{ij} \sum_{\{n_k\}} |\alpha_{\{n_k\}}|^2 \frac{n_i}{N} \tag{2.37}$$

where n_k are the occupation numbers of the different momentum modes

$$|0_{\text{num}}\rangle = \sum_{\{n_k\}} \alpha_{\{n_k\}} |\{n_k\}\rangle \tag{2.38}$$

and the δ_{ij} is a direct consequence of the fact that we consider an angular momentum eigenstate with

$$\sum_k k\, n_k = L_{\text{tot}} = 0 \tag{2.39}$$

for all nonzero $\alpha_{\{n_k\}}$.

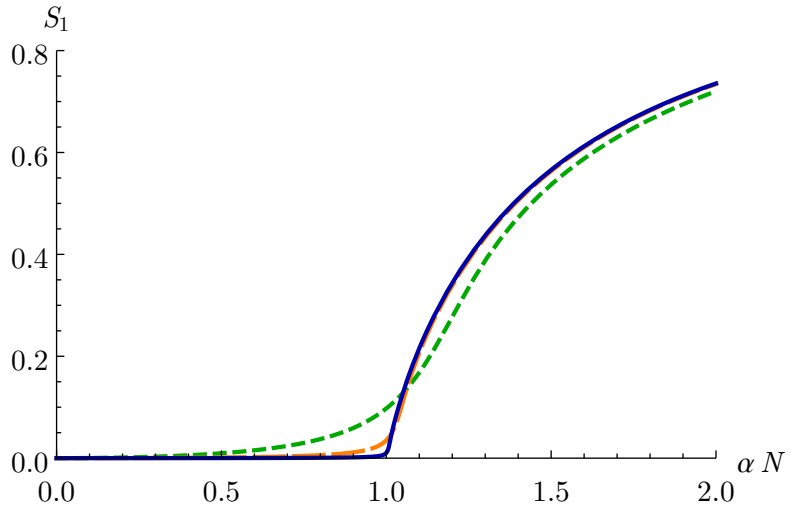

Figure 2.3: One particle entanglement as a function of the effective coupling αN; calculated numerically for $N = 50$ (green, small dashes), $N = 500$ (orange, long dashes) and $N = 5000$ (blue, solid curve) with modes truncated to $l = -1, 0, 1$. A version of this plot was included in [FPW13].

The figure 2.3 shows the numerical results for the one-particle entanglement evaluated with respect to the collective coupling. Different curves are displayed for different simulations with increasing particle number (50, 500, 5000).

At very weak coupling, we know that the particles form a homogeneous Bose-Einstein condensate and mean-field should be a good approximation even for low particle numbers. On this side of the phase transition, the one-particle entanglement is expected to be tiny and the figure confirms this expectation. As the phase transition is approached, however, we expect collective effects to become important as the ground state is reorganized. This effect is also clearly observed.

After the phase transition, the figure shows a marked increase in the one-particle entanglement. At stronger coupling, the entanglement grows further, even though we argued previously (see section 2.4.2) that mean field should become a good description again for stronger couplings, in the large particle number limit. The effect we observe here is the superposition of would-be-solitons discussed already in 2.4.3. Actual symmetry breaking only occurs for an infinite number of degrees of freedom. For any finite particle number, as in the numerical calculation, there is no superselection and the observed ground state has to be interpreted as an s-wave superposition of solitons localized at different center of mass.

In our simulation, we only took three momentum modes into account ($l = -1, 0, 1$). The finite size of the density matrix then bounds the entropy $S_1^{\text{num}} \leq \log 3$. For the range of effective coupling shown in the plot, this truncation gives a qualitatively good approximation. For even larger αN, the soliton becomes narrower, more momentum modes are involved and the true one-particle entanglement would increase further, albeit slowly.

Let us also comment on the change of shape as the particle number is varied. The curve becomes much sharper as the number is increased. Already for 5000 particles, the curve has a visibly sharp kink close to $\alpha N = 1$. This is easily explained, because level repulsion becomes weaker as the number of degrees of freedom is increased. For infinitely many particles, actual level crossing would occur, changing the derivative of the one-particle entanglement instantaneously. The one-particle entanglement itself does not become discontinuous in this limit, however, as its growth may be attributed to the superposition of mean-field solitons and the soliton develops continuously from the homogenous solution.

2.5.3 Ground State Fidelity

Above, we have seen that the phase transition results in a sharp increase of the one-particle entanglement. We related the monotonic growth of this quantity to the fact that the observed ground state in the solitonic regime behaves like a superposition of mean-field solitons. Thus, the one-particle entanglement has a large contribution arising from the classical order parameter and basic quantum mechanics[13]. In this section, we will introduce another indicator for the phase transition, that does not receive this kind of semiclassical contribution, before we develop an improved measure of quantumness in the next section.

The so-called ground state fidelity was conceived [ZP06] to detect quantum phase transitions. It indicates the overlap between ground states of the same system at slightly different couplings[14].

$$F_0(gN, gn + \delta) = |\langle 0_{gN} | 0_{gN+\delta} \rangle| \tag{2.40}$$

Around generic values of the coupling, the ground state changes adiabatically. The fidelity is therefore close to unity.

[13]The effect is not any more spectacular than the statement that the ground state wave function of any macroscopic object - in the absence of interactions and decoherence - is still an s-wave.

[14]The name “fidelity” is imported from the quantum information community, where state overlaps are used to quantify the distinguishability of states.

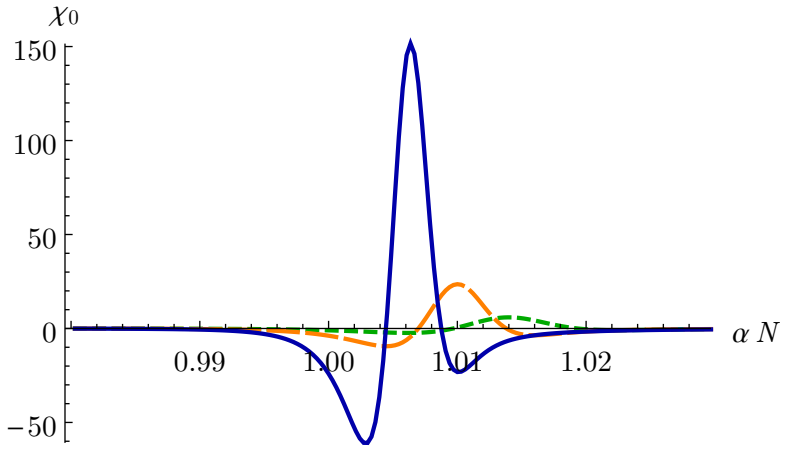

Figure 2.4: The ground state fidelity susceptibility as a function of the effective coupling αN; calculated numerically for $N = 3000$ (green, small dashes), $N = 10000$ (orange, long dashes) and $N = 5000$ (blue curve) with modes truncated to $l = -1, 0, 1$. A version of this plot was included in [FPW13].

At the quantum critical point of an infinitely large system, however, level crossing occurs. The ground state suddenly changes into a state of (infinitesimally) different energy eigenvalue - the two are orthogonal. The fidelity across a phase transition is therefore exactly zero. For a large but finite system, its levels still repel [15], but the reorganization of the ground state nevertheless diminishes the overlap around the would-be phase transition point. This kind of "orthogonality catastrophe" has been known for a long time in one form or another [And67], but provides a good generic characteristic for phase transitions.

The definition of the ground state fidelity suffers from an arbitrary choice of a small-but-finite parameter δ. An improved characteristic can be constructed from the second derivative of the ground state fidelity. This fidelity susceptibility [CGZ07] can be defined as

$$\chi_0(\alpha N) = \lim_{\delta \to 0} \frac{2 \log F_0(\alpha N, \alpha N + \delta)}{\delta^2} \tag{2.41}$$

where it was used that $F(\alpha N, \alpha N) = 1$ is a local maximum with respect to its second argument.

In [Yan07] it was later shown that, for a broad class of physical systems, first and second order quantum phase transitions (as well as transitions of

[15] Barring systems with different superselection sectors.

the Berezinksii-Kosterlitz-Thouless type) are associated with a divergence in the ground state fidelity susceptibility.

We have argued above that the ground state fidelity has a dip at the critical point. In figure 2.4, the expected shape for the fidelity susceptibility is clearly observed. Note that the fidelity susceptibility is nonzero only in a small region around the phase transition point. As the number of particles is increased in our simulation, the peak moves closer to $\alpha N = 1$. The peak also becomes sharper and is expected to behave like $\chi_0 \to \delta''(\alpha N - 1)$ in the limit.

As it signals a dramatic change in the structure of the ground state, the ground state fidelity (and its derivatives) are a useful tool to localize a phase transition. In the next section, we strive to create a measure of quantumness that is triggered by the quantum correlations at the transition.

2.6 Quantumness at the Critical Point

In this section, we will construct two measures of quantumness. One to demonstrate that quantum effects are really important at criticality, even at large particle number. And another one, suitable for numerical calculations, that is not dominated by the trivial form of quantum superposition inherent to the true s-wave ground state of any localized object of finite mass.

These original results were also published in [FPW13]. Section 2.6.4 represents an improvement upon the arguments contained in said work.

2.6.1 Fluctuation Entanglement

First, we would like to extract the entanglement of the fluctuations of the momentum modes on top of a classically observed c-valued "mean field" $\delta a_k = a_k - a_k^{\mathrm{mf}}$ with the rest of the system. One reason we are interested in the modes a_k of the physical particles as opposed to the Bogoliubov excitations (2.22) is that we imagine an external observer weakly coupled to the Bosonic system in the fundamental Lagrangian. In the simplest setup, they would couple linearly to the Bosonic field - i.e. the a_k operators.

We will also concentrate on the entanglement of a given momentum mode with the rest of the system - as opposed to, e.g., the one-particle entanglement. One reason for doing so is that we imagine the observer measuring macroscopically long wavelengths in order to characterize the system. The motivation for using momentum modes of the field is that for linear couplings to the environment, field values (and their Fourier components) represent

the environmentally selected pointer states and not localized single-particle states [AZ96].

As a working definition we will calculate the von Neumann entropy of the reduced density matrix $\delta\rho_k$ for the fluctuations of one mode k on top of a suitable mean-field coherent state $|\mathrm{mf}\rangle$

$$S_k = -\operatorname{Tr}[\delta\rho_k \log \delta\rho_k] \tag{2.42}$$

$$(\delta\rho_k)_{nm} \propto \frac{1}{\sqrt{m!\,n!}} \operatorname{Tr}\left[\rho\,(\delta a_k^\dagger)^m |\mathrm{mf}\rangle\langle\mathrm{mf}|(\delta a_k)^n\right] \tag{2.43}$$

with a suitable normalization and a mean-field state corresponding to the field value that would be observed classically.

The fluctuation entanglement may be regarded as a (different) form of quantum discord - a notion that we will introduce in the next section.

2.6.2 Bogoliubov Treatment

Above, we have defined the fluctuation entanglement as a suitable measure of quantumness. In the large N limit with fixed αN, we know that the Bogoliubov approximation becomes good. Let us, therefore, calculate the fluctuation entanglement expected in the limit.

A Bogoliubov state can be written as a displaced and multi-mode squeezed vacuum. It is a Gaussian state in the sense that its Wigner function [Wig32]

$$W(z, z^\star) \equiv \frac{1}{\pi^2} \int d^2\xi\ \exp(-i\xi z^\star - i\xi^\star z)\ \operatorname{Tr}[\rho\ \exp(i\xi a^\dagger + i\xi^\star a)] \tag{2.44}$$

is Gaussian, because squeezing and displacement preserve this property. Integrating out certain modes also preserves Gaussianity in the remaining modes. Hence, the density matrix $\delta\rho_k$ that we want to study is still Gaussian and can therefore be written in the most general Gaussian form

$$\delta\rho_k = C \exp\left[-\lambda\left(\delta a_k^\dagger \delta a_k - \frac{\tau^\star}{2}\,\delta a_k^\dagger \delta a_k^\dagger - \frac{\tau}{2}\,\delta a_k \delta a_k\right)\right] \tag{2.45}$$

where λ and τ are coefficients characterizing the state and C is the appropriate normalization. Formally, this density matrix may be diagonalized using yet another Bogoliubov transformation of $a_k, a_k^\dagger$. Note that this formal transformation is a priori not related to the physical Bogoliubov transformation in a homogeneous mean-field state involving $a_k, a_{-k}^\dagger$.

After diagonalizing the density matrix with this transformation, we can easily determine its normalization

$$C = 2\,e^{-\lambda/2} \sinh\left(\frac{\lambda}{2}\sqrt{1-|\tau|^2}\right) \tag{2.46}$$

Our final goal, the von Neumann entropy, directly follows

$$\begin{aligned} S_k &= \mathrm{Tr}[\delta\rho_k \log \delta\rho_k] = -\lambda\, C\, \frac{d(1/C)}{d\lambda} - \log C \\ &= \frac{\lambda}{2}\sqrt{1-|\tau|^2}\left[\coth\left(\frac{\lambda}{2}\sqrt{1-|\tau|^2}\right) - 1\right] - \log\left(1 - e^{-\lambda\sqrt{1-|\tau|^2}}\right) \end{aligned} \tag{2.47}$$

The parameters λ and τ still need to be determined. We can do so by comparing

$$\langle \delta a_k^\dagger \delta a_k \rangle \equiv \mathrm{Tr}[\delta\rho_k \delta a_k^\dagger \delta a_k] = \frac{1}{2\sqrt{1-|\tau|^2}} \coth\left(\frac{\lambda}{2}\sqrt{1-|\tau|^2}\right) - \frac{1}{2} \tag{2.48}$$

and

$$\langle \delta a_k \delta a_k \rangle \equiv \mathrm{Tr}[\delta\rho_k \delta a_k \delta a_k] = \frac{\tau^\star}{2\sqrt{1-|\tau|^2}} \coth\left(\frac{\lambda}{2}\sqrt{1-|\tau|^2}\right) \tag{2.49}$$

where the left hand side needs to be calculated explicitly in the desired Bogoliubov state.

In the weak coupling regime, the mean-field ground state is homogeneous and the Bogoliubov squeezing acts between $a_k, a_{-k}^\dagger$. The left hand sides of (2.48) and (2.49) are calculated by inserting (2.22):

$$\langle \delta a_k^\dagger \delta a_k \rangle = v_k^2, \quad \langle \delta a_k \delta a_k \rangle = 0 \tag{2.50}$$

which implies

$$\lambda = \log(u_k^2/v_k^2), \quad \tau = 0 \tag{2.51}$$

so that the fluctuation entanglement is

$$S_k = u_k^2 \log u_k^2 - v_k^2 \log v_k^2 \tag{2.52}$$

Using the explicit forms for the Bogoliubov coefficients (2.23), we see that the fluctuation entanglement for the first momentum mode diverges at the critical point. By expanding (2.52) for $\alpha N \to 1_-$, we can quantify the divergence

$$S_1 \sim \frac{1}{2}\log(1-\alpha N) \tag{2.53}$$

Note also that the entanglement in higher-k modes stays finite at the critical point, underscoring that it is an infrared effect, insensitive to the short distance structure of the theory.

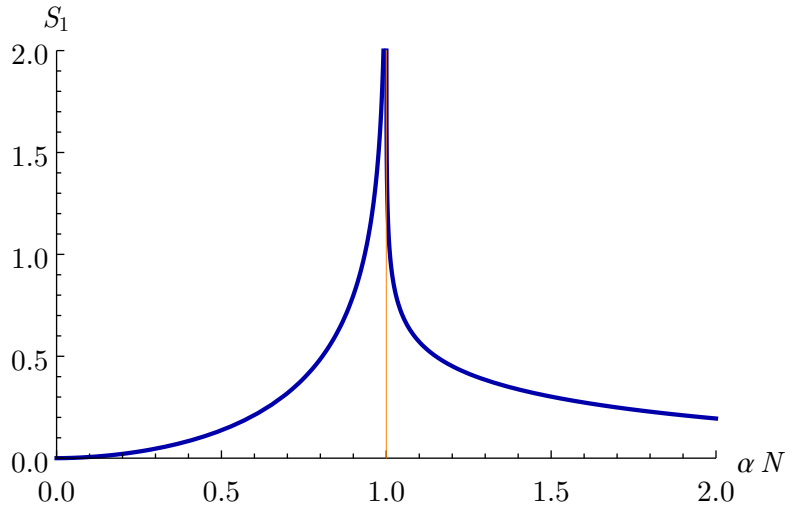

Figure 2.5: Fluctuation entanglement calculated in the Bogoliubov approximation. The orange line highlights the phase transition point. A version of this plot was included in [DF+13].

In the solitonic phase, the treatment is complicated by the fact that the Bogoliubov transformation mixes, not only modes of opposite momentum, but all momentum modes. The calculation of the left hand side of (2.48) and (2.49) now involves the Fourier components of all Bogoliubov de Gennes mode functions

$$\langle \delta a_m^\dagger \delta a_n \rangle = \sum_k \left(\int d\theta e^{im\theta} v_k(\theta) \right) \left(\int d\theta e^{-in\theta} v_k(\theta)^\star \right) \tag{2.54}$$

$$\langle \delta a_k \delta a_k \rangle = \sum_k \left(\int d\theta e^{-im\theta} u_k(\theta) \right) \left(\int d\theta e^{-in\theta} v_k(\theta)^\star \right) \tag{2.55}$$

Close to the phase transition, the first mode (2.29) gives the dominant contribution to these expressions and thus the fluctuation entanglement. We have not attempted to find an analytic expression for these Fourier components, but rather relied on numerical integration to evaluate them. The parameters λ and τ are then determined numerically in turn and the fluctuation entanglement can be evaluated. It, again, shows a divergence at the phase transition point. The numerical data is consistent with a logarithmic divergence. The coefficient of the logarithm is close to 0.25, i.e. different from the coefficient on the weak coupling side.

Our figure 2.5 visualizes the Bogoliubov results for the fluctuation entanglement with respect to the effective coupling αN. The divergence at the

critical point is clearly visible and very sharp.

A divergence of the entanglement entropy close to a quantum critical point has already been observed in spin-chains and other lattice models [VL+03; ON02]. In these cases, the entanglement was between nearest neighbor sites, i.e. on length scales comparable to the cutoff of the corresponding field theory. In contrast to these cases, the phase transition of the Bosons exhibits huge entanglement in modes of macroscopically large wavelength at the phase transition. To our knowledge, this is the first case with divergent long range entanglement. We will discuss the implications for the black hole portrait later.

2.6.3 Quantum Discord

Now, we will construct another measure of quantumness that, unlike the previous one, can meaningfully be evaluated for finite-N systems. It is not dominated by the trivial form of quantum superposition inherent to the true s-wave ground state of any localized object of finite mass. Instead, it isolates the truly quantum correlations that characterize the phase transition point.

We want to isolate the quantum part of correlations from just classical ones. This task has already been addressed in the quantum information literature. A measure called quantum discord was devised for bipartite systems in [OZ02] (see [HV01] for simultaneous and closely related developments). We need to introduce this measure, before we can explain our generalization for indistinguishable Bosons. The next few paragraphs follow the presentation of [OZ02].

For a classical ensemble of a bipartite system, the mutual information is a measure of correlations between the two subsystems A and B

$$J(A:B) = H(A) - H(A|B) \tag{2.56}$$

Where $H(A) = -\sum p_a \log p_a$ is the Shannon entropy for the probabilities p_a of subsystem A and $H(A|B) = \sum p_b H(A|B = b)$ the conditional entropy involving all possible measurement outcomes of subsystem B. There is a classically equivalent way to write the mutual information

$$I(A:B) = H(A) + H(B) - H(AB) \tag{2.57}$$

where $H(AB)$ is the entropy of the joint probability distribution, i.e. that of the total system.

We judiciously used a different letter, here because after adapting both quantities for quantum mechanical systems, they will not coincide any more.

In this adaptation, the Shannon entropy is naturally replaced by the von-Neumann entropy S. Only the conditional entropy $H(A|B)$ needs more thought. As it classically involves probabilities of A after a measurement on subsystem B, the proposed quantum generalization involves a set of orthogonal projection operators Π_b onto different measurement outcomes that sums up to unity. In order to make the quantity independent of the choice of measurements, we minimize over all possible choices

$$S(A|B) \equiv \min_{\{\Pi_b\}} \sum_b p_b \, S\left[\frac{\Pi_b \, \rho_{AB} \, \Pi_b}{\mathrm{Tr}(\Pi_b \, \rho_{AB} \, \Pi_b)}\right] \tag{2.58}$$

where naturally $p_b = \mathrm{Tr}(\Pi_b \, \rho_{AB})$. The quantum discord is then defined as

$$\delta(A:B) = I(A:B) - J(A:B) \tag{2.59}$$

$$= S(A|B) - S(AB) + S(B) \tag{2.60}$$

and still involves the minimization over all possible sets of measurements. This clearly is a measure of quantum correlations, as it involves two different correlation measures, but vanishes for classical ensembles. In [OZ02], it was also argued that the measurements minimizing the quantum discord should correspond to proper pointer states of the system.

If the system B was composed of a single particle, projectors onto orthogonal orbitals $\{\psi(x)\}$ would be used:

$$\Pi_i = a_\psi^\dagger \, a_\psi \tag{2.61}$$

where a_ψ is the annihilation operator corresponding to the orbital ψ. If, furthermore, the system A consisted of other distinguishable particles, entropies of its density matrix could be used.

2.6.4 Numerical Result

In the Lieb-Liniger model, the Bosons are not distinguishable however and no subset of particles forms a proper sub-system. Nevertheless, we will follow the same prescription as above to formulate a measure of quantumness that is closely inspired by the quantum discord. As it still has some intuitive physical merit, we will not worry too much about the non-factorization issue[16] For reasons of practical calculability, we restrict both A and B to a single Boson each. Thus, the entropy of A is implemented as that of the one-particle

[16] Of course, the formal proofs of properties of the quantum discord may not apply to our generalization.

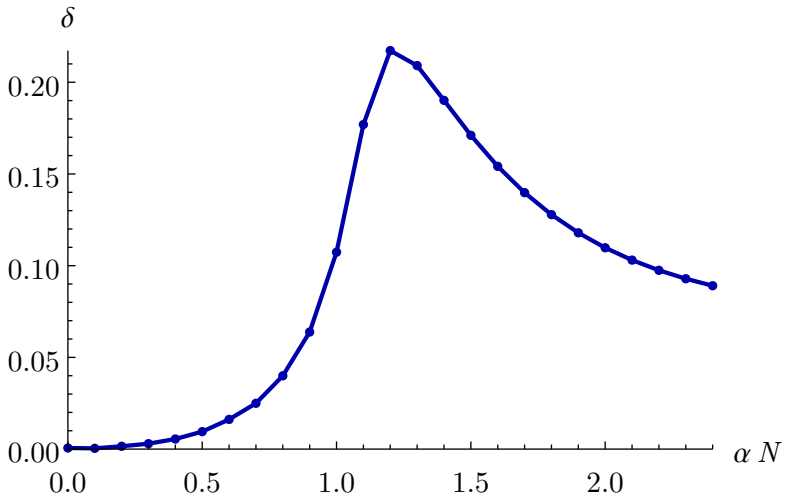

Figure 2.6: The two-Boson quantum discord as a function of the effective coupling αN; calculated numerically for $N = 40$, including the modes $|l| = 0, 1, 2$.

density matrix, the joint entropy is that of the two-particle density matrix and measurements on B are just single-particle (density) measurements (2.61) in different orbitals. Thus our two-Boson quantum discord is calculated as

$$\delta = S(1|1) - S(\rho_2) + S(\rho_1) \tag{2.62}$$

with

$$S(1|1) = \min_{\{\psi\}} \operatorname{Tr}(a_\psi^\dagger a_\psi \, \rho) \, S[\rho_1(a_\psi^\dagger a_\psi \, \rho \, a_\psi^\dagger a_\psi)] \tag{2.63}$$

and $\rho_1(\cdot)$ the normalized one-particle density matrix of its argument.

The physical appeal is that $S(1|1)$ is the expected one-particle entanglement after measuring the density in an optimal orbital. If the system is in a pure condensate state, with all particles occupying the same mode, the optimal measurement will use just this mode. For a pure condensate state, $S(\rho_1)$, $S(\rho_2)$ and also $S(1|1)$ thus vanish. If the system is in a superposition of condensate states (in orthogonal orbitals), the optimal one-particle projectors each just isolate one of the condensates out of the superposition and $S(1|1)$ therefore still vanishes. Only in more complex quantum states does $S(1|1)$ contribute.

For the Lieb-Liniger model in the strong coupling regime, with large but finite particle number, the superposition of solitons contains not just orthogonal modes. Nevertheless, the density measurement of $S(1|1)$ has the potential to pin down the position of the condensate, after which the one-particle en-

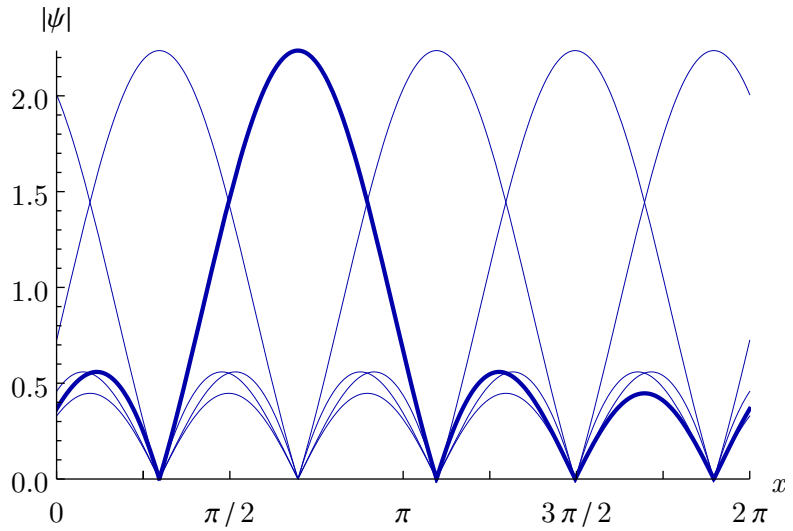

Figure 2.7: The optimal modes in the two-particle quantum discord at $\alpha N = 2.0$ calculated for $N = 40$, including the modes $|l| = 0, 1, 2$.

tropy should be considerably reduced compared with a state of genuinely strong quantum correlations.

For our explicit implementation, we exploited the fact that (2.63) can be calculated exactly from the three-particle density matrix. Thus, we first determined the three-particle density matrix of the ground state and performed the optimization of the basis $\{\psi(x)\}$ in this formulation.

Figure 2.6 shows the two-Boson quantum discord in the ground state for varying coupling. It is strongly peaked at the would-be phase transition point. The offset of the maximum away from $\alpha N = 1$ is consistent with that observed in the minimum of the excitation gap at this number of particles. The discord vanishes at weak coupling, where the state becomes a pure condensate. At strong coupling, the discord does not tend to zero, as the superposition of solitons is arguably still quantum - although dominated by classical correlations.

We calculated the discord for $N = 20, 30, 40$ (including momentum modes $l = 0, 1, 2$) and found it to be quite stable with changing particle number. The peak slightly narrows as more particles are included. The height of the peak does not change significantly. The divergence of the quantumness attested with the fluctuation entanglement in the Bogoliubov approximation cannot be seen with the limited resolution of one- and two-particle density matrices.

It is also quite insightful to look at the optimal measurement orbitals.

These (actually their absolute value) are displayed in figure 2.7 for two values of the effective coupling. At αN exceeding the phase transition, the best orthogonal orbitals contain strongly localized modes (keep in mind that the basis contains only $|l| \leq 2$ modes). This, on the one hand, nicely confirms our interpretation of the state as a superposition of solitons; on the other hand, it illustrates the point of Ollivier and Zurek that the projectors select the classically stable pointer states.

2.7 Quantumness of Black Holes

Above, we have studied the Lieb-Liniger model close to its critical point $\alpha N = 1$. While this toy model is, of course, much simpler to treat than the graviton condensate that we envision to constitute a black hole, we should, nevertheless, extract some tentative lessons.

To understand how the graviton condensate black hole would differ from the standard picture outside the horizon, we may reason in terms of k-particle density matrices, or equivalently, equal time correlators. So we can attribute a gravitational mean field that probably coincides with the Schwarzschild prediction up to backreaction effects, which may be small. The main difference lies in the existence of nontrivial more-particle density matrices, or equivalently, higher-point equal-time correlations. These are prominent around the phase transition in the toy model and we expect them to play an important role in black hole physics as well. In principle, such correlations have the power to imprint information in outgoing Hawking radiation, and we would expect them to do so.

An obvious question then is, whether such correlations could be observable for astrophysical black holes. Sadly, we are not in a position to answer this important question, but we can at least dissect it a little. There are two issues that play a role. One is, how strong the correlations actually are, another, how far outside the would-be horizon the correlations manifest themselves. The former part of the question may be amenable to a semiclassical treatment. Under the assumption that the correlations are just about strong enough to release the minimal required amount of information in Hawking radiation, one might be able to set a bound on the strength of correlations. The latter part of the question is much harder to answer. The philosophy of the graviton condensate model, that the relevant physics plays out in long wavelength modes, suggests that the effect decays only on length scales comparable to the Schwarzschild radius. Redshift effects are, however, not taken into account in this consideration.

Given that there should be nontrivial quantum correlations of the metric around a black hole, according to the graviton condensate picture, we should also pose the question in which way these may be observed. An obvious idea is to use interference of coherent light traveling past the black hole in close proximity. The effect on the expected interference pattern then depends on the nature of the correlations. Here it is worthwhile to remind the reader that the unstable circular orbit of light around a Schwarzschild black hole has a radius of $r = 1.5R_S$. This is also the minimum distance at which one can shine light (of distant stars) past a black hole. So this feature of the Schwarzschild metric severely limits the observability of the conjectured correlations. Using a coherent light source spiraling into the black hole would present a way around this limitation. It is worth investigating the observational prospect further, because planned telescopes are apparently approaching the required resolution [FD+11]. See also [Gid14] for a recent discussion of other observational consequences of (nonlocal) modifications of black hole physics.

We should also point out that the ring-down after a black hole merger, as recently observed in gravitational waves [AA+16c; AA+16b], represents an extreme form of radiation emitted close to the horizon. It would be very helpful to figure out, whether the effects of the graviton condensate picture measurably change the endpoint of the expected black hole merger waveform (see [Gid16] for an immediate first attempt in this spirit, motivated, however, by different models).

We must also briefly address the recent controversy about "firewalls". From an interesting thought experiment, Almheiri et al. concluded, that information release in Hawking radiation and a perfect mean field outside the black hole horizon force the horizon itself to be full of extremely short wavelength excitations in the eyes of an infalling observer [AM+13]. Although the claim has been vigorously debated (see, e.g., [MS13; Bou13; VV13]), the thought experiment seems to teach some lessons for the semiclassical black hole picture. The graviton condensate picture, in contrast, already violates one of the basic assumptions of the firewall argument - an infalling observer cannot simply diagnose empty space as the equivalence principle for the mean-field background would suggest. By performing appropriate measurements (even of higher equal-time-correlators in one point), the observer would conclude that the state he observes is not just the perturbative vacuum. Thus we believe that firewalls need not occur in the graviton condensate model, because the quantum structure of black hole states is already modified outside the horizon.

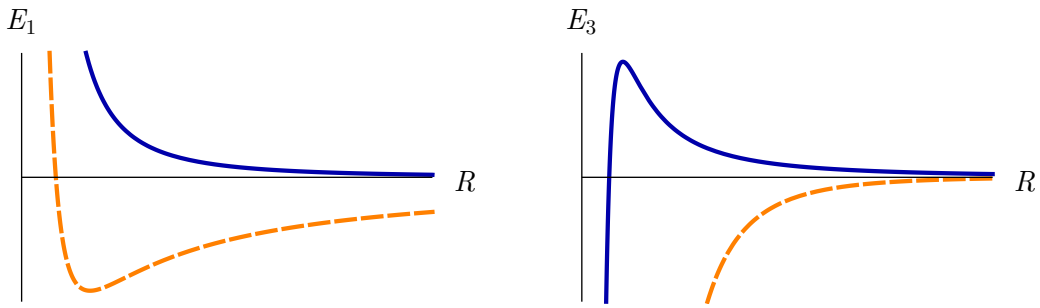

Figure 2.8: Schematic behavior of the mean-field energy with respect to the characteristic size of the condensate for one dimensional (left) and three-dimensional (right) condensates. The two curves show the subcritical (blue, solid curve) and supercritical (orange, dashed) regimes. A similar illustration has appeared in our publication [DF+13].

2.8 Higher-Dimensional Condensates

So far, we have been discussing Bose-Einstein condensates of attractive particles in only one spatial dimension. While this toy model with its phase transition has revealed a number of interesting features that may be relevant for a proper description of black holes, it is still worthwhile to widen the scope and consider condensates in more than one spatial dimension. In this section, we will briefly highlight some of the more interesting properties of such condensates. These will motivate us to study the physics of unstable systems and, in particular, condensates in the following sections.

2.8.1 Instability to Collapse

To get an idea about the qualitative behavior of Bose Einstein condensates with attractive contact interaction in higher dimensions, let us consider the scaling of the energy of a condensate of size R in an arbitrary number d of spatial dimensions,

$$E_d \sim \frac{N}{R^2} - \alpha N \frac{N}{R^d} \tag{2.64}$$

where the first term represents the kinetic energy and the second the mean-field attraction in spirit of the discussion of section 2.3.1. While the coefficients of order one (suppressed here) in both terms depend on the shape of the condensate, the qualitative behavior is reproduced correctly. In figure 2.8 we display this energy functional in $d = 1$ and 3 and for both, a small and a large value of the effective coupling αN. As we know very well by now, there is a stable mean-field ground state for the condensate in $d = 1$ at all values of

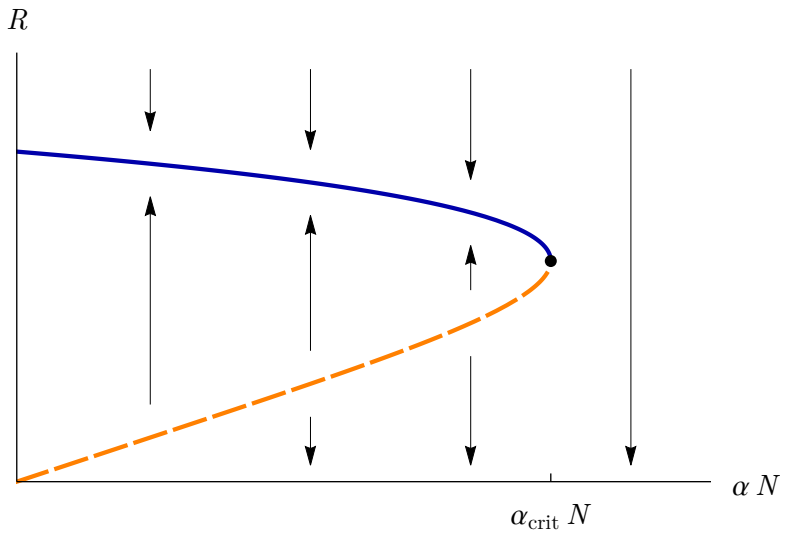

Figure 2.9: Stable (blue, solid curve) and unstable (orange, dashed) solutions of the three-dimensional Gross-Pitaevski equations. We show the characteristic size of the condensate over the effective coupling αN. The solution is obtained as a Gaussian ansatz in a harmonic trapping potential as in [PM+97]. The arrows indicate the stability properties around the bifurcation point.

the coupling. The curves of the energy functional also indicate the existence of the phase transition. At low αN, the ground state expands as much as the compactification allows, while at large αN, there is a preferred size. In $d \geq 3$, the physics is very different. While there is a (meta-) stable mean-field state for small effective coupling, that tends to maximize its size, condensates with tiny radius are already unstable towards shrinking further. When the effective coupling exceeds $O(1)$, the situation worsens and the stable solution ceases to exist. This situation is concisely represented in figure 2.9, which shows the actual stable solution for a condensate in a harmonic trap in three dimensions (with a Gaussian ansatz of its shape) as in [PM+97]. The arrows indicate the stability properties. At the critical point, the stable and unstable solutions disappear in a saddle node bifurcation.

The marginal case of $d = 2$ cannot be decided on simple dimensional grounds. It turns out, however, that it is unstable in a similar way to the three dimensional case.

This instability of the nonlinear Schrödinger equation has been studied in great detail mathematically (see [SS07] for an extensive treatment) and displays an intriguing structure involving self similarity of the limiting collapse solution. For our purposes, however, the collapse is accompanied by a

second phenomenon that prevents the energy from being redistributed into very short wave length modes as we will discuss below.

Nevertheless, the fact that higher dimensional Bosonic condensates are unstable after the would-be critical point, is a key insight that informs our subsequent ideas.

2.8.2 Explosion of the Condensate

Above, we have seen that supercritical condensates in $d \geq 2$ are unstable and prone to collapse. In experiments involving ultra-cold atoms, however, the observed behavior is qualitatively different [SG+99; CC+00]. The collapsing condensate emits particles at an unexpectedly high rate, a phenomenon dubbed "explosion" of the condensate. This effect has been explained theoretically [DS01] within the effective theory of point-like interactions, so the cutoff scale (atomic radius of the Bosons) does not seem to come into play.

The ejection of Bosons from the condensate is mainly mediated by two-body scattering processes during which two condensate particles interact, ejecting one of them while the other is absorbed by the condensate again (three body decay). This process is obviously forbidden by momentum conservation for homogeneous condensates, but produces sizable particle losses for trapped condensates. Another process that contributes even in the homogeneous case has two condensed particles scattering and both leaving the condensate (two body decay). As the question for particle losses is properly phrased as one for the non-equilibrium time evolution of given initial conditions, the Schwinger-Keldysh formalism is the right tool to answer it. The total amplitude for the two processes may then be calculated from self energy diagrams using the optical theorem. Detailed derivations may be found in [Sto99].

This account for the explosion of an attractive Bose condensate is strongly reminiscent of the processes that are thought to be responsible for Hawking evaporation in the graviton condensate picture (see section 2.3.2).

In [FW15], Foit and Wintergerst tried to push the analogy with Hawking radiation even further. Their aim was to make the attractive Bose condensate more akin to actual gravity by introducing a relativistic dispersion relation $H_{\text{kin}} \sim |\vec{k}| a_k^\dagger a_k$ for the Bosons. Under favorable assumptions about the dominant contribution to incoherent scattering, they were able to reproduce many of the evaporation properties expected from actual black holes.

In the present work, we do not want to take Bosonic toy models quite as literally. Instead, we will use the key insight that higher dimensional condensates are unstable, to develop a novel idea how the mysterious fast scrambling time might arise.

2.9 Ehrenfest Time for Unstable Systems

In the previous section we have seen that higher dimensional attractive condensates are unstable in the supercritical regime. This motivates us to consider more closely the quantum mechanical properties of systems that feature a classical instability. As is well known in the study of quantum chaos, such systems generically deviate from their classically expected time evolution after a relatively short "quantum break time". In the next section, we will then continue to apply this insight to black holes.

Already in the early days of quantum mechanics, a natural question to ask was, how long a system with given initial conditions could be described classically (quantum break time). In recognition of Ehrenfest's contribution [Ehr27] to this problem, the timescale in question is also called Ehrenfest time. The characteristic duration after which quantum effects become important usually scales like some power of the typical action S in units of $\hbar$. It was only realized much later that the quantum break time is significantly shorter in systems at a dynamical instability [BZ78] or in chaotic dynamics. There, it generically scales like

$$t \sim \lambda^{-1} \log(S/\hbar) \tag{2.65}$$

where λ is the dominant (local) Lyapunov exponent of the instability.

2.9.1 Derivation of Ehrenfest Time

The reason for the quick deviation between the classical and quantum time evolution at an instability is especially transparent in a phase space picture. The derivation presented here is similar to the argument in [Zur03].

A classical ensemble may be represented by a probability density on phase space $\rho(t, q, p)$. Its dynamics is, of course, implemented by the Poisson bracket $\{\cdot, \cdot\}_{\mathrm{PB}}$

$$\partial_t \rho = \{H, \rho\}_{\mathrm{PB}} \tag{2.66}$$

with the classical Hamiltonian H.

A quantum state may be represented by a distribution function on phase space as well. In section 2.6.2, we already briefly used the Wigner function (2.44) and will apply it again, here. It shares a critical property with a classical probability density - expectation values may be calculated as

$$\mathrm{Tr}(\rho A) = \int d^2 z \, W(z, z^\star) \, A^{\mathrm{W}}(z, z^\star) \tag{2.67}$$

where the function A^{W} is obtained by bringing the operator A into Weyl order and then replacing creation and annihilation operators with $z^\star, z$. Unlike a

classical density distribution, however, the Wigner function is not strictly positive, and can therefore not be given a naive probabilistic interpretation.

The time evolution of the Wigner function is implemented by the following differential equation (see, e.g., the comprehensive review [Lee95] and original references therein).

$$\partial_t W = \frac{2}{\hbar}\sinh\left[\frac{1}{2}\left(\frac{\partial}{\partial z_1^\star}\frac{\partial}{\partial z_2} - \frac{\partial}{\partial z_1}\frac{\partial}{\partial z_2^\star}\right)\right]\times H^{\mathrm{W}}(z_1, z_1^\star)\, W(z_2, z_2^\star)\Big|_{\substack{z_1=z_2=z\\ z_1^\star=z_2^\star=z^\star}} \tag{2.68}$$

where H^{W} is the Hamilton function obtained by Weyl-ordering the Hamiltonian and then replacing operators by c-numbers.

As the complex phase space coordinates contain a power of $z \propto \hbar^{-1/2}$, the leading order in $\hbar$ of the above equation is just the classical Hamiltonian flow (2.66). The important point, however, is that higher orders in $\hbar$, i.e. quantum corrections, are suppressed by additional derivatives of the density measured in characteristic scales of the problem.

To see the implications of this fact, let us start with a quantum state localized in phase space at an instability, but with small derivatives of its Wigner function, so that quantum effects are initially weak. The instability will exponentially stretch the density distribution in the direction of the largest Lyapunov exponent λ. By the Liouville theorem, however, the leading order Hamiltonian flow is volume preserving. So while being stretched in one direction, the density distribution must be exponentially compressed in some other direction with an expected Lyapunov of $-\lambda$, so that its width evolves as

$$\Delta(t) \sim \Delta_0\, e^{-\lambda t} \tag{2.69}$$

As soon as the state is compressed to the characteristic scale of (2.68), quantum effects become equally important to the classical flow. This width is reached after the logarithmic timescale (2.65) which, indeed, is the quantum break time for this system.

2.9.2 Illustrative Example

Above, we have invoked the compression of the phase space distribution to argue for the logarithmic quantum break time near an instability. Let us illustrate the argument in a minimal setup[17] - quantum mechanics of a

[17] This kind of exercise is certainly not new.

particle of mass m in one dimension near the top of a symmetry breaking potential

$$V(x) = -\alpha x^2 + \beta x^4 \tag{2.70}$$

At this point of phase space, there is a (local) dynamical instability with Lyapunov exponent $\lambda = \sqrt{2\alpha/m}$.

Figure 2.10 shows the evolution of a minimum uncertainty wave packet starting at $x = p = 0$. The images in the top row show density plots of the Wigner function at several points in time [18]. The bottom row shows the corresponding evolution of a classical density distribution. The Wigner function is stretched similar to the classical probability density. As soon as it becomes narrow, however, the $\hbar$ corrections change the evolution. Most notably, the Wigner function develops negative values (highlighted in orange) in some patches of phase space - a direct indication of nonclassical behavior.

2.9.3 Chaos and Thermalization

So far, we have only discussed the effect of an instability that is localized in phase space. If the classical version of the dynamical system also exhibits chaotic behavior, the conclusions are more far reaching.

If generic classical paths experience an instability throughout their evolution, then outcomes are very sensitive to initial conditions. If the dynamics, furthermore, mixes trajectories in phase space, the system is said to be chaotic [Gut91].

The quantum mechanical versions of such systems also exhibit characteristic phenomena regarding, e.g., their statistics of level spacings [Ber87] and assisted tunneling [LB90]. Another feature that has only recently been uncovered are fast thermalization timescales [AH12b; AH12a]. Quantum chaotic systems may effectively thermalize on timescales of the order of the Ehrenfest time. The argument is an extension of the reasoning presented above. In a chaotic system, the quantum mechanical phase space distribution is not only stretched, which leads to a form of diffusion in the transverse direction, it is also mixed in phase space. The spreading happens in a time scale that goes like the Ehrenfest time. The diffusion then ensures that the state becomes effectively featureless, i.e. thermal (although it remains pure).

While our model system is integrable and does certainly not exhibit chaos, the potential for fast thermalization should be kept in mind for our discussion of possible graviton condensate behavior.

[18] These images were obtained by numerically evolving the wave function according to the Schrödinger equation and using (2.66) to obtain the values of the Wigner function.

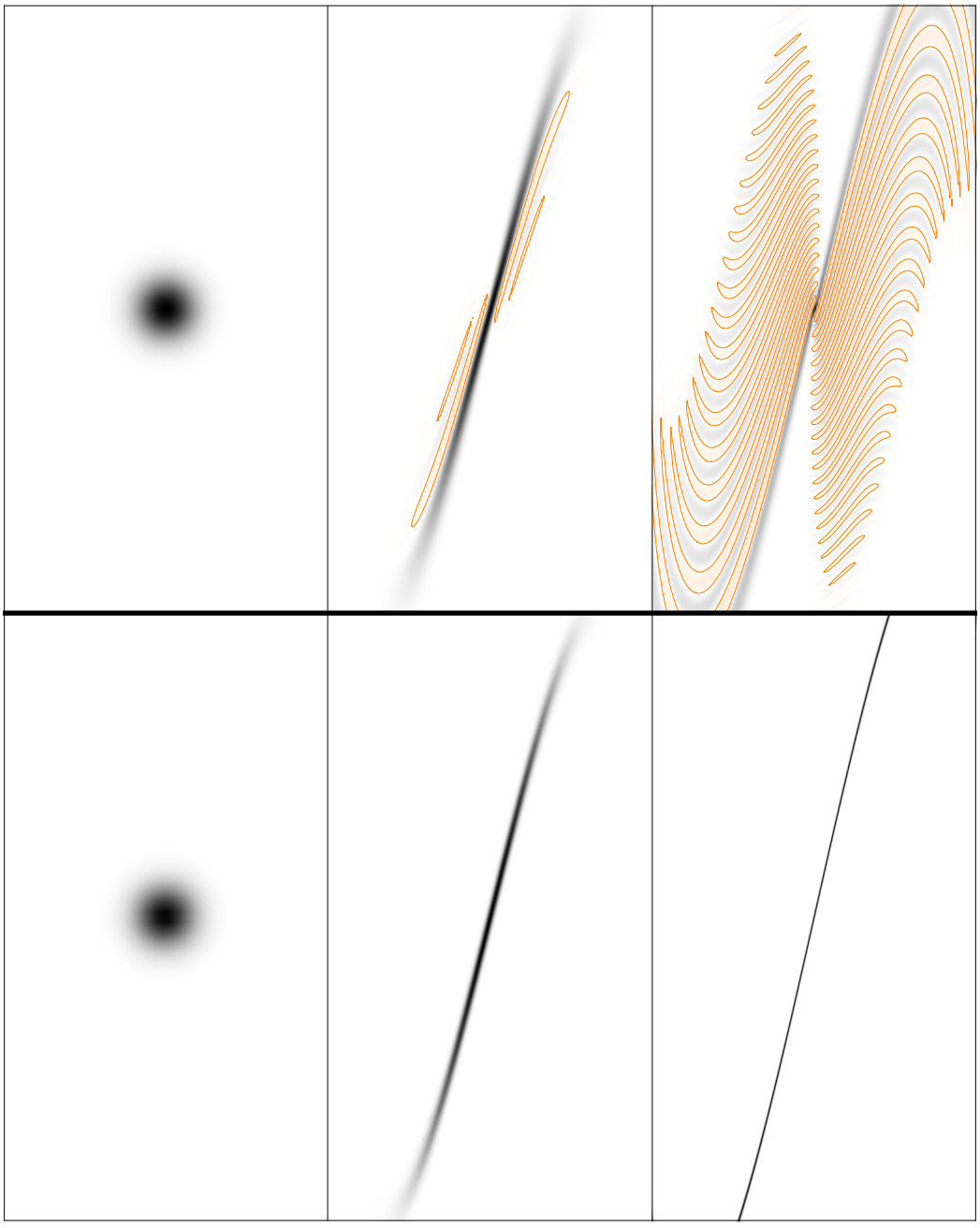

Figure 2.10: Wigner quasi density distribution (top row) and classical density (bottom row) as they evolve for a state centered at an instability. The horizontal axis represents the phase space coordinate x and the vertical axis p. Positive values of the densities are shaded in grey, negativ values in orange. The contour lines highlight regions with negative value of the Wigner function.

2.10 Scrambling in Condensate Black Holes

Above, we have surveyed several important aspects, that we will assemble in this section to give a potential explanation for fast scrambling in the black hole N-portrait. We have published these ideas and the simulations of the subsequent section in [DF+13].

In section 2.8.1, we have explained that higher dimensional attractive Bose condensates are unstable towards collapse. Of course, we do not know reliably, how a condensate of gravitons would behave - their interactions are, of course, much more intricate than those of heavy, nonrelativistic scalars. It is, however, suggestive that graviton condensate black holes would exhibit a similar dynamical instability. The only characteristic length scale of a black hole that survives in the classical limit is the Schwarzschild radius. Therefore, the Lyapunov exponent of a classical dynamical instability of the graviton condensate would also be $\lambda \sim R_{\rm S}^{-1}$.

Above, we have also shown that systems at a dynamical instability exhibit a relatively short quantum break time that scales with the logarithm of $\hbar$. Applying this insight to the putative instability of the graviton condensates leads us to conjecture that their quantum break time would scale like

$$t_{\rm qb} \sim R_{\rm S} \log(S/\hbar) \tag{2.71}$$

according to (2.65). Here S is the typical action of a black hole, which scales like N - just as the black hole entropy does.

We instantly recognize the time scale as that of fast scrambling. Therefore we putatively claim that quantum breaking due to the instability of the graviton condensate is at the origin of fast scrambling in black holes.

Above, we have always been careful to differentiate quantum breaking from thermalization. In the conventional wisdom, black hole scrambling is really an expression of complete thermalization, although it is doubtful whether the thought experiments invoked so far are actually sensitive towards high order correlators.

It is therefore worth pointing out that, if the presumed instability persists during the evolution of the black hole condensate, according to section 2.9.3, the condensate would also be expected to thermalize in a timescale proportional to $t_{\rm qb}$ - in agreement with most assumptions about scrambling.

2.11 Quantum Breaking of the Toy Model

In the previous section, we have put forward a proposal for the origin of fast scrambling in graviton condensate black holes. Sadly, we are not yet in a position to check all the assumptions made on the way. It is, therefore, all the more important to test at least those parts of the overall picture, that are accessible with standard techniques. Below, we will revisit the one dimensional condensate toy model and numerically analyze its behavior at an instability[19]. At the least, this will prove that some Bosonic condensates at an instability do actually exhibit crucial elements of the qualitative behavior described previously.

We have also reported on the results of these simulations in [DF+13].

2.11.1 Quench across the Critical Point

In contrast to higher dimensional condensates, there is a stable mean-field solution for all values of the effective coupling in the Lieb-Liniger model. In order to study the behavior of this condensate in an unstable regime, we have to prepare the instability willfully. The steps, however, are well motivated by a comparison to higher dimensional condensates. For a real three dimensional Bose gas, we might probe the instability by assembling a condensate in a trap at weak coupling and then tuning the coupling past criticality. Thanks to Feshbach resonance techniques, this is exactly how some experiments actually look at the instability of the condensate [CC+00]. We can perform the same steps on a one dimensional condensate and also arrive at an instability. Starting in a homogeneous ground state of N Bosons, we will instantly dial the coupling α to the strong coupling regime and then observe the evolution of the state.

The procedure just outlined is also known as a quench and the study of quantum systems quenched across a critical point is a fruitful direction, even for its own sake [SPS04]. Note that there is no choice of bringing the system to the strong coupling side adiabatically in the large-N limit. As the excitations become light at the critical point, the corresponding characteristic time scale diverges (critical slowing down) and no change of the coupling can be regarded as adiabatic.

To elucidate, why quenching the homogeneous condensate to the strong coupling side results in unstable behavior, remember the discussion about

[19] Of course, it would be desirable to directly study a higher dimensional condensate. The requisite computational effort, however, would be disproportionately high.

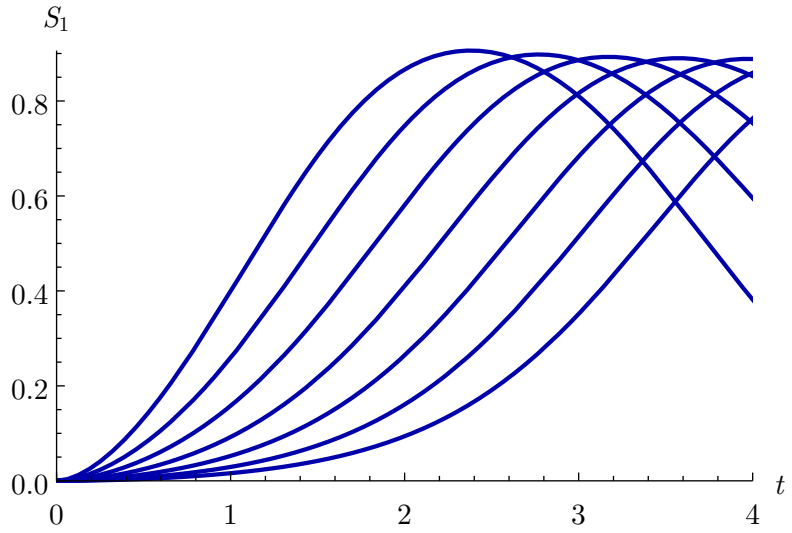

Figure 2.11: Evolution of one-particle entanglement after a quantum quench $\alpha N = 0 \to 1.8$ for different numbers of particles $N = 16, 32, 64, 128, 256, 512, 1024$ (from left to right). A version of this plot was included in [DF+13].

the Bogoliubov approximation. We already know the energy of fluctuation modes around the homogeneous condensate (2.24), which we repeat here for convenience:

$$\epsilon_k = \sqrt{k^2(k^2 - \alpha N)} \tag{2.72}$$

The $k = 1$ fluctuation receives an imaginary energy in the solitonic regime $\alpha N > 1$. It is therefore an exponentially growing mode and will invariably lead away from the pure condensate. The expected Lyapunov exponent is just

$$\lambda = \sqrt{\alpha N - 1} \tag{2.73}$$

An in-depth analysis in this direction can be found in [CD96]. We will rather study the resulting time evolution numerically, below.

2.11.2 Numerical Results

In order to diagnose scrambling, we would split the system into two initially unentangled parts and track their entanglement during time evolution. For a Bose condensate of N particles, k-particle subsets are a natural candidate to consider in this prescription. Of course, due to Bose-symmetry, any k-particle subsystem does not form a subspace within the physical Hilbert

space, but k-particle sub-density matrices nevertheless provide a convenient tool to parametrize entanglement with the rest of the system.

$$\rho^{(k)}_{\{m\}\{n\}} = C \operatorname{Tr}\left[\rho \left(\prod_l (a_l^\dagger)^{m_l}\right)\left(\prod_l a_l^{m_l}\right)\right] \tag{2.74}$$

Here $\{m_l\}$ and $\{n_l\}$ are integer partitions of k and label the occupation numbers of l-orbitals in the k-particle basis of the reduced density matrix. The normalization C is determined by the condition $\operatorname{Tr}\rho^{(k)} = 1$.

A Bose gas would be a fast scrambler, if its time evolution would generate large entropy in all sub-density matrices $\rho^{(k)}$ for $k \ll N$ in a timescale that scales like $\log N$.

We do not expect our toy model to be a fast scrambler, however. Already the intuition that it will evolve "towards" the stable mean-field ground state tells us that the required instability cannot persist and the system will stop to generate entanglement efficiently. Still, we can use the one-particle density matrix to detect quantum breaking. As discussed already (section 2.5.2), any mean-field state has zero entropy in the one particle density matrix and its entropy thus measures deviations from classicality.

The numerical calculations will, again, be carried out using exact diagonalization as described in section 2.4.4. The homogeneous initial state is projected onto the spectrum of energy eigenstates. Time evolution is trivial on each of these. The one-particle entanglement can then be calculated for any instant in time.

In figure 2.11, we display the evolution of the von Neumann entropy of the one particle density matrix after a quench. Here the quench takes a perfect homogeneous condensate, the ground state for $g = 0$, to $gN = 1.8$. This is already significantly past the phase transition to make the Lyapunov exponent (2.72) sizable for the one dimensional condensate. Different curves exhibit the entanglement evolution for different numbers of particles N. We see that the entanglement rises steeply and comes close to saturating the maximal possible value $S_{\max} = \log 3 \approx 1.10$ in the restricted basis $l = -1, 0, 1$. The subsequent time evolution shows incoherent oscillations, which we do not consider very interesting for our purposes, as non-integrable systems might behave differently.

It is more insightful to analyze the behavior of the quantum break time with respect to N. In figure 2.12 we evaluated the quantum break times for different particle numbers. The break time is implemented as the time at which the one-particle entanglement reaches its first maximum. Similar results are obtained by measuring the time to exceed a given threshold. The

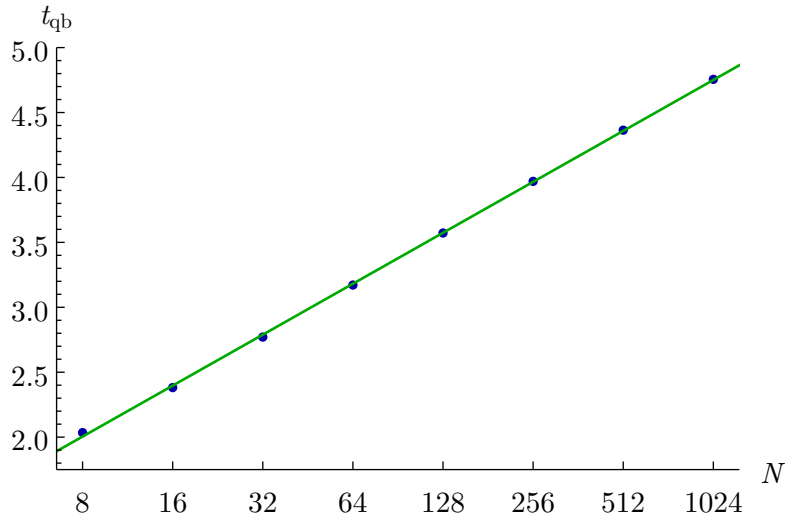

Figure 2.12: Quantum break time for the condensate as a function of particle number. The horizontal axis is logarithmic in the particle number. The green line represents a linear fit in this logarithmic-linear space. A similar plot was included in [DF+13].

solid line represents the best fit of the form $a \log(b\, N)$. The excellent agreement between the numerical experiments and the $\log N$ relation is a great confirmation for the logarithmic in N quantum break time that we have argued for. The observed prefactor $a \approx 0.57$ is not very close to the Bogoliubov prediction (here $\lambda = 0.89$), but at least in the same ballpark. It is not too worrisome, though, because it represents the averaged Lyapunov exponent during the time until the maximum is reached and not just the local value.

A look at the density of states (figure 2.13) offers a complementary perspective on the fast quantum break time at the instability. In the figure, one can locate the condensate in the line extrapolating the weak coupling ground state. It is apparent that the density of states is relatively high around this line on the strong coupling side. In fact, we have checked that the density scales logarithmically with N

$$\frac{\Delta n}{\Delta E} \sim \lambda \log N \tag{2.75}$$

We have also checked that the condensate has large overlap only with the states in this band. Thus, we again see the quantum break time arise, now from the dephasing of different energy eigenstates.

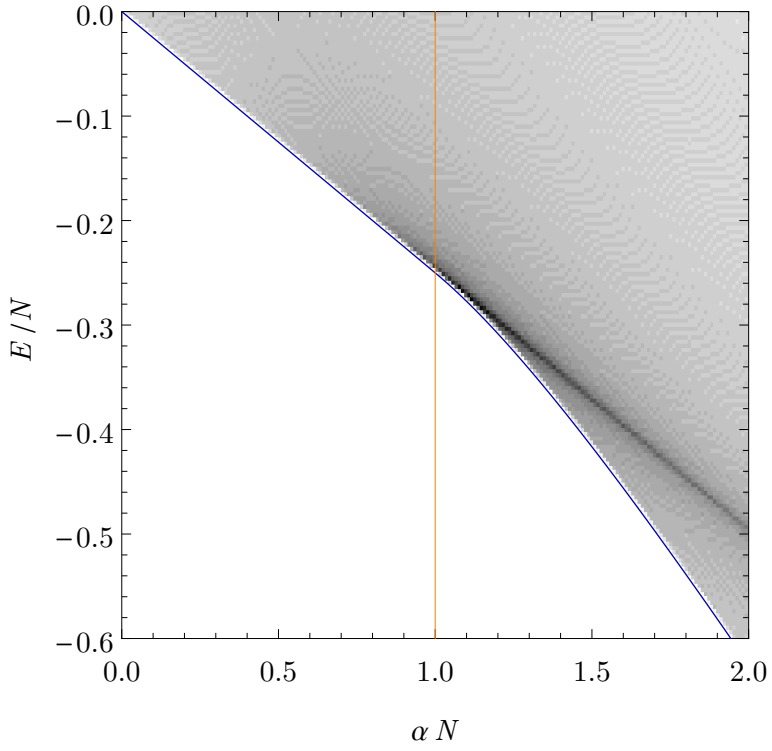

Figure 2.13: Density of states in the total momentum zero sector as a function of the effective coupling αN and energy per particle E/N. Darker is higher density. The orange line highlights the phase transition point, the blue line represents the ground state energy. A similar plot was included in [DF+13].

These numerical results for the one-dimensional condensate underscore, that Bose condensates with an instability naturally produce the $\lambda^{-1} \log N$ timescale that matches the scrambling time of black holes. As we have discussed before, such an instability is automatically present for higher dimensional condensates slightly past the critical point. And if Hawking evaporation happens at the appropriate rate, the black hole graviton condensate may be stuck at the instability during its whole evolution. In this way, the numerical results support our picture of scrambling in the black hole condensate portrait.

2.12 Outlook

This chapter was concerned with the graviton condensate portrait for black holes. Following a suggestion by Dvali and Gomez, we used the Lieb-Liniger

system as a toy model and studied its phase transition. At the quantum critical point, the first Bogoliubov mode becomes light, increasing the density of states. The number of nearly degenerate states is not excessive, however, because the minimal mass gap scales like $N^{-1/3}$, a far cry from the exponential degeneracy of black holes. It is still one of the important unsolved questions of the graviton condensate picture to plausibly explain the black hole entropy. Simply replacing the Lieb-Liniger coupling α with a momentum dependent term proportional to k^2 looks somewhat plausible with the graviton interaction in mind and would hint at many more Bogoliubov modes becoming light in (2.24). Whether the resulting model is viable, however, is a completely separate question. A momentum dependent coupling was already introduced in [BM+13] and analyzed more closely with the black hole entropy in mind in [DF+15]. More investigations regarding the entropy are, however, clearly mandated, especially as BMS transformations at the horizon [HPS16] have also been considered to provide the required states in the graviton condensate model [AD+16].

We have, moreover, found clear additional signs of the phase transition in the form of a sudden increase in the one particle entanglement and a dip in the ground state fidelity even at relatively low particle number.

We, then, focused our attention on quantumness at the critical point. We have seen that, on top of the fixed mean-field background (which corresponds to the large particle number limit), the momentum modes of fluctuations are most entangled at the critical point. Actually, we have seen that this fluctuation entanglement diverges. We can therefore claim that quantumness really is an important phenomenon at the phase transition point. It is also noteworthy that the entanglement resides in the first momentum mode only, i.e., that it is a long wavelength or infrared phenomenon. The latter observation is important for our black hole picture, where a central claim is that black hole physics is governed by Einstein-effective-theory and not the choice of UV-completion.

At finite particle number, the divergence in the fluctuation entanglement is not a great quantity to consider, because the true ground state always has zero momentum and therefore represents a quantum superposition of solitons (at large coupling). The entanglement due to this superposition drowns out the relevant effect. Instead, at finite particle number, we have studied the quantum discord for two Bosons in the condensate. It has become clear that, at large coupling, an initial measurement localizes the soliton and the correlations are then actually classical. At the critical point, in contrast, the initial measurement has little power to pin down the state - the correlations are relatively strong and purely quantum. Because of the specific way, we constructed this measure, it stays finite at the critical point,

unlike the fluctuation entanglement. Still, it clearly points to the fact that there exist important long range correlations in the system at criticality.

It is now an obvious challenge to experimentalists to make appropriate measurements on ultracold atomic condensates to observe the predicted quantum correlations at criticality. Entanglement, however, seems to be difficult to quantify in the way experiments are currently conducted.

In section 2.7, we have already addressed the observational challenges posed by the graviton condensate portrait to astronomical observations of real-life black holes.

In the second half of this chapter, we have attacked the question of fast scrambling in the black hole portrait. Using insights from atomic condensates and from quantum chaos, we have presented a plausible mechanism in which higher dimensional condensates slightly past criticality naturally exhibit quantum breaking during the logarithmic timescale of the fast scrambling time. We have underpinned this using simulations in the one-dimensional Lieb-Liniger model in analogous conditions. We have then argued that graviton condensate black holes, that are supposed to be stuck at criticality during their evaporation and shrinking, should exhibit full-blown fast scrambling.

We have previously pointed out a parallel between the graviton condensate portrait and the BFFS matrix model of black holes. We can now apply the new insights to matrix models. While matrix models of black holes were already used as evidence for fast scrambling in by Sekino and Susskind [SS08], we can now reinterpret their scrambling behavior in terms of instability and chaos. Very recently, the Lyapunov exponent (actually the whole Lyapunov spectrum) of the classical matrix model has been determined in numerical simulations [GHS16] (see [ABT11] for closely related earlier studies). While "classical scrambling" as the complete de-localization of a perturbation was observed and attested in this work, we would like to emphasize the fact that the observed classical instability directly implies quantum breaking and most likely thermalization as well.

It is quite remarkable, that chaos as an important ingredient in black hole physics has recently enjoyed much attention from an independent line of research. It emanated from studies of the time evolution of the Ryu-Takayanagi entropy in a black hole spacetime with infalling perturbations [SS14]. With the potential of holographic computations, more investigations into the relationship between black holes and chaos followed, see, e.g., [MSS15; Pol15]. We would like to take this as independent indications that chaotic behavior plays a decisive role in the evolution of a black hole as a dynamical system.

Chapter 3

Bethe Ansatz at Large-N

3.1 Motivation

In the previous chapter, we have treated the Lieb-Liniger model as a toy model for black hole behavior. So far, we have neglected one important property of this system, its integrability. That is, the spectrum and energy eigenstates can be obtained exactly from the roots of a set of transcendental equations, the Bethe equations [LL63], - as opposed to solving the differential Schrödinger equation[1]. Integrability may thus serve as a fourth alternative approach to studying the model, next to the perturbative methods, numeric simulations as in the previous chapter, and experiment. It has already proven useful in the Lieb-Liniger model for the study of various properties, such as zero-temperature correlation functions [CC07b], quenches [PDC13], and dynamics [CC07a; KS+13] and for making a connection with the KPZ-problem [CL14].

With another tool at hand for solving the Lieb-Liniger system, we are naturally interested in probing strong collective behavior, i.e., the phase transition, again. This has not been undertaken with methods of integrability yet, although for finite particle number, precursors to the phase transition were observed in the numerical Bethe solution, e.g., in [SDD07; SS+05]. The potential to study the phase transition in the Bethe ansatz was also mentioned in [OL07]. In this chapter we will close this obvious gap.

In the process of solving the Bethe ansatz in the infinite particle number limit for fixed effective coupling, we realize that there is an exact equivalence between the ground state of the Lieb-Liniger system and two-dimensional

[1]For a classical system, integrability is equivalent to the existence of infinitely many conserved quantities. About the difficulties of transferring this definition to the quantum mechanical case, see, e.g., [CM11]

nonabelian Yang-Mills theory in the 't Hooft limit. The Lieb-Liniger phase transition turns out to be exactly related to the Douglas-Kazakov phase transition of Yang-Mills [DK93], a confinement-deconfinement transition.

After a short review of the Bethe ansatz in the context of the Lieb-Liniger model (section 3.2), we derive the large particle number limit of the Bethe equations (s. 3.3). While this limit is quite easily obtained for repulsive systems and has already been treated in [LL63], additional technical complications need to be overcome for attractive systems. The phase transition is directly apparent from the solution to the Bethe equations that we present. We calculate the ground state energy in this framework to verify the order of the phase transition. Then we review the necessary basics of two-dimensional Yang-Mills theory in 3.5 and state the newly obtained equivalence. We have published the newly obtained results of sections 3.3 and 3.5 in [FFP15].

3.2 Review of the Bethe Ansatz

In this section, we will quickly review the Bethe ansatz in its application to the Lieb-Liniger model, before we proceed to present our generalization of the method to large particle number, in the next section.

The easiest way to obtain the Bethe equations in the current model is the so-called coordinate-form Bethe ansatz. The solution method goes back to H. Bethe [Bet31], who, in 1931, studied the antiferromagnetic Heisenberg spin chain using analogous techniques. Lieb and Liniger successfully adapted the idea to their model in [LL63] and this section roughly follows their very clear exposition. See [KBI93] for a more complete review of the Bethe-ansatz technique.

We will first make an ansatz for the Schrödinger wave function of an energy eigenstate of Hamiltonian (2.10), which we repeat here for convenience (again, we choose units in which $\hbar = 2m = 1$)

$$H = -\sum_{i=1}^{N} \partial_i^2 - c \sum_{i \neq j} \delta(x_i - x_j) \tag{3.1}$$

Whenever the coordinates x_i of all N Bosons are distinct from one another, the interaction potential is zero and the wave function is a superposition of

plane waves in all coordinates. We therefore write

$$\Psi(x_1,\ldots,x_N) = \sum_{\pi\in S_N} a_\pi \prod_{j=1}^{N} \exp\left[i\, k_{\pi(j)}\, x_j\right] \qquad \text{for} \quad 0 \le x_1 < \cdots < x_N < 2\pi R \tag{3.2}$$

where we have guessed that there must be a sum over all permutations, π, of momentum assignments, but leave the momenta k_j and coefficients of each permutation a_π to be determined. Whenever the coordinates x_j are not increasing with j, the wave function is dictated by Bose symmetry. We will later comment, whether this apparently restrictive ansatz captures all states in the spectrum.

We will first determine the a_π in terms of the k_j. Integrating the time independent Schrödinger equation over infinitesimal intervals around $\Delta_{jl} = x_j - x_l = 0$ produces familiar looking junction conditions

$$-(\partial_j - \partial_l)\Psi\Big|_{\Delta_{jl}=0^-}^{0^+} = 2c\,\Psi\Big|_{\Delta_{jl}=0} \tag{3.3}$$

where the superscript plus and minus indicate the directional limits; or, using Bose symmetry,

$$-(\partial_{j+1} - \partial_j)\Psi = c\,\Psi \quad \text{for} \quad x_j = x_{j+1}^- \tag{3.4}$$

From the sum in (3.2), focus on the terms for a certain permutation π and of the permutation $\tilde{\pi} = \pi \circ (j\ j{+}1)$, in which the elements assigned to j and $j{+}1$ are interchanged. If (3.4) is satisfied for each such pair of terms, it is satisfied for the total wave-function as well. For these two terms, (3.4) reduces to

$$-[ik_{\pi(j+1)} - ik_{\pi(j)}]\, a_\pi - [ik_{\tilde{\pi}(j+1)} - ik_{\tilde{\pi}(j)}]\, a_{\tilde{\pi}} = c\,(a_\pi + a_{\tilde{\pi}}) \tag{3.5}$$

which holds, if the coefficients satisfy

$$a_{\tilde{\pi}} = a_\pi\, \frac{ik_{\pi(j+1)} - ik_{\pi(j)} + c}{ik_{\pi(j+1)} - ik_{\pi(j)} - c} \tag{3.6}$$

Choosing the normalization for the wave-function $a_{\mathrm{id}} = 1$, it is easy to see that this relation implies well defined assignments for all a_π. With a bit of counting, one can also confirm that there are enough conditions from (3.4) for this choice of a_π to be unique up to normalization (see the original work of Lieb and Liniger). Thus, the Bethe wave function is determined by the set of psudo-momenta k_j. Note that the relation also implies that Ψ vanishes, if any two pseudo-momenta are equal.

One additional step is required, however. We still need to impose the periodic boundary conditions (2.11) with $L = 2\pi R$. Periodicity in the first coordinate, for example, implies

$$\Psi(0, x_2, \ldots, x_N) \stackrel{!}{=} \Psi(L, x_2, \ldots, x_N) \quad = \Psi(x_2, \ldots, x_N, L) \tag{3.7}$$

$$\partial_1\Psi(0, x_2, \ldots, x_N) \stackrel{!}{=} \partial_1\Psi(L, x_2, \ldots, x_N) = \partial_N\Psi(x_2, \ldots, x_N, L) \tag{3.8}$$

where the first equality in each line expresses the periodic boundary conditions and the second one is due to Bose symmetry. Because these must hold for all choices of $x_2, \ldots, x_N$ and because the k_j are distinct, we can identify terms in the wave function on the left hand side and on the right hand side that must satisfy the equality separately. The terms for

$$\pi_{\mathrm{L}} = \left(\begin{smallmatrix} 1 & 2 & \ldots & N \\ \pi(1) & \pi(2) & \ldots & \pi(N) \end{smallmatrix}\right) \quad \text{and} \quad \pi_{\mathrm{R}} = \left(\begin{smallmatrix} 1 & 2 & \ldots & N \\ \pi(2) & \pi(3) & \ldots & \pi(1) \end{smallmatrix}\right) \tag{3.9}$$

need to satisfy the equation. Their coefficients are related by (3.6) as

$$a_{\pi_{\mathrm{R}}} = a_{\pi_{\mathrm{L}}} \times \frac{ik_{\pi(2)} - ik_{\pi(1)} + c}{ik_{\pi(2)} - ik_{\pi(1)} - c} \times \frac{ik_{\pi(3)} - ik_{\pi(1)} + c}{ik_{\pi(3)} - ik_{\pi(1)} - c} \times \cdots \tag{3.10}$$

Including the $\exp[ik_{\pi(1)}L]$ factor, we finally obtain the so-called Bethe equations for $j = 1 \ldots N$.

$$e^{ik_jL} = \prod_{l \neq j} \frac{k_j - k_l - ic}{k_j - k_l + ic} \tag{3.11}$$

They determine the allowed sets of pseudo-momemta or Bethe roots $\{k_j\}$ and will be the main focus of our formal derivations presented in section 3.3. The fact that we only need to solve a set of transcendental equations to characterize the Lieb-Liniger model as apposed to a partial differential Schrödinger equation is one face of integrability.

At this point we should pause and take note of some relevant properties of the Bethe states (characterized by the set roots $\{k\}$). They are, of course, energy eigenstates with associated eigenvalue

$$E_{\{k\}} = \sum_j \frac{\hbar^2}{2m} k_j^2 \tag{3.12}$$

and they are also momentum eigenstates with

$$P_{\{k\}} = \hbar \sum_j k_j \tag{3.13}$$

while the pseudo-momenta are not directly measurable. Therefore we will just refer to them as Bethe roots from here on. Note also that we can shift all k_j simultaneously by multiples of $2\pi/L$ which corresponds to a Galilei boost on the whole solution.

3.2.1 Weak coupling limit

In the weak coupling limit $c \ll \frac{1}{NL}$, by physical arguments, the Bethe roots will deviate very little from the allowed free particle wave vectors $k_j \approx n_j 2\pi/L$ with integer n_j. Solutions can be found for arbitrary numbers of roots clustered around each of the free wave vectors. Of course, the roots still don't coincide and we will see later that their deviations from the free momenta are much larger than c, yet much smaller than $1/L$. We can thus persuade ourselves in the weak coupling limit that the Bethe equation gives enough solutions to account for all states of the free particle Fock space. By continuity[2], the Bethe ansatz wave functions are therefore a complete set of the physical Hilbert space of the system at arbitrary coupling. This completeness argument is analogous to the one formally proven by Yang and Yang [YY69] in the case of repulsive interactions.

The roots in the weak coupling (i.e., thermodynamic) limit were already described in [Gau71] and will later arise as a by-product of our general derivation.

3.2.2 Strong Coupling Limit Solution

In the strong coupling limit $c \gg \frac{1}{NL}$, in contrast, the ground state spacing of k_j is very close to ic. The state, derived in [Tha81], is therefore also known as a string (like "pearls on a string"). For convenience, we will index the Bethe roots with $j \in -\frac{N-1}{2}, \ldots, \frac{N-1}{2}$ in this section. To parametrize the strong coupling state, we introduce

$$k_{j+1} - k_j \equiv i(c + \delta_{j\,j+1}) \tag{3.14}$$

with $0 < \delta_j \ll c$ as we will see self consistently. In the Bethe equations (3.11), the neighboring roots now dominate, giving a contribution

$$\frac{k_j - k_{j-1} - ic}{k_j - k_{j-1} + ic} \times \frac{k_j - k_{j+1} - ic}{k_j - k_{j+1} + ic} \approx \frac{\delta_{j-1\,j}}{\delta_{j\,j+1}} \tag{3.15}$$

For roots away from the center of the string, a relevant term due to the asymmetric contribution from the boundary arises. For l such that $|j - l| > n/2 - |j|$, there is no matching term from the opposite side of j, so that a suppressed contribution remains

$$\prod_{l=-\frac{n}{2}}^{-\frac{n}{2}+2j} \frac{k_j - k_l - ic}{k_j - k_l + ic} \approx \frac{(1 - 2j/N)^2}{(1 + 2j/N)^2} + \mathcal{O}(1/N) \tag{3.16}$$

[2] In the infinite N limit, we encounter a phase transition. For any large but finite N however, no discontinuities should occur.

for fixed j/N at large N.

Taking both into account, we get a relation between the offsets δ

$$\frac{\delta_{j-1\,j}}{\delta_{j\,j+1}} \approx \exp[-jcL + 4\,\mathrm{arctanh}(2j/N)] \tag{3.17}$$

Similar considerations determine the offset δ at the boundary of the string

$$e^{-(N-1)cL/2} \approx \frac{\delta_{(N-3)/2\,(N-1)/2}}{2c} \times \frac{2}{N^2} \tag{3.18}$$

Together, (3.17) and (3.18) determine all Bethe roots. For sufficiently large coupling c, all offsets δ are small and the string solution is self consistently valid.

As a note of caution, numerical simulations need to be implemented carefully, not to lose track of these exponentially small deviations δ, as we will detail in section 3.4.

3.3 Continuum Limit of the Bethe Ansatz

In this section we will present a proof of our main formal result in the attractive Lieb-Liniger system, an $N \to \infty$ formulation of the Bethe equations, as well as its ground state solutions in the homogeneous and solitonic regimes. The derivations in this section were all contributed by the author.

As we have discussed in 2.4.1, and in agreement with the validity of the weak and strong coupling limits discussed in 3.2.1 and 3.2.2, the effective coupling

$$g = cNL \tag{3.19}$$

needs to be fixed as $N \to \infty$ in order to preserve the phase transition. We will use units in which $L = 1$ from here on.

It has been shown in [McG64] that the Bethe roots of the ground state are purely imaginary, because the ground state is a bound state of the attractive Bosons (of course, the soliton only forms after the phase transition). Adding a real part to all roots corresponds to giving total momentum to the bound state. For convenience, we will thus redefine

$$k_j \to ik_j \tag{3.20}$$

This redefinition contributes, for example, a negative sign to the expression for the ground state energy (3.12) and should therefore be kept in mind.

We arrive at a convenient form of the Bethe equations (3.11)

$$k_j = \sum_{l \neq j} \log \frac{k_j - k_l + g/N}{k_j - k_l - g/N} \tag{3.21}$$

where we have chosen the branch of the logarithm that corresponds to the ground state. It is clear from the discussion of section 3.2.1 that other branches are associated with excited states of the system (and produce Bethe roots that are not purely imaginary).

We will show below that the Bethe equations are asymptotically satisfied, if the roots are described by

$$k_j \equiv g\, k(j/N) \tag{3.22}$$

and will determine the continuous function $k(x)$.

3.3.1 Constraint on the Root Distribution

Let us already notice a crucial constraint on the root distribution arising from 3.21. The roots need to satisfy

$$|k_i - k_j| > g/N \tag{3.23}$$

We have mentioned before that this inequality holds at weak coupling and will see so, explicitly, below. Actually the inequality is true for all g by continuity. Assume that, as we increase g, at some point, $k_{j+1} - k_j = g/N$ for some pairs of roots. Focus on the smallest root for which the inequality is violated. For this root, there is only one diverging term on the right hand side of (3.21) and the Bethe equation cannot be satisfied.

In the continuum limit, this constraint implies

$$k'(x) \geq 1 \tag{3.24}$$

where, in the limit, the relation weakens to greater-equal.

3.3.2 The Integral Equation

We will now derive the continuum limit of the Bethe equations (3.21) for all points where $k'(x) > 0$ and $k''(x) \neq 0$. For this purpose, let us split the sum on the right hand side into a contribution from those l that fall in a given

interval of the continuum variable $y = l/N \in [x-\epsilon, x+\epsilon]$ around $x = j/N$ and the rest.

$$k_{j=xN} = \sum_{\Delta=1}^{\epsilon N} \log\left(1 + \frac{2}{N}\frac{k_{j-\Delta} + k_{j+\Delta} - 2k_j}{(k_{j+\Delta} - k_j + g/N)(k_j - k_{j-\Delta} - g/N)}\right) + \sum_{|l-j|>\epsilon N} \log\frac{k_j - k_l + g/N}{k_j - k_l - g/N} \tag{3.25}$$

Although ϵ is initially arbitrary, we will consider the limit $\lim_{\epsilon\to 0}\lim_{N\to\infty}$ of going to the continuum before shrinking the interval.

Let $c > 1$, then, for ϵ sufficiently small, we can bound the magnitude of the sum in the first line by

$$\sum_{\Delta=1}^{\epsilon N}\left|\log\left(1 + \frac{2}{N}\frac{c\,k''(x)}{\min[k'(x-\epsilon)^2, k'(x+\epsilon)^2] - 1}\right)\right| \tag{3.26}$$

which, in the limit $N \to \infty$ goes to

$$\epsilon \times \left(\frac{2c|\bar{k}''(x)|}{\min[k'(x-\epsilon)^2, k'(x+\epsilon)^2] - 1}\right) \tag{3.27}$$

and vanishes as $\epsilon \to 0$. So, for any point with $k' > 1$, $k'' \neq 0$, only the second sum in (3.25) contributes in the continuum limit.

For the sum in the second line of (3.25), the contributing root differences become much larger than g/N as $N \to \infty$ for any given ϵ. Therefore

$$\lim_{N\to\infty} \log\frac{k_j - k_l + g/N}{k_j - k_l - g/N} = \frac{2g}{N}\frac{1}{k_j - k_l} \tag{3.28}$$

In the continuum limit, we can then write an integral instead of the sum

$$g\,k(x) = 2\int\limits_{\substack{[-1/2, x-\epsilon)\\ \cup(x+\epsilon, 1/2]}} dy\,\frac{1}{k(x) - k(y)} \tag{3.29}$$

Defining the density of roots

$$\rho(k) = \frac{1}{k'[x(k)]} \quad \text{with} \quad \int_{k_{\min}}^{k_{\max}} \rho(u)du = 1 \tag{3.30}$$

we can bring the integral equation into its final form

$$g\,k = 2\,\mathcal{P}\!\int_{k_{\min}}^{k_{\max}} du\,\frac{\rho(u)}{k-u} \tag{3.31}$$

where $\mathcal{P}$ indicates principal value integration - a remnant of the ϵ excision in the sum. This form of the Bethe equations is the main result of this section.

3.3.3 Homogeneous Phase Solution

The solution to the integral equation (3.31) is well known - a semi-circle [Pip91]

$$\rho(k) = \frac{1}{\pi}\sqrt{g - \frac{g^2k^2}{4}} \tag{3.32}$$

with $k_{\max} = -k_{\min} = 2/\sqrt{g}$. Where it does not violate the constraint, this root distribution uniquely characterizes the state of the system. We will later see examples, how physical observables can be calculated from this information.

In the weak coupling limit, in agreement with section 3.2.1, all roots deviate relatively little from the free ground state $k_i = 0$ in comparison to the natural momentum scale of the compactification. Furthermore, their distances are still large compared to the constraint as assumed in section 3.3.1.

$$\max k' = \frac{\pi}{\sqrt{g}} \tag{3.33}$$

Yet, we see that the constraint is violated for $g \geq \pi^2$ (Note that the normalization of the collective coupling differs from the one in chapter 2, where the phase transition was always at $\alpha N = 1$). In the derivation of the integral equation, we assumed that $k'(x) > 1$. Before we can treat the regime of larger effective couplings, we have to revisit the situation of $k'(x) \approx 1$.

3.3.4 Continuum Limit of the String

When the distance of adjacent Bethe roots is nearly saturating the constraint, i.e., $k_{j+1} - k_j = c + \delta_{j\,j+1}$ with small δ, we have already seen that (3.17) determines the δ. Let us translate this relation into continuum variables

$$\delta_{j\,j+1} \equiv \frac{N}{g}\,\delta(j/N) \tag{3.34}$$

then

$$(\log\delta)'(x) = N[gx - 4\,\mathrm{arctanh}(2x)] \tag{3.35}$$

For roots in the center, x close to zero, this implies

$$\log\delta(x) \approx \frac{N}{2}(g-8)x^2 \tag{3.36}$$

Figure 3.1 shows a logarithmic plot of the δ obtained from a numeric solution of the Bethe equations at $N = 250$ in the strong coupling regime ($g = 16$), as well as a polynomial fit. The fit parameter nicely confirms the functional form just obtained.

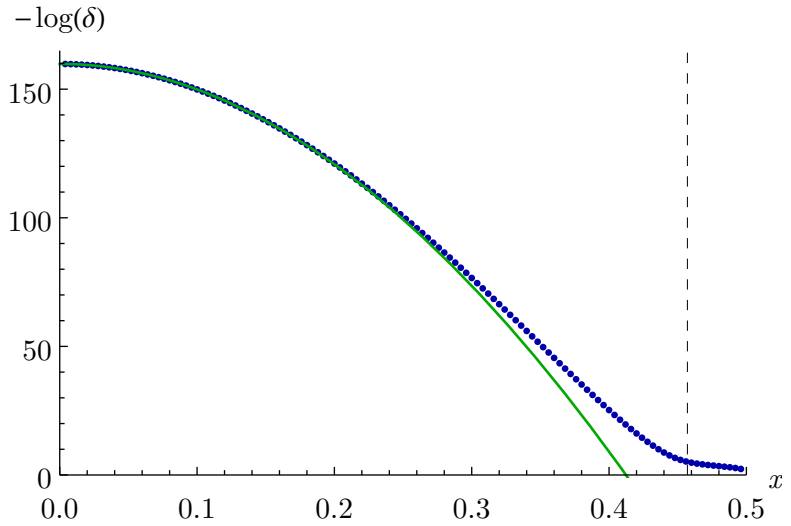

Figure 3.1: Numerical solution to the Bethe equation for $N = 250$ at $g = 16$, which is well on the strong coupling side, parametrized by $\delta(x)$ as in our treatment of the continuum string. The green line represents a fit of $ax^2 + bx^3 + c$. The fit coefficient $a = -1006.5$ is in good agreement with the theoretical prediction $-(g-8)N/2 = -1000$ given the value of N. The dashed line indicates the theoretical prediction for the boundary of the string interval (see section 3.3.5).

Here we only assume that the constraint is nearly saturated for some range of j and do not yet reason about the outermost roots as in (3.18). Instead, let us consider the point y where the continuum function reaches $k'(y) = 1 + \epsilon$ with $\epsilon > 0$, but where we still trust the nearest neighbor-only approximation. Then, as $\delta(x) = k'(x) - 1$, we can integrate (3.35) and determine the integration constant.

The shape of the resulting function is explicitly N dependent and tends to zero for $x < y$ as N is sent to infinity[3]. At $x = y$, the derivative

$$k''(y) = \delta'(y) = \delta(y)\,(\log\delta)'(y) \tag{3.37}$$

$$= \epsilon N[gx - 4\,\mathrm{arctanh}(2x)] \xrightarrow[N\to\infty]{} \infty \tag{3.38}$$

diverges in the limit.

[3]This check can only be completed after the fact, when we determine the interval, in which continuum solution actually contains a string, because the arctanh contribution could in principle change the sign of the derivative. With hindsight, we can confirm that this doesn't happen.

We thus have to allow for an interval, in which the continuum root density saturates the constraint. In this interval, the root density does not need to obey the integral equation. At the boundaries of the interval, its derivative must be discontinuous. By looking at the string solution again, we also know that the interval should be centered about $x = 0$.

3.3.5 Solitonic Ground State

In light of the last section, we make the ansatz that the density saturates the constraint in an interval

$$\rho(k) = \begin{cases} 1 & k \in [-b, b] \\ \tilde{\rho}(k) & k \in [-a, -b) \cup (b, a] \end{cases} \tag{3.39}$$

Inserting this form into (3.31) yields a modified integral equation for $\tilde{\rho}$

$$\frac{g}{2}k + \log\frac{k-b}{k+b} = \mathcal{P}\!\int\limits_{\substack{[-a,-b]\\ \cup[b,a]}} du\, \frac{\tilde{\rho}(u)}{k-u} \tag{3.40}$$

Luckily, the solution to this integral equation is known [DK93] and can be derived using methods detailed in [Pip91] and contour integration. The solution reads

$$\tilde{\rho}(k) = \frac{2}{\pi a|k|}\sqrt{(a^2-k^2)(k^2-b^2)}\ \Pi_1\left(\frac{b^2}{k^2}, \frac{b^2}{a^2}\right) \tag{3.41}$$

where Π_1 is the elliptic function of the third kind (see appendix A for definitions of the special functions[4]).

The boundaries of the interval, a and b need to be determined from the following conditions

$$\begin{gathered} 4\,\mathrm{K}(x)\left[2\,\mathrm{E}(x) - (1-x)\,\mathrm{K}(x)\right] = g, \\ ag = 4\,\mathrm{K}(x) \quad \text{and} \quad x = b^2/a^2 \end{gathered} \tag{3.42}$$

in order for (3.41) to fulfill the integral equation. E and K are elliptic functions of the first and second kind.

It is interesting to note that for $g \to \pi^2$, the strong coupling solution approaches the semi-circle law (3.32) so that the root distribution is a continuous function of g, even at the phase transition.

[4]Especially the convention regarding the square of the arguments varies across the literature.

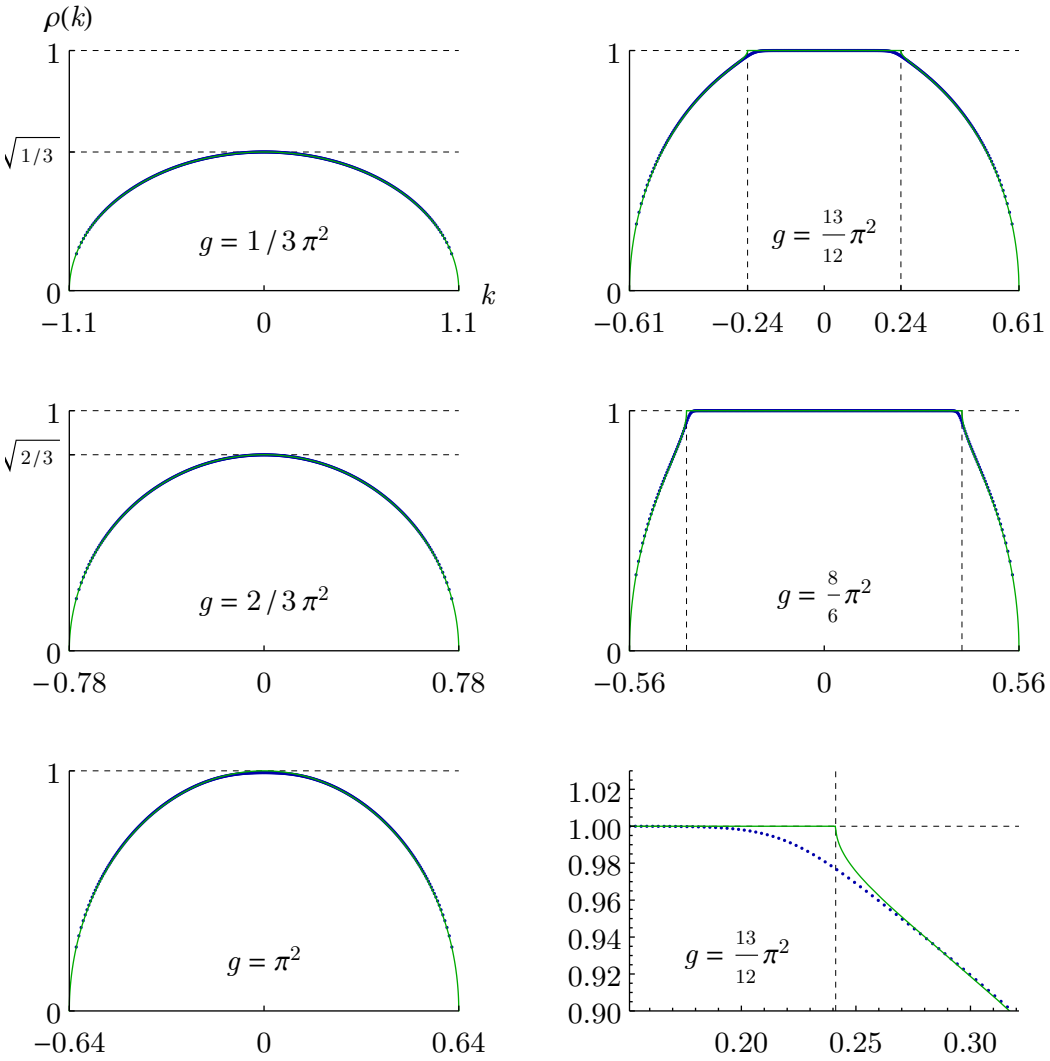

Figure 3.2: Solutions of our continuum Bethe equations (green curve) in contrast to numerical results with $N = 400$ (blue dots) for various values of the effective coupling g. The root density $\rho(k)$ is displayed as a function of k. The bottom right plot shows a zoom to the end of the interval in which the density saturates the constraint. A version of this plot was included in [FFP15].

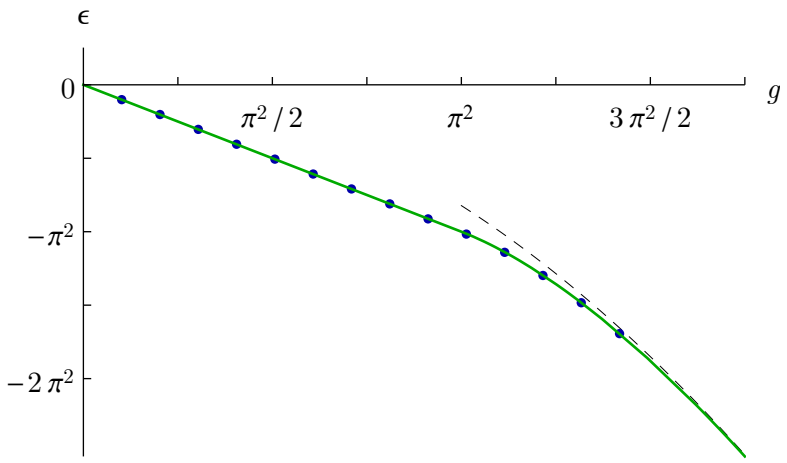

Figure 3.3: Energy of the ground state of the Lieb-Liniger model calculated analytically in the continuum Bethe ansatz (green curve) and numerically for $N = 400$ particles. The black dashed line indicates the strong coupling limit. A version of this plot was included in [FFP15].

3.3.6 Ground State Energy

Above, we have derived an integral equation governing the distribution of Bethe roots in the ground state at large N and obtained analytic expressions for the regimes $g^2 \gtrless \pi^2$. The root distributions contain the full physical information of the state - calculating observables from them, however, is usually nontrivial. Here we will determine the ground state energies associated with these root distributions. They serve as a sanity check because we can compare to the values obtained in mean-field theory (see section 2.4.1).

From (3.12), we conclude that the energy per particle is finite in the continuum limit

$$\epsilon_g = \frac{E_g}{N} = -g^2 \int k^2 \rho(k)\, dk \tag{3.43}$$

where the negative sign is a result of our redefinition $k \to ik$. On the weak coupling side, the value can easily be obtained by partial integration. On the strong coupling side, it is beneficial to use the integral representation of Π_1 and exchange the two integrals. Contour integration techniques then yield the desired result. Using (3.42), the energy can be written in concise form

$$-\epsilon = \begin{cases} g & \text{for} \quad g \leq \pi^2 \\ \frac{1}{48} g^2 \left[8(a^2+b^2) + g(a^2-b^2)^2 \right] & \text{for} \quad g > \pi^2 \end{cases} \tag{3.44}$$

The order of the quantum phase transition is defined through the order of continuity of the ground state energy. From (3.42), we can obtain a series expansion of a and b around $g \sim \pi^2$ and insert these in (3.44) to obtain

$$-\epsilon = g + \frac{2}{\pi^2}(g-\pi^2)^2 + \mathcal{O}\Big[(g-\pi^2)^3\Big] \quad \text{for} \quad g > \pi^2 \tag{3.45}$$

Thus, the ground state energy and its first derivative are continuous at the phase transition, unlike its second derivative. So the phase transition is of second order, as mentioned before.

As an analytic check on our results, we will verify that the ground state energy coincides with the mean-field result as it should (see section 2.4.2) for a discussion of the validity of mean field). The parameters x from (3.42) and m from (2.18) are related as

$$x = \left(\frac{1-\sqrt{1-m}}{1+\sqrt{1-m}}\right)^2 \tag{3.46}$$

Expression (3.44) can then be transformed identically into (2.20), using the alternative evaluation relations[5] for elliptic functions (17.3.29) and (17.3.30) from [AS64].

3.4 Numerical Validation

In this section, we will perform some numerical checks to validate our results obtained above. To this end, we solve the Bethe equations numerically for large-but-finite N and compare the ensuing root distribution with our analytic prediction for the continuum. Below, we will first outline the numerical techniques that we implemented, before presenting the simulation results and comparing them with the prediction.

The method we have used is similar to the one described in the purely numerical studies of [SDD07]. We parametrize the roots as

$$k_j \equiv c(j + \Delta_j) \tag{3.47}$$

Using the $\{\Delta_j\}$ as variables allows us to make good use of the floating point format to capture the exponentially small deviations in the string solution at strong coupling (see 3.2.2). Thus we can perform the calculations in

[5] We are indepted to M. Crescimanno for pointing these out.

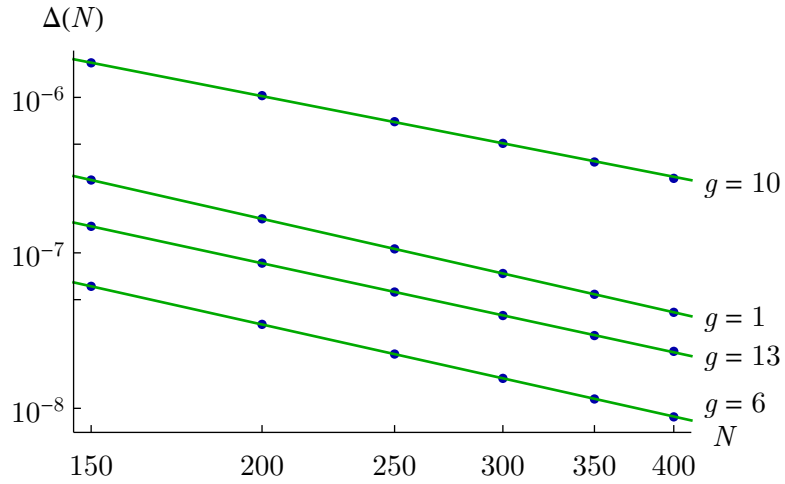

Figure 3.4: Deviation of the numerical finite-N root distribution (blue dots) with respect to our continuum prediction as a function of N for various values of the effective coupling g in a doubly logarithmic scaling. The green lines represent power law fits to the error. A version of this plot was included in [FFP15].

hardware supported double precision floating point numbers. As we know that the ground state root distribution has to be symmetric, we can also save some amount of calculation by explicitly manipulating only half of the roots.

We then minimize the sum of squared errors

$$\sum_j [\mathrm{LHS}_j - \mathrm{RHS}_j]^2 \tag{3.48}$$

where LHS_j (RHS_j) refer to the left (right) hand side of the j-th Bethe equation (3.21). The minimization uses the Levenberg-Marquardt algorithm implemented in Mathematica. Special care is required to make the algorithm robust towards roots that overshoot and momentarily violate the bound on their distance. Replacing

$$\log(k_i - k_j \pm c) \to \log \max[(\Delta_i - \Delta_j) + (i - j \pm 1), \epsilon_{\mathrm{flt}}] + \log c \tag{3.49}$$

for $i > j$, with ϵ_{flt} the smallest nonzero floating point number, proved useful.

In the weak coupling regime $g \ll 1$, the algorithm is quite insensitive towards different choices of initial conditions and converges quickly. To obtain solutions at strong coupling, we found it convenient to solve at weak coupling first and track the solution, while increasing the coupling step by step. We

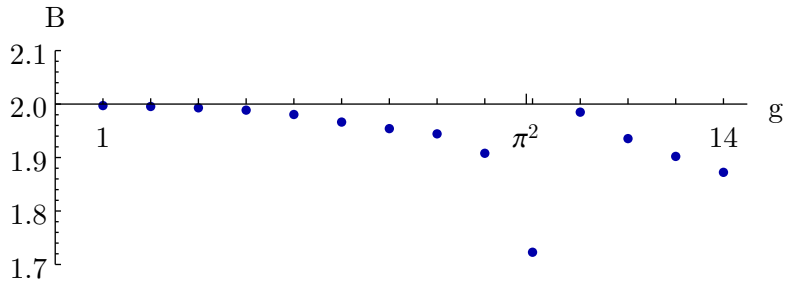

Figure 3.5: Power law in N that governs the convergence of the numerical finite-N solution to the continuum limit. A version of this plot was included in [FFP15].

initialized each step directly by the previous solution and observed satisfactory convergence speeds. Another speedup might possibly be achieved by extrapolating in a suitable fashion for each initialization.

This setup allowed us to easily simulate systems with $N \sim 400$ roots and g significantly exceeding the phase transition on a commodity personal computer.

The numerical roots were already displayed in fig. 3.2, where they are hard to discern from the predicted continuum solution by eye. In the bottom-right plot of the figure, we show a magnification of the strong coupling solution around the end of the flat section. This is, where the deviation from the continuum solution is most marked and finite-N effects are important.

To quantify the deviations, we used the following measure

$$\Delta(N,g) = \frac{1}{N}\sum_{i=1}^{N}\left[k_i - g\,k(i/N)\right]^2\Big|_g \tag{3.50}$$

where $k(x)$ was obtained from the analytic root density $\rho(k)$ of (3.32, 3.39) by numerical integration. We should remark that the inherent numerical errors of the finite-N Bethe roots were estimated to be much smaller than these deviations.

In fig. 3.4, the doubly logarithmic plot reveals that, for each effective coupling g, the deviations decrease as a power law in N, to good approximation. The exponent fit parameter for these power laws are reproduced in fig. 3.5. Based on those numbers, we conjecture that the finite-N deviations scale like

$$\Delta(N,g) \sim N^{-2} \tag{3.51}$$

at large N.

It may also be observed that the convergence to the continuum solution is faster away from the critical point $g = \pi^2$.

3.5 Equivalence with 2D Yang-Mills Theory

In this section we will first review some necessary basics of Yang-Mills theory quantized on a Euclidean two-manifold. We will then point out a surprising equivalence between the description of the large N_{color} saddle of Yang-Mills and our continuum limit of the Bethe equations. This equivalence was not yet known and our main reason to publish [FFP15].

3.5.1 Review of 2D Yang-Mills

The action of pure Yang-Mills theory in two dimensions has the standard form

$$S = -\frac{1}{4e^2}\int_M d^2x\sqrt{g}\ \mathrm{Tr}[F^{\mu\nu}F_{\mu\nu}] \tag{3.52}$$

where $F_{\mu\nu}$ is the nonabelian field strength associated with the gauge field A_μ and e is the coupling. Below, we will focus on $\mathrm{U}(N)$ gauge groups. We have already written the integral to be over a two-manifold M with metric $g_{\mu\nu}$.

Like two-dimensional electromagnetism, this theory does not propagate any degrees of freedom. It should also be noted that it is super-renormalizable. Furthermore, it does not depend on the metric $g_{\mu\nu}$, but only on the associated measure $d^2x\,\sqrt{\det g}$. This fact can be readily appreciated after introducing an auxiliary field ϕ and rewriting [DI99]

$$S = \frac{i}{2}\int_M d^2x\,\epsilon^{\mu\nu}\,\mathrm{Tr}[F_{\mu\nu}\phi] - \frac{e^2}{2}\int d^2x\sqrt{g}\ \mathrm{Tr}\,\phi^2 \tag{3.53}$$

The invariance under area preserving diffeomorphisms is such a powerful symmetry that the theory is, in fact, exactly soluble [Mig75].

Nevertheless, 2d Yang-Mills shares some important characteristics with its higher-dimensional cousins, namely confinement and a deconfining phase transition, and has variously served as a toy model or a theory on its own right. It also has important applications in mathematics that we will not elaborate here.

The concrete form of the partition function will be relevant for us, later, so we will give a brief sketch how it comes about. The original derivation was given by Migdal [Mig75] using a lattice regularization on $\mathbb{R}^2$ and generalized by Rusakov [Rus90] to arbitrary topologies. The outline presented here follows a more field theoretic treatment due to Witten ([Wit91] and [DI99]).

The only invariant constructed from the Riemannian measure is the total area $a = \int dx\sqrt{g}$, so we can already anticipate that the partition function can only depend on the combination ae^2.

As an initial step, let us canonically quantize the theory on a cylinder with circular equal-"time" slices of length L. The wave functional is a gauge-invariant functional from gauge connections into $\mathbb{C}$. Due to gauge invariance it can only be a function of the holonomy of the connection $w[A] = \mathcal{P}\exp(i\int A_1 dx)$. It must still be invariant under the adjoint action of the gauge group $w \to g\, w[A]\, g^{-1}$, or in other words, it must be a class function. Characters provide a convenient basis of class functions and, accordingly, we choose them as the basis for the Hilbert space.

$$\Psi_R[A] = \chi_R(w[A]) \tag{3.54}$$

The Hamiltonian is

$$H = \frac{e^2}{2}\int dx\ \operatorname{Tr}\pi_1^2 \tag{3.55}$$

which is the square of the canonical momentum. Acting as a differential operator on the wave function gives

$$H\Psi_R[A] = \int dx \sum_a \frac{\delta}{\delta A^a(x)}\frac{\delta}{\delta A^a(x)} \operatorname*{Tr}_R w[A] = \frac{e^2 L}{2} c_2(R)\, \Psi_R[A] \tag{3.56}$$

where $c_2(R)$ is the quadratic Casimir in the representation R. Thus, Ψ_R are energy eigenfunctions and the matrix element relevant for the partition function is

$$\langle R|e^{-HT}|R\rangle = e^{-e^2 a\, c_2(R)/2} \tag{3.57}$$

What remains to be done in order to calculate the partition function, is to decompose the manifold into cylindrical patches, glue those together and trace over all states. Invariance under area preserving diffeomorphisms greatly simplifies the task. Consider a junction (pair-of-pants topology) where the state on each of the three boundary circles is described by a representation as above. For an insertion of a Casimir operator, we can deform the metric so that the operator is close to any one of the boundaries and effectively measures the state at the chosen boundary. Because the matrix elements still have to agree in any case, the partition function with prescribed boundaries can only be nonzero, when the representations on all boundaries are equal. Because diffeomorphisms also allow us to deform the geometry to be dominated by three cylindrical tubes, the partition function must be

proportional to the right hand side of (3.57). See [DI99] for more detailed derivations.

Furthermore, a cylinder may be decomposed into a pair-of-pants and a disk. This fact allows us to fix the partition function on the disk with fixed boundary to be proportional to (3.57) as well, with inverse proportionality constant. Plugging these building blocks together and summing over all representations gives the final form for the partition function

$$Z_M = \sum_R (\dim R)^{2-2g}\, e^{-ae^2 c_2(R)/2} \tag{3.58}$$

where $(\dim R)$ is the proportionality constant for each junction which obviously has to appear in power of the Euler characteristic of the manifold.

We have completely sidestepped issues of renormalization, which just amount to a multiplicative renormalization of the Euler characteristic and an additive renormalization of the quadratic Casimir for this theory. The renormalization conditions implicitly adopted above are in line with lattice regularization.

In [DK93], Douglas and Kazakov have constructed the large-N limit of this partition function for U(N) gauge groups on a sphere. We will explicitly exhibit the main steps to clarify the quantities that appear in our equivalence with the Lieb-Liniger Bethe ansatz.

We characterize each representation of U(N) by a sequence of N decreasing (and not necessarily positive) integers $n_1 \geq n_2 \geq \cdots n_N$, the components of highest weight. These numbers may be usefully related to either one Young tableau with (positive) row lengths given by shifted n_i or to two Young tableaux, one defined by the set of positive, another by the negative n_i [DZ83].

All required quantities can easily be expressed in terms of the components of highest weight:

$$\begin{aligned} \dim R &= \prod_{i>j} \left(1 - \frac{n_i - n_j}{i-j}\right) \\ c_2(R) &= \sum_i n_i(n_i - 2i + N + 1) \end{aligned} \tag{3.59}$$

In the 't Hooft large-N limit, the following continuum variables are introduced

$$\begin{aligned} \lambda &= e^2 N \quad \text{('t Hooft coupling)} \\ x &= i/N \\ h(x) &= (i - n_i)/N - 1/2 \end{aligned} \tag{3.60}$$

The fact that the n_i are necessarily decreasing translates into a constraint on $h(x)$

$$h'(x) \geq 1 \tag{3.61}$$

Using (3.59), the partition function (3.58) on a sphere can be rewritten as a path integral over the row lengths of the Young tableau.

$$\begin{aligned} Z_{\text{sphere}} &= \int Dh\, e^{-N^2 S[h]} \\ S[h] &= -\int dx\, dy\, \log[h(x) - h(y)] + \frac{a\lambda}{2}\int dx\, h(x)^2 - \frac{a\lambda}{24} \end{aligned} \tag{3.62}$$

In the large-N limit, the partition function is dominated by the saddle point. The corresponding representation is determined by the following "equation of motion"

$$a\lambda\, h = 2\,\mathcal{P}\!\int dv\, \frac{\rho(v)}{h - v} \tag{3.63}$$

where we have introduced the density $\rho(h) = 1/h'[x(h)] \leq 1$ to parametrize the growth of the Young tableau.

Douglas and Kazakov also solved the resulting integral equation with constraint and identified a third order phase transition. This confinement-deconfinement phase transition is usually referred to as Douglas-Kazakov transition. As the transition is triggered by varying the radius of a Euclidean sphere, one may think of it as a thermal transition.

3.5.2 Connection Between LL and YM

In the previous section, we have reviewed the large-N limit of U(N) Yang-Mills theory on a two-sphere. Equation (3.63), together with a constraint on the density $\rho(h)$, determines the dominant representation contributing to the partition function. After introducing all this background, it is now trivial to observe a direct equivalence with equation (3.31) governing the distribution of Bethe roots in the ground state of the Lieb-Liniger model. Also the constraint on the density agrees. Thus, after identifying the dimensionless combination of area and 't Hooft coupling $a\lambda$ with the effective Lieb-Liniger coupling g, the solutions are in one-to-one correspondence. The distribution of Bethe-roots has the exact same behavior as the growth of the dominant Young tableau.

$$\begin{array}{ccc} \text{Lieb-Liniger} & \Leftrightarrow & U(N_{\text{c}})\ \text{Yang-Mills} \\ N & \Leftrightarrow & N_{\text{c}} \\ g = cLN & \Leftrightarrow & a\lambda = e^2 aN \\ \rho(k) & \Leftrightarrow & \rho(h) \end{array} \tag{3.64}$$

The Douglas-Kazakov phase transition turns out to have a direct equivalent in the homogenous/solitonic phase transition in the Lieb-Liniger model.

The appearance of the Douglas-Kazakov phase transition is all the more exciting for it is deeply connected with random matrix theory [MS14] and diverse other physical and mathematical questions (e.g. [FMS11; CP13]).

In this context, we should give credit to various relations between the (supersymmetric) Yang-Mills theory and integrable systems that have already been reported (see, e.g., [GS04; NS09] and references therein). In the known examples, however, the integrable system was mapped to the moduli space of the gauge theory, and the roots were identified with eigenvalues of the complex scalar in the vector multiplet. In our mind the existence of additional relations makes it even more intriguing to fully understand the relation between the various theories involved. Note also that [GMN16] has already made good use of our correspondence in conjunction with such other relations.

3.6 Outlook

In this chapter, we have concentrated on the integrability property of the Lieb-Liniger model and formulated the Bethe ansatz equations in the large-N limit. We have thus been able to determine the ground state of the system for arbitrary effective coupling. We have then pointed out an exact equivalence between the Bethe ansatz ground state of the Lieb-Liniger model and the 't Hooft limit of two-dimensional $U(N)$ Yang-Mills theory on a sphere.

It is especially the potential duality that mandates further investigation. To elevate its status from a mere mathematical curiosity, one would have to identify a useful dictionary between physical observables on both sides. The Wilson loops of two-dimensional Yang-Mills, for example, have been determined long ago [DK94]. The remaining task, of course, is to formulate physical observables in the continuum description and possibly identify ones with a meaningful equivalent on the gauge theory side. A deeper understanding of the reason underlying the equivalence would, of course, also be desirable.

Another future direction is to include $1/N$ corrections in our formalism. Versions of the Euler-Maclaurin formula exist [Lyn85] that make it possible to write the leading error incurred in the continuum limit in suitable form. Carefully taking into account all possible sources of contributions suppressed by $1/N$, it should be possible to arrive at an integral equation for the subleading terms of the root distribution as well. Of course, the formulation

of observables is then complicated by similar $1/N$ corrections. In the end, however, the $1/N$ corrections would yield answers that are not easy to come by with mean-field and Bogoliubov techniques, and thus of genuine interest.

Chapter 4

High-Multiplicity Scattering

4.1 Motivation

It is well known that perturbation theory in quantum mechanics and field theory[1] only produces an asymptotic series for most physical quantities [Lip77]. The classic argument for this behavior was given by Dyson [Dys52]. He argued that, if the perturbative series had a finite radius of convergence, one would be able to analytically continue physical quantities to small negative couplings. We know, however, that even the vacuum of QED becomes unstable to electron-positron production for negative fine structure constant - suggesting that analytic continuation is impossible. The mathematical origin for the asymptotic growth of the terms in the perturbation series is (at least) twofold. On the one hand, the number of Feynman diagrams contributing to a given process grows drastically with the number of vertices in the diagrams. On the other hand, in field theories that require renormalization, even the value of an individual diagram of a certain build at each order may grow factorially after momentum integration[2]. We will focus on the former in this work, also because our concrete calculations are restricted to quantum mechanics, where renormalization is not required.

In practice, the asymptotic nature of the perturbative series does usually not play a role in weakly coupled field theories[3]. The leading first few orders of perturbation theory are sufficiently accurate to match experimental results - compare, e.g., the impressive accuracy of the electron $g-2$ prediction in the Standard Model [GH+06]. The asymptotic growth of perturbation the-

[1] Similar conclusions are, of course, also reached in string theory [She90; ASV12].

[2] This phenomenon is known as renormalon. See [Ben99] for a review and [AU12] for recent advances in the context of resurgence theory.

[3] Unless the analytic continuation to complex or large values of the coupling is sought for [CKÜ15].

ory is a more urgent issue for scattering amplitudes with a high multiplicity of particles in the final or initial state, as even the leading Feynman diagram is of high order in the coupling [Gol90; Cor90]. Motivated by the study of lepton number violating sphaleron processes, amplitudes with high multiplicity attracted considerable attention in the early 1990s. References to some important works of the time can be found in the reviews [Vol94; Rub95; LRT97]. While Rubakov, Son and Tinyakov [RST92; Son96] have developed a semiclassical technique to approximate scattering into the dominant coherent state, we still lack the ability to calculate more general amplitudes with high-multiplicity final states. The associated question, how they avoid to endanger unitarity [Zak91] is also still unresolved. These issues have become more urgent, recently, as Khoze has pointed out the possibility that high-multiplicity amplitudes of the electro-weak sector may be accessible at future particle-colliders [Kho14; JK15].

In this chapter, we will analyze scattering amplitudes of many interacting particles with inspiration from resurgence theory. In order to gain a better understanding and to develop calculational techniques, we use analogs of scattering amplitudes in low dimensional toy models (simple integrals and quantum mechanics).

After quickly reviewing the saddle-point approximation in section 4.2 and commenting on the quantities of interest in the model systems (s. 4.3), we study the breakdown of perturbation theory for the quartic integral in considerable detail in section 4.4. While the amplitudes of this model have received a fair amount of attention in the past, we contribute new and concise estimates about the critical coupling for the demise of the tree approximation and the breakdown of perturbation theory. In performing resummation, we encounter higher-order poles in the Borel-plane that point towards the possibility of non-perturbative dominance. In section 4.5, we explore the possibility to obtain high-multiplicity amplitudes from tree-level information of all saddle points, only. We succeed in all cases under considerations and find an appealing situation in non-Borel-summable models, where a non-perturbative (complex) saddle completely dominates the amplitudes. Some of the more technical aspects of our derivations are collected in 4.7. The observations of 4.4 and 4.5 will be the content of our upcoming publication [Fla16].

4.2 Review of Perturbative Series

The saddle point approximation (also referred to as “steepest descent” or “constant phase”) is widely applied in various fields of physics. In quantum

field theory, it is the way to obtain the perturbative series from the (Euclidean) path integral. As we will study the limits to perturbation theory and the relevance of non-perturbative contributions, it is worth to revisit the method.

In this section, we will quickly review the saddle point method and we point out how it naturally leads to resurgent transseries[4] for physical quantities. Much of the material in this section is covered in [Din73], with references to some more recent developments indicated specifically.

4.2.1 Saddle Point Method and Borel-Summation

As a model for a (Euclidean) path integral, consider the simple integral over an exponential of the form

$$Z = \int_{-\infty}^{\infty} d\phi \, e^{-S(\phi)} \tag{4.1}$$

where the action S is assumed to fall off sufficiently quickly. If $\tilde{S}$ has sufficiently deep minima, these (actually a certain set of saddle points) will dominate the integral. We can make the statement more precise if there is a small (positive) coupling constant λ, by which we can scale the exponent

$$Z = \frac{1}{\sqrt{\lambda}} \int_{-\infty}^{\infty} d\phi \, e^{-\frac{1}{\lambda}\tilde{S}(\phi)} \tag{4.2}$$

with $\tilde{S}(\phi)$ independent of λ. The prefactor $1/\sqrt{\lambda}$ is appropriate, if the quadratic term of $S(\phi)$ was canonically normalized. We will preserve the tilde on $\tilde{S}$ in the following paragraphs to remind the reader of the possibly relevant rescaling of the fields.

We will reformulate this integral and finally find that this formulation is equivalent to standard Borel-resummed perturbation theory. Going step by step, however, will naturally reveal that specific subleading saddle points with their respective perturbative series need to be included as well.

As a first step, we complexify the integration variable and identify all saddle points of the action in the complex plane. For simplicity, we will assume the saddles are isolated. We then construct contours through the saddle points, along which the imaginary part of the exponent is constant.

$$\mathrm{Im}(\tilde{S}/\lambda) = \text{const.} \tag{4.3}$$

[4] We will, however, not attempt to introduce J. Écalle's theory in full glory, but instead refer the reader to some mathematical review articles on the subject.

Two such contours pass perpendicularly through each saddle point. The real part of the exponent increases monotonically, away from the saddle point along one of the contours and decreases along the other. In a generic situation, the contour does not run into other saddle points. We will however come back to this important special case, later.

We can now continuously deform the initial integration path (initially along the real axis) in such a way that it runs along a set of constant phase contours. The integral can thus be computed as a sum of line integrals along constant phase contours. Not all saddle points of the action necessarily lie on this deformed integration path, however. Figure 4.1 illustrates the procedure: there, the integral can be computed as a sum of contour integrals along constant phase contours I and III (through saddles A and C). The contours of constant phase are also known as Lefschetz thimbles and Picard-Lefschetz theory is the branch of mathematics that studies such structures.

Let us now turn to the evaluation of a single integral along the constant phase contour γ through saddle point G. The treatment follows the elegant outline of [BH91]. The integral can be rewritten as

$$Z_\gamma = e^{-\tilde{S}_G/\lambda} \int_0^\infty ds\, e^{-s} \left[\frac{\sqrt{\lambda}}{\tilde{S}'(\phi_\gamma^+(s))} - \frac{\sqrt{\lambda}}{\tilde{S}'(\phi_\gamma^-(s))} \right] \tag{4.4}$$

where $\phi_\gamma^{+/-}(s)$ are the inverse functions on the contour γ in both directions, such that $[\tilde{S}(\phi_\gamma^{+/-}(s)) - \tilde{S}_G]/\lambda = s$. One can easily check that the term in square brackets is reproduced by another contour integral narrowly encircling an appropriate section of the original steepest descent contour.

$$Z_\gamma = e^{-\tilde{S}_G/\lambda} \int_0^\infty ds\, e^{-s} \frac{\sqrt{\lambda}}{2\pi i \sqrt{s}} \oint d\chi \frac{\sqrt{(\tilde{S}(\chi) - \tilde{S}_G)/\lambda}}{\tilde{S}(\chi) - \tilde{S}_G - \lambda s} \tag{4.5}$$

The square root is defined positive along one direction of the constant phase contour and is thus negative on the other side of the branch point, reproducing the necessary signs. The integrand of the second integral may be expanded in a power series in λs.

$$Z_\gamma = e^{-\tilde{S}_G/\lambda} \int_0^\infty ds\, e^{-s} \frac{1}{2\pi i \sqrt{s}} \oint d\chi \sum_{n=0}^\infty \frac{(\lambda s)^n}{(\tilde{S}(\chi) - \tilde{S}_G)^{n+1/2}} \tag{4.6}$$

If, on the one hand, we pull out the summation sign and perform the ds integral first, we arrive at a series representation for Z_γ. This interchange of integration and summation is usually not legal and, consequently, the resulting series is not convergent, but rather asymptotic (therefore no equality

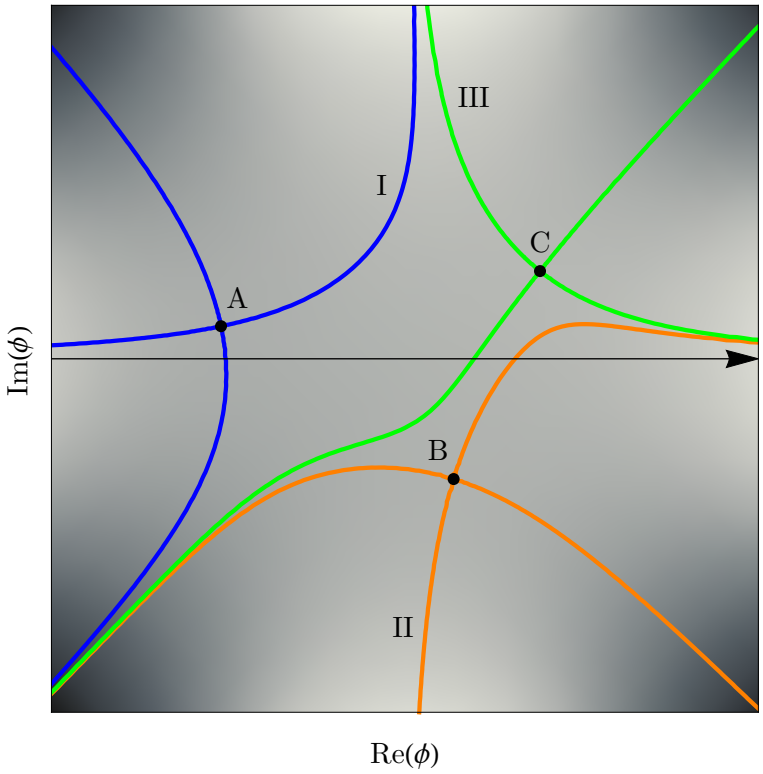

Figure 4.1: Illustration of the saddle point method with a polynomial action $\tilde{S}$ with complex coefficients (explicitly: $\tilde{S} = \phi^4 - 4\phi^3 + 5\phi^2 - 2i\phi$). The gray level represents its real part (lighter is bigger). The points A, B and C are saddle points of the action. The blue, orange and green curves are the lines of constant imaginary part of the exponent emanating from the respective saddles. Along the curves I, II and III, the real part of the exponent is monotonically decreasing and renders the line integral over $\exp(-\tilde{S}/\lambda)$ finite. In order to obtain the intended integration path (black arrow), contours I and III through saddles A and C need to be summed.

sign).

$$Z_\gamma \sim \sum_{n=0}^{\infty} a_n \lambda^n \quad \text{with} \quad a_n \equiv \frac{1}{2\pi i} \oint d\chi \frac{(n-1/2)!}{(\tilde{S}(\chi) - \tilde{S}_G)^{n+1/2}} \tag{4.7}$$

where the $d\chi$ integration loop may now be contracted to a small circle around the saddle point. This is the standard perturbative series at the saddle point G.

If, on the other hand, we only switch the $d\chi$ integration and summation in (4.6), we get an expression that is the Borel-summation of the previous series. This interchange of integration and summation is usually valid for at least a certain range of s and $\mathcal{B}Z_\gamma$ needs to be analytically continued along the real axis before performing the integral.

$$Z_\gamma = e^{-\tilde{S}_G/\lambda} \int_0^\infty ds\, e^{-s}\, \mathcal{B}Z_\gamma(s\lambda) \quad \text{with} \quad \mathcal{B}Z_\gamma(s) \equiv \sum_0^\infty \frac{a_n\, s^n}{n!} \tag{4.8}$$

Here we used the integral representation of the Euler beta function to trade powers of s against the argument of the factorial.

So, to summarize this short review,

- the perturbative series is only asymptotic
- its Borel-summation yields the value of contour integration along one steepest descent contour
- in order to reproduce the full integral, an appropriate set of saddle points with their corresponding steepest descent integrals (or equivalently, resummed perturbative series) needs to be taken into account.

For multi-dimensional integrals, the treatment is a bit more subtle and logarithmic terms arise as well. More details about these issues can be found in [How97].

The general structure of the result, consisting of power series, exponentials (in the case above), and logarithms (in the more general case), is known as a transseries of a resurgent function. On the mathematical side, Ecalle pioneered the investigation of such structures [Eca81] (see, e.g., [Dor14] for an accessible review and [Sau07] for a more mathematical flavor). The application of related ideas to physics started probably independently with the work of [Bog80; Zin81].

4.2.2 Stokes Phenomenon and Resurgence

Let us now emphasize a relation that connects the perturbation series from different saddle points.

When considering the Borel plane of complex parameter s, the form of (4.4) makes clear that the integrand has poles for those s corresponding to the difference in action with other saddle points. As long as these poles do not lie on the positive real axis, resummation is not hampered.

Asymptotics of high derivatives of $\mathcal{B}Z_\gamma(s)$, i.e. late perturbative coefficients a_n, are then dictated by the closest pole by Darboux' lemma [Dar] (see [KW89] for an elegant derivation). Explicitly, for a function of which the closest singularity near zero has the form $f(t) \sim c\,(s_0 - s)^{-w}$ the derivatives are

$$f^{(k)}(0) \approx c\,\frac{k!\,k^{w-1}}{\Gamma(w)\,s_0^{w+k}} \tag{4.9}$$

asymptotically for large k.

A closer analysis reveals that successively better approximations to high perturbative coefficients may be obtained by including not just the leading order information of the adjacent saddle points, but by using the next-to-leading, etc. information as well (see, e.g., [BDU13] for an illustrative example). The resulting relations are known as resurgence-relations, because they suggest that the same information is encoded in the perturbation series of all different saddle point. A more surprising manifestation of such resurgence has been found in quantum mechanics [ZJ04; DU14].

4.3 Amplitude-Analogs

In this section, we will introduce the amplitude analogs that we are going to consider in the rest of this chapter. In field theory, scattering amplitudes may be calculated from the partition function, which has the following path integral representation

$$Z(j) = \int D\phi\, \exp\left[\frac{i}{\hbar}\left(S + \int d^dx\, j\phi\right)\right] \tag{4.10}$$

where ϕ stands for the set of fields, j for the respective sources, and S for the local field theory action. Below, we will use units such that $\hbar = 1$. Usually, Wick rotation to Euclidean space is performed to give meaning to the formal path integral. The oscillatory exponent iS is thus replaced by the much better convergent Euclidean action $-S_\mathrm{E}$. The perturbative expansion

for Z contains all Feynman graphs. It is also useful to define the generating functional of connected diagrams

$$W(j) = -i \log Z(j) \tag{4.11}$$

In Euclidean space, we will omit the i from this definition $W_{\mathrm{E}} = -\log Z_{\mathrm{E}}$.

Amplitudes can be obtained from this generating functional

$$a(p_1, \ldots, p_N) = \frac{\partial}{i\,\partial j(p_1)} \cdots \frac{\partial}{i\,\partial j(p_N)}\, iW(j) \bigg|_{j=0} \tag{4.12}$$

where only the momenta of the participating particles p_i are indicated and other labels like helicity are suppressed. To be precise, the quantity a, above, is a connected Green's function and the LSZ-theorem for the calculation of scattering processes requires the residue of its on-shell pole in momentum-space. We will, however, still continue to use the term "amplitude", as is often done in the literature.

The models that we are going to consider are "field theories" in $0+0$ and $0+1$ dimensions - the former are integrals, the latter are quantum mechanical systems. The great advantage of using such models is that reference values for amplitudes are available, so that new calculational techniques can be assessed more easily.

In $0+0$ dimensions and with a single real scalar field, the exponent of the Euclidean action $\exp[-S_{\mathrm{E}}(\phi)]$ can be regarded as a (not yet normalized) probability distribution over the real line. Then the Euclidean partition function $Z(j)$ is nothing but the moment-generating function for this probability distribution. Its logarithm, $W(j)$, is the generating function of cumulants. Thus, the analog of high multiplicity amplitudes in $0+0$ dimensions are high-order cumulants. We will use the terms "cumulant" and "amplitude" interchangeably during the discussion. These toy models are also sometimes advertised as the zero-momentum sector of the path integral, but we would rather like to emphasize the formal similarities.

In $0+1$ dimensions, i.e., quantum mechanics, the connected generating functional is closely related to the ground state energy, E_0, which may be calculated from the Euclidean partition function with periodic boundary conditions in imaginary time (see e.g. [Col88]):

$$Z_T = \mathrm{Tr}\, e^{-HT} \tag{4.13}$$

Thus

$$E_0 = -\lim_{T\to\infty} \frac{1}{T} \log Z_T \tag{4.14}$$

Of course, the partition function may just as well be calculated in the path integral. So, high-multiplicity amplitudes have a formal analog in high derivatives of the ground state energy with respect to a static source. Naturally, the sources used for physical field theory scattering amplitudes are on-shell and therefore time-dependent. We will however restrict ourselves to static sources, because exact reference values can feasibly be obtained in this case.

In both, $0+0$ and $0+1$ dimensions, we do not ampute our amplitudes. In both cases, the difference amounts to a finite rescaling of the source. For field theory, more care should probably be taken.

4.4 Fate of Perturbation Theory

Here we want to gain a better understanding of the way in which perturbation theory breaks down for high-multiplicity amplitudes. One important reason for the breakdown is the rapidly increasing number of Feynman diagrams. For concreteness, we choose ϕ^4 integral. While this example has been considered numerous times before, e.g., [GV91; AH+01; HJ15], we nevertheless contribute some new observations as detailed below.

Because our focus is on combinatorics, we can use a $0+0$ dimensional toy model, i.e., a simple integral, in place of a field theoretic path integral [CLP78].

$$Z(j) = \int_{-\infty}^{\infty} d\phi \, \exp\left(-\frac{\mu^2}{2}\phi^2 - \frac{\lambda}{4!}\phi^4 + j\phi\right) \tag{4.15}$$

As mentioned above, the cumulants a_N of this integral are the equivalents to field theory amplitudes with N external legs. They can be computed perturbatively, in the familiar language of Feynman diagrams, as connected graphs where the propagators are all just $1/\mu^2$. The combinatorics, however, is the same as for ϕ^4 field theory.

$$W(j) = \log Z(j) = \sum_n a_{2n} \frac{j^{2n}}{(2n)!} \tag{4.16}$$

$$= \sum_n \left(a_{2n}^{\text{tree}} \frac{\lambda^{n-1}}{\mu^{6n-4}} + a_{2n}^{1-\text{loop}} \frac{\lambda^n}{\mu^{6n}} + \cdots\right) \frac{j^{2n}}{(2n)!} \tag{4.17}$$

Because of the Z_2 symmetry of the action, only even cumulants are nonzero. Below, we will use units in which $\mu = 1$ to simplify the results.

When using the saddle point approximation to this simple integral, just one saddle point contributes and the theory is Borel-summable. Nevertheless, we expect the perturbative expansion of a_{2n} in powers of λ to be an asymptotic expansion, only.

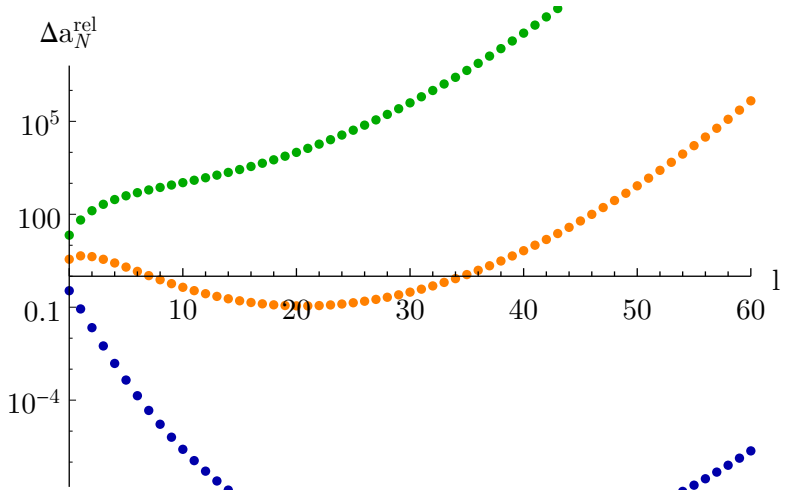

Figure 4.2: Relative error of the partial sums of the perturbative series (with respect to reference results) as a function of loop order l in the quartic integral with $\lambda = 1/25$. The three series of dots represent partial sums for the cumulants with $N = 6$ external legs (blue, bottom-most curve), $N = 16$ (orange, center), and $N = 26$ (green, top-most).

To streamline the presentation, we will postpone the discussion of our techniques used to calculate cumulants and their perturbative coefficients to section 4.7.

4.4.1 Qualitative Behavior

In figure 4.2, we display the relative error of partial sums of the perturbative series (4.17) for the cumulants as a function of loop order and for different multiplicities $N = 2n$.

In a weakly coupled theory, the naive expectation would see tree level as a first approximation, while the next few orders are expected to give subleading corrections that improve upon the result. Only if the series is summed past the term of smallest magnitude (point of optimal truncation), does the diverging nature beset calculations[5]. The figure (blue curve) confirms that the perturbative series for small N meets this expectation.

In an intermediate regime of N (orange curve), tree level ceases to be a good approximation to the actual result and the one-loop contribution even exceeds tree level. Nevertheless, summing up sufficiently many perturbative terms yields a satisfactory approximation to the cumulant. At higher loop

[5]Some form of this reasoning is, e.g., inherent in all tree-level unitarity arguments.

order, the series diverges again.

For even larger values of N, no partial sum of the perturbative series is faithful to the true cumulant (green curve).

That loop-level becomes as important as tree-level parametrically before $\lambda N = 1$, has already been observed for on-threshold-production in ϕ^4-theory [Vol93], but has apparently not been widely appreciated. The existence of the intermediate regime is noteworthy, because general considerations about the validity of perturbation theory must not be taken as evidence for the accuracy of often-used tree-level results.

Later, we will see that Borel-Padé resummation is a practical tool to obtain arbitrarily good approximations in all three regimes. And in the second half of the chapter, we will explore alternative methods to evaluate high-multiplicity amplitudes without calculating so many perturbative orders.

4.4.2 Regime Boundaries

One important task is to determine the boundaries between the three regimes described above, i.e., the critical value of the particle number at fixed coupling or vice versa.

In order to determine the limit of validity of tree level, we can compare the magnitude of the tree level with the one-loop contribution.

$$a_{2n}^{\text{tree}}\,\lambda^{n-1} \stackrel{!}{=} a_{2n}^{1-\text{loop}}\,\lambda^{n} \tag{4.18}$$

As soon as the latter exceeds the former, we should not trust the tree approximation any more.

We have been able to prove a new closed-form expression for the tree-level cumulants in the present theory

$$a_{2n}^{\text{tree}} = (-1)^{n-1}\frac{(3n-3)!}{(n-1)!\,6^{n-1}} \tag{4.19}$$

which at large number of particles becomes

$$a_{2n}^{\text{tree}} \xrightarrow{n\to\infty} \frac{4}{3\sqrt{3\pi}}\,(2n-2)!\left(\frac{9}{8}\right)^{n}\left[\frac{1}{\sqrt{n}} + \mathcal{O}(n^{-3/2})\right] \tag{4.20}$$

This asymptotic form was previously obtained in [GV91; Vol92].

We have also derived an asymptotic form for the one-loop coefficient of the cumulants

$$a_{2n}^{1-\text{loop}} \sim (-1)^{n}\frac{(3n)!}{n!\,6^{n}}\,\frac{1}{\sqrt{n}} \tag{4.21}$$

We, thus, get the critical number of external legs $N = 2n$ that marks the demise of the tree level approximation

$$N_{\text{crit}} \propto \lambda^{-2/3} \tag{4.22}$$

Numerical checks, of course, confirm this result.

It is significantly harder, to establish where perturbation theory, finally, breaks down. By standard reasoning, optimal truncation makes sense as long as there is a local minimum in the magnitude of the l-loop contribution with respect to l (compare the shapes of curves in figure 4.2).

$$\frac{\partial}{\partial l}\, a_{2n}^{(\mathrm{l})}\, \lambda^{n-1+l} = 0 \tag{4.23}$$

Therefore, we use the point where this minimum disappears to determine the second regime boundary. Alternatively, we may write

$$\log \lambda_{\text{crit}} = -\min_{l} \frac{\partial \log a_{2n}^{(l)}}{\partial l} \tag{4.24}$$

We have found approximations for the perturbative terms a_{2n}^{l} that become better as the loop order is increased (see section 4.7.1). The leading-order approximation of this sort is

$$\left(a_{2n}^{(l)}\right)_{\text{lo}} \approx \frac{(-1)^{l+n}}{2^{n+2l-2}\, 3^{n+l-1}} \frac{(2n+2l-3)!!\,(4n+4l-5)!!}{(n+2l-2)!} \tag{4.25}$$

Using this expression in (4.23) and expanding for large $N = 2n$ indicates that the asymptotic critical relation is

$$N_{\text{crit}} \propto 1/\lambda \tag{4.26}$$

with a constant of proportionality of 8/9. This is an indication rather than a proof, because we would still need to establish that the leading order approximation (4.25) is sufficiently accurate. Instead, we will rely on numerical calculations to corroborate this relation.

Figure 4.3 shows the critical values λ_{crit} as a function of N, obtained using (4.24), in a doubly logarithmic plot. A linear fit to the data points is also included. As the fit reproduces the data points extremely well, its slope -1.006 forcefully supports the conjectured regime boundary (4.26). Even the exponent of the intercept 0.882 is in good agreement with the constant of proportionality obtained analytically.

To summarize,

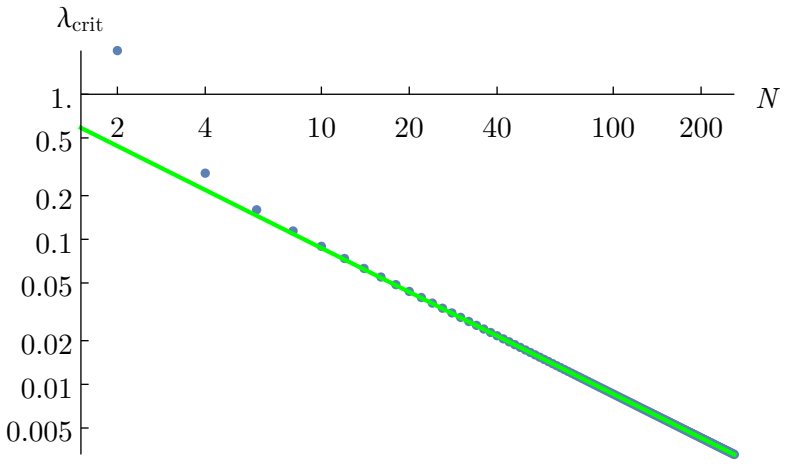

Figure 4.3: Critical coupling of the breakdown of perturbation theory (second regime boundary) as a function of the multiplicity. Obtained directly from the perturbative coefficients on the basis of (4.24). The green line is a linear fit to the doubly-logarithmic data points that has a slope -1.006 and intercept -0.125.

- for few external legs $n \lesssim \mathcal{O}(\lambda^{-2/3})$, the naive assumptions about perturbation theory are valid.
- for intermediate values of N, tree level results may be off by many orders of magnitude, but perturbation theory gives a good approximation when sufficiently many loop orders are taken into account.
- for a large number of external legs $N \gtrsim \mathcal{O}(1/\lambda)$, perturbation theory breaks down and resummation or completely different methods are required.

4.4.3 Physical Picture

While it may be too early to draw physical conclusions, the appearance of a critical point at $\lambda N \sim 1$ allows us to highlight the parallel with the critical point of the Bosonic system studied in the previous chapters.

We can paint a tentative physical picture for high energy scattering processes that is consistent with our results. In a high-energy collision, one should focus on the interaction volume. As particles are produced in the collision, as soon as their number in the interaction volume exceeds $\lambda N \sim 1$, we expect collective effects to become important. This may imply unstable behavior as described in 2.8.1 and, most probably, a fast quantum break time.

Then it is natural to expect that perturbation theory does not give useful results any more, which is just, what we have observed.

4.4.4 Resummation

After having studied the perturbative series and its demise in so much detail, we will now try to obtain accurate results from the perturbative coefficients. This is an application of known techniques, but we will make an interesting observation in the process.

As we have seen in 4.2, Borel-resummation is, in principle, suited to obtain the exact result. A direct application of the Borel transform and a Laplace re-transform to a truncation of the perturbative series, however, does not improve upon the result. Together, both operations leave a polynomial invariant. We need a more powerful method to approximate the Borel-plane function outside its circle of convergence.

In the past, Padé approximants have already proven handy in resummation (a recent example is [AW12]), and we follow the same strategy, to find a Padé approximant for the Borel transform of the truncated series, before applying the inverse Laplace transform. A Padé approximant is a rational function of the form

$$\mathcal{P}_{(n,n)}f(s) = \frac{\sum_{k=0}^{n} a_k\, s^k}{1 + \sum_{k=1}^{n} b_k\, s^k} \tag{4.27}$$

that coincides with $f(s)$ in the first $2n+1$ Taylor coefficients. Padé approximants are useful, because they can, to some extent, reconstruct the pole structure of f, even when only a limited number of Taylor coefficients are known. In the inverse Laplace transform, care must be taken to select an integration path that does not miss some of the reconstructed poles.

In figure 4.4, we highlight how Borel-Padé resummation really yields extremely precise results, when many perturbative terms are included. It must, however, also be noted that a sufficient number of terms have to be used to achieve better than order-one results. For high-multiplicity amplitudes this minimum number is already quite demanding.

An important observation can be made in the Borel-plane. On the negative real axis of the Borel-plane (complex variable s), there is an expected singularity corresponding to the non-perturbative saddles of this theory. The location of these saddles in ϕ is purely imaginary and their steepest descent contours do not contribute directly in this model. Through resurgence relations, they are, however, strongly intertwined with late perturbative coefficients.

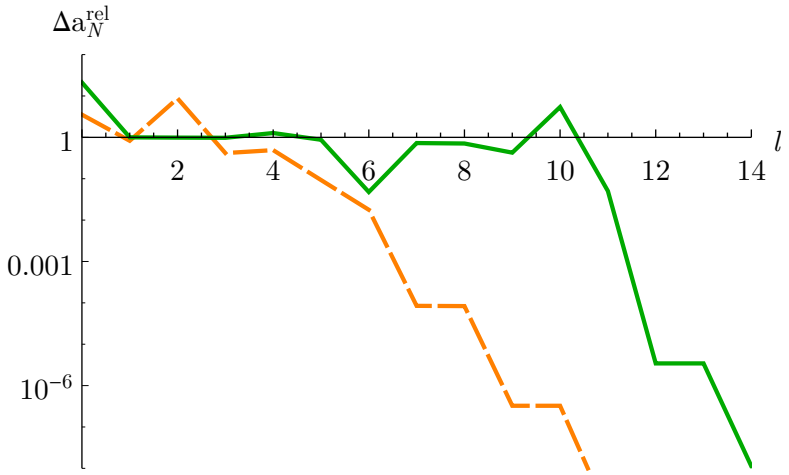

Figure 4.4: Relative error of the Borel-Padé resummation of the cumulants as a function for the loop order to which the approximation was calculated. The parameters match figure 4.2 with $\lambda = 1/25$ and $N = 16$ for the orange, dashed curve and $N = 26$ for the green curve.

It is a formal, but interesting, observation that for higher cumulants, these poles in the Borel plane are also of higher order. Which is to say, the Borel transform of the cumulant a_N generically looks like

$$\mathcal{B}\, a_N \sim \frac{1}{(s - S_{\mathrm{np}})^{N/2+1}} \tag{4.28}$$

at the pole in the Borel parameter s. The resurgence relations have to be adapted accordingly. To be precise, for the ϕ^4-model the analytic structure can be evaluated exactly. In this case, it is actually a pole of order $N/2$, superimposed with the start of a branch cut.

The higher-order nature of the pole in the Borel plane (convolutive model), is a reflection of the fact that the perturbation series around the "non-perturbative" saddle starts at negative order for higher cumulants

$$a_N^{\mathrm{np}} = e^{-S_{\mathrm{np}}} \sum_{k=0}^{\infty} c_k\, \lambda^{k-N/2} \tag{4.29}$$

This in turn can be explained by the fact that the derivatives $\partial/\partial j$ also act on the saddle action in the exponent and bring down successive inverse powers of the coupling. This phenomenon is important, because sufficiently high inverse powers in λ can overcome the non-perturbative exponential suppression. We take it as a first indication that non-perturbative saddle points might take center-stage for high-multiplicity amplitudes and will actually observe this in practice in section 4.5.2.

4.5 Resurgence of High-Mult. Amplitudes

Previously we have been occupied with the perturbative series of high multiplicity amplitudes in a zero-dimensional model. Now, we will turn to the actual physical values of amplitudes, exemplified in integrals and a quantum mechanical (i.e. one-dimensional) model. Quite surprisingly, we see that, in all cases we have considered, the value of the amplitudes can be approximated with only the knowledge of the tree-level approximation to all (nonperturbative) saddle points. This phenomenon is quite distinct from standard resurgence relations, that connect late perturbative orders (in the coupling) with early terms in the expansion about nonperturbative saddles. We will, therefore, refer to our new observation as "resurgence of high-multiplicity amplitudes".

First, we will again consider the quartic integral from the previous sections. Then we change the situation to be non Borel-summable and take a closer look at cumulants of the non-degenerate double well. Finally, we generalize this consideration to quantum mechanics and look at a quantum mechanical particle in a non-degenerate double-well potential. In the two latter models, the correct saddle-point approximation contains exponentially suppressed contributions from "nonperturbative" saddles. Though still exponentially suppressed, these come to dominate high multiplicity amplitudes.

While we do not yet have a unified description for the three manifestations we studied, it is nevertheless suggestive that the phenomenon itself should have broader import, likely also for field theoretic calculations in more than one dimension.

4.5.1 Quartic Integral Cumulants

For a first occurrence of resurgence of high-multiplicity amplitudes, let us consider the integral with quartic action (4.15), again. We have seen in section 4.4.1 that perturbation theory "breaks down" for high multiplicity amplitudes, as soon as the effective coupling λN exceeds unity. We have also seen that the physical values of the amplitudes could still be recovered from the perturbative series by Borel or, in practice, Borel-Padé summation (therefore the quotation marks around the "breakdown"). The procedure, however, was very tedious and required many terms in the perturbative series, a requirement that would be hard to fulfill in an actual $3+1$ dimensional field theories.

Here we will go down another route and see how to achieve an approximation to the high order cumulants/amplitude-analogs (4.16) directly. After the fact, we became aware that some of the arguments of the following dis-

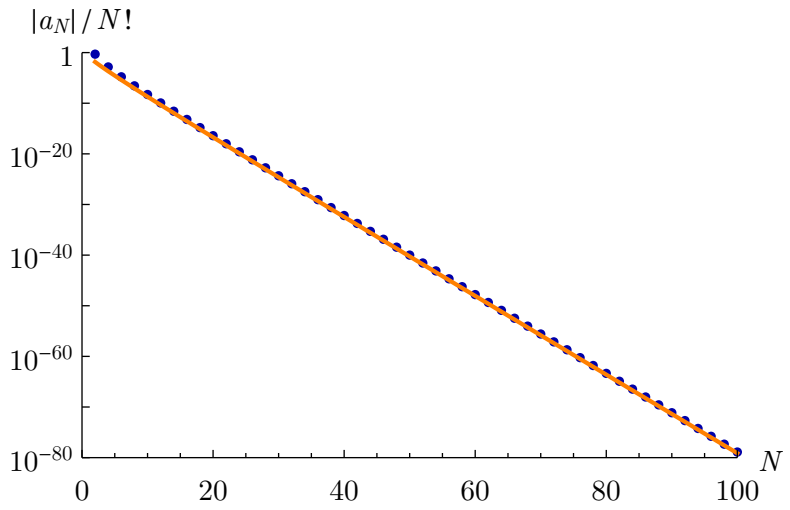

Figure 4.5: Numeric absolute values of the cumulants (rescaled by $N!$) of the quartic integral as a function of the number of external legs N for $\lambda = 1/25$ (blue dots). The orange line is a prediction based only on tree-level approximations to the saddle points.

cussion were already formulated in [GV91], as we will indicate below.

In figure 4.5, we present a logarithmic plot of the reference values for the cumulants (obtained using the techniques of 4.7.1) rescaled by $N!$. It is clear that they follow an exponential law to good accuracy. The orange line is not a fit to the data, but a prediction based only on tree-level knowledge. The rest of this section explains, how it can be obtained.

Recall that the cumulants/amplitudes are defined as derivatives of the generating function $W(j)$. An asymptotic behavior of factorial-times-exponential type in high derivatives is, of course, reminiscent of the Darboux theorem (4.9), which states that high derivatives are dominated by the position and behavior of closest pole or branch cut in the function. It remains to be explained, however, why and where $W(j)$ is singular in the source j. For real values of source and the coupling, $Z(j)$ is obviously positive and nonsingular. For complex values of the source, however, the partition function $Z(j)$ may vanish exactly and W then incurs a logarithmic branch cut.

To understand the vanishing of $Z(j)$, let us analyze the steepest descent contours for the integral. For any real j, there is one saddle point on the real line and its steepest descent path is identical to the originally intended integration contour. If we consider purely imaginary values of the source $j = ij_{\text{im}}$, however, this saddle point moves into the complex ϕ-plane as

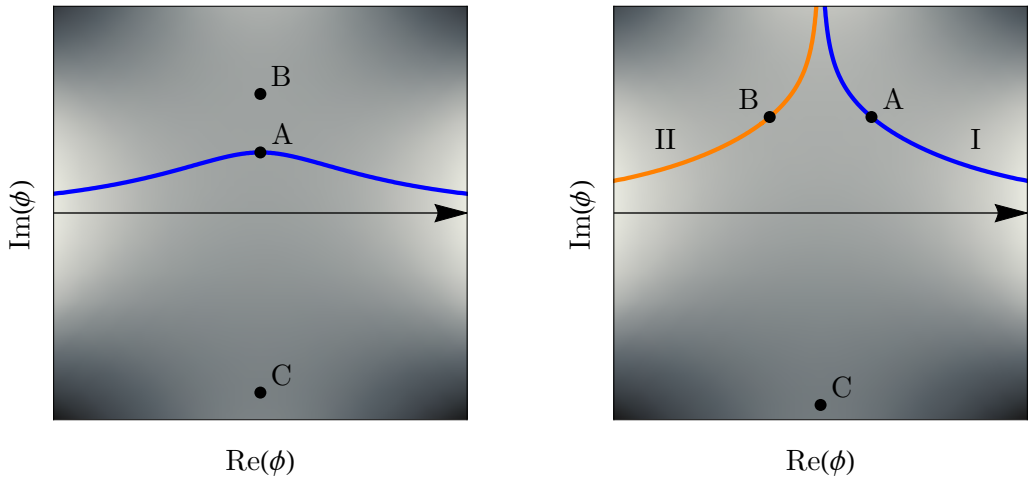

Figure 4.6: Saddle points and relevant steepest descent contours in the quartic integral ($\lambda = 1/25$) for two different values of purely imaginary source. Before the bifurcation, all saddles lie on the imaginary axis (left for $j = 4i$), after, two move out and both their steepest descent contours become relevant (right for $j = 7i$).

we increase j_{im} and the integral acquires an imaginary part. For even larger values of j_{im}, the perturbative saddle and one complex nonperturbative saddle bifurcate[6]. Afterwards, both saddles take symmetric positions in the complex plane and both of their steepest descent contours need to be taken into account to calculate $Z(ij_{\text{im}})$. This situation is depicted in figure 4.6.

$$Z(j = ij_{\text{im}}) = \int_{\text{I}} d\phi\, e^{-S_j} + \int_{\text{II}} d\phi\, e^{-S_j} \tag{4.30}$$

Due to the symmetry of the action in the complex ϕ-plane for purely imaginary source, the integrals along the two saddle point contours I and II produce values that are exactly complex conjugate to each other. Thus, $Z(j)$ is real and has a zero when the real part of the integrals (4.30) vanishes. The cumulant generating function $W(j)$ naturally has a logarithmic singularity, there.

The associated (purely imaginary) value of $j = ij_{\text{crit}}$ can be approximated from the leading order of perturbation theory

$$\text{Re} \int_{\text{I}} d\phi\, e^{-S_j(\phi)} \Big|_{j=ij_{\text{crit}}} \approx \text{Re} \sqrt{\frac{2\pi}{S_j''(\phi_{\text{A}})}}\, e^{-S_j(\phi_{\text{A}})} \Big|_{j=ij_{\text{crit}}} \stackrel{!}{=} 0 \tag{4.31}$$

[6]This point has strong implications for the asymptotics of tree-level amplitudes as was emphasized in [GV91].

Equipped with the knowledge, where $W(j)$ has a logarithmic singularity, we can predict the asymptotics of the (even) cumulants using Darboux theorem

$$a_N/N! \approx \frac{(-1)^{N/2+1}}{N\, j_{\text{crit}}^N} \tag{4.32}$$

In figure 4.5, we have already seen that this expression predicts the cumulants very well. In table 4.1, we compare the values of j_{crit} determined by a fit to reference values with the values from the leading order saddle point approximation (4.31). Arguably the accuracy of our prediction is satisfactory for a leading order calculation, although it seems to. Higher accuracy may, of course, be achieved by substituting successively better approximations in (4.31).

λ	0.1	0.05	0.02	0.01	0.005	0.002	0.0001
$j_{\text{crit, ref}}$	4.377	5.461	7.731	10.353	14.102	21.634	30.221
$j_{\text{crit, pred}}$	4.366	5.452	7.730	10.377	14.180	21.810	30.464

Table 4.1: The value of j_{crit} in (4.32) that determines the asymptotics of quartic cumulants. Comparison between the numerical reference value and the tree-level prediction.

The zero in $Z(j)$ was already observed numerically by Goldberg and Vaughn [GV91], who also foresaw that it would determine high multiplicity amplitudes. They did, however, not realize that its position could be predicted from appropriate tree-level information, which is the main theme of the present discussion.

While we have expended much energy in the previous section to obtain perturbative coefficients for the high order cumulants - even before resummation -, we have now obtained a surprisingly good approximation for the actual value of the cumulants. For this approximation, we just used the leading order perturbative coefficients of the saddle points, as well as knowledge, how the different saddles interact.

4.5.2 Double-Well Integral Cumulants

Above we have studied the cumulants of a zero-dimensional field theory model that is Borel-summable. We were able to approximate cumulants from knowledge of the interplay of (complex) saddle points and leading order perturbative information. Here we will turn to a non-Borel-summable case and see that the situation in this model is conceptually even simpler.

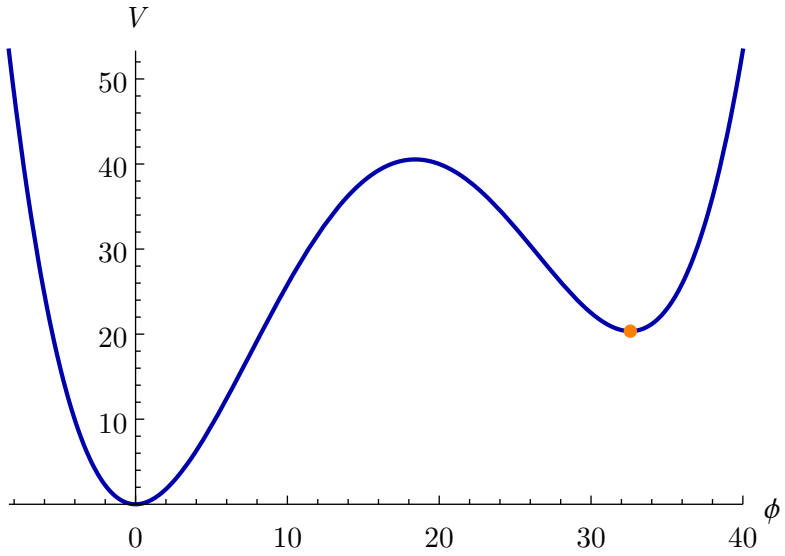

Figure 4.7: Action (or, for $0+0$ dimensions, equivalently "potential") as a function of the integration variable of the zero dimensional amplitude. The orange dot indicates the nonperturbative saddle point.

For now, we stay with a zero-dimensional model, but use a non-degenerate double-well action (see fig. 4.7).

$$Z(j) = \int_{-\infty}^{\infty} d\phi \, \exp\left(-\frac{\mu^2}{2}\phi^2 + \frac{\tau\lambda}{3!}\phi^3 - \frac{\lambda^2}{4!}\phi^4 + j\phi\right) \tag{4.33}$$

The action $S(\phi)$ is plotted in figure 4.7. It has a global minimum at $\phi = 0$ and a local minimum. It is clear that the decomposition of the integration path into steepest descent thimbles must take contours through both saddles into account. A clearer view of the involved paths can be gained by adding small imaginary parts to the parameters and the situation can be deformed to look very similar to figure 4.1.

The partition function $Z(j)$ can thus be written as a sum of two steepest descent integrations. One through the absolute minimum (perturbative saddle) and one associated with the second minimum (nonperturbative saddle), where the latter contribution is exponentially suppressed $\exp(-S_{\text{np}})$ by the saddle action.

For the cumulant generating function $W(j) = \log Z(j)$, the logarithm can be expanded, treating the nonperturbative exponential as a small parameter. The result is a sum of all different powers of $\exp(-S_{\text{np}})$, each accompanied by a power-series in the coupling λ. A full-blown trans-series structure. To obtain very precise results, each power-series needs to be resummed in turn.

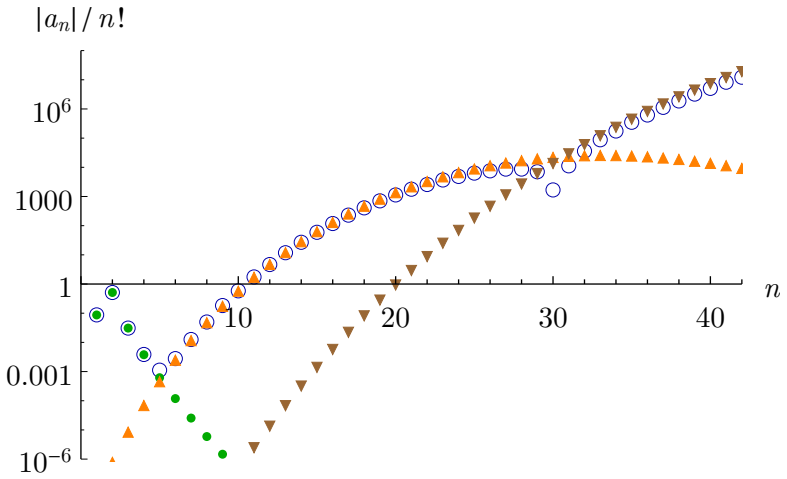

Figure 4.8: Comparison of contributions to the amplitudes of the zero-dimensional non-degenerate double-well integral (4.33) with parameter choices $\lambda = 1/10$, $\tau = 17/10$. Empty blue circles represent numerical reference values; green dots are resummed perturbative contributions; orange triangles are nonperturbative saddle contributions; brown inverted triangles are contributions from the square of the non-perturbative saddle.

For our purposes, however, we will only use the tree-level approximation to the nonperturbative contributions

$$a_n^{(\mathrm{np},1)} = \frac{d^n}{dj^n} \frac{1}{\sqrt{S''_{\mathrm{np}}}} e^{-S\mathrm{np}} \tag{4.34}$$

and similarly for the contribution from the second nonperturbative power $a_n^{(\mathrm{np},2)}$.

In figure 4.8, we compare the reference values for the cumulants, shown as blue circles, with different contributions (see section 4.7.2 for details on the calculations). The resummed perturbative series is plotted as green dots. The lowest order nonperturbative terms (4.34) are displayed as orange triangles and the second order nonperturbative terms $a_n^{(\mathrm{np},2)}$ as brown inverted triangles.

For very low multiplicity amplitudes, the (resummed) perturbation theory agrees very well with the reference values and the error is exponentially small - consistent with the nonperturbative saddle contribution. But what we can clearly take away from this figure is that, for higher cumulants, the dominant contribution comes from the nonperturbative saddle (later even

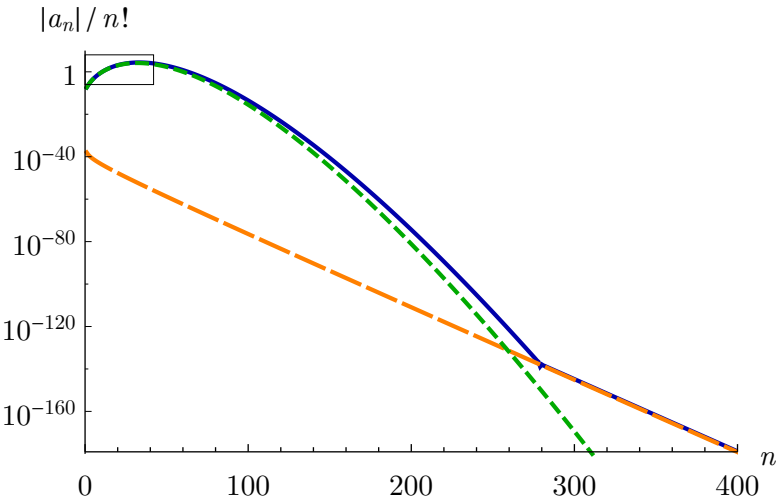

Figure 4.9: Asymptotic behavior of the first nonperturbative contribution $a_n^{(\mathrm{np},1)}$ to the zero dimensional amplitudes. Actual values (blue curve), as well as far asymptotics (orange, long dashes) and derivative acting repeatedly on exponent (green, short dashes). The small rectangle indicates the detail visible in fig. 4.8.

the second order nonperturbative term). What is even more striking is that the plot contains the contribution from the leading order about the saddle point, only. The emerging picture is therefore similar to the previous model insofar as tree level information from all saddles is sufficient. It is much simpler, however, in another respect, as the contribution of the nonperturbative saddle, alone, dominates the amplitudes.

It is also quite interesting to see how the shape of the nonperturbative contribution $a_n^{(\mathrm{np},1)}$ comes about. Figure 4.9 illustrates its behavior. While the far asymptotics matches the prediction from the nearest singularity in $\exp(-S_{\mathrm{np}})/\sqrt{S''_{\mathrm{np}}}$ using Darboux theorem, the relevant part of the curve is explained by another effect. Acting repeatedly on the exponent with $\partial/\partial j$ gives

$$a_n^{(\mathrm{np},1)} \approx \frac{1}{\sqrt{S''_{\mathrm{np}}}} \left[\partial_j S_{\mathrm{np}}\right]^n e^{-S\mathrm{np}} \tag{4.35}$$

and reproduces the observed behavior well. This form is the counterpart to the higher-order pole in the Borel-plane that we discussed in section 4.4.4.

4.5.3 Quantum Mechanical Double-Well

Finally, we turn our attention to a quantum mechanical model. As discussed before, the appropriate analogs of high multiplicity amplitudes are high derivatives of the ground state energy in a quantum mechanical system.

Previously, we have studied both, a Borel-summable and a non-Borel-summable case and found that high multiplicity amplitudes could be determined with only leading order (in the coupling) information of all saddle points. In the latter case, the application to quantum mechanics seems simpler, as the high multiplicity amplitudes are dominated by the nonperturbative contribution (in its lowest perturbative approximation) alone. We will therefore consider a non Borel-summable case in which the nonperturbative saddle contribution is known.

We will even take the direct generalization of the double-well example in the form of a quantum mechanical particle in the non-degenerate double-well potential, governed by the Hamiltonian

$$H = -\partial_\phi^2 - \phi^2 + \beta\,\phi^4 + (j_0 + j)\phi \tag{4.36}$$

where a rescaling of ϕ and the energy were used to set the kinetic and harmonic prefactors to unity, for convenience. The constant β is the quartic coupling, while j_0 is the lifting of the minima, and j the source.

It has already been found a long time ago by Balitsky and Yung that a nonperturbative saddle point contributes in the path integral for physical quantities, like the ground state energy [BY86]. It is well known that the decay of a state in the false vacuum is governed by a bounce field configuration (see [Col77] for a lucid explanation and the famous application to field theory). The bounce starts in the false vacuum, runs up to the turning point with equal potential and back again. Balitsky and Yung noticed that the analytically continued field configuration, actually contributes as a relevant saddle point to the path integral of the model. This complex bounce starts in the absolute minimum and runs to a complex turning point and back again and is illustrated in figure 4.10. It may be interpreted as a complex instanton/anti-instanton pair and the vacuum of the non-degenerate double-well may be viewed to contain a dilute gas of these molecules. See [BD+15] for a recent analysis in the context of resurgence.

They explicitly calculated the contribution to the ground state energy due to the dilute gas of these pairs. The main complication in the calculation arises from the fact that the separation between instanton and anti-instanton costs very little energy and cannot be treated in the Gaussian approximation. A more thorough quasi-zero-mode integration is required. Actually, when j_0

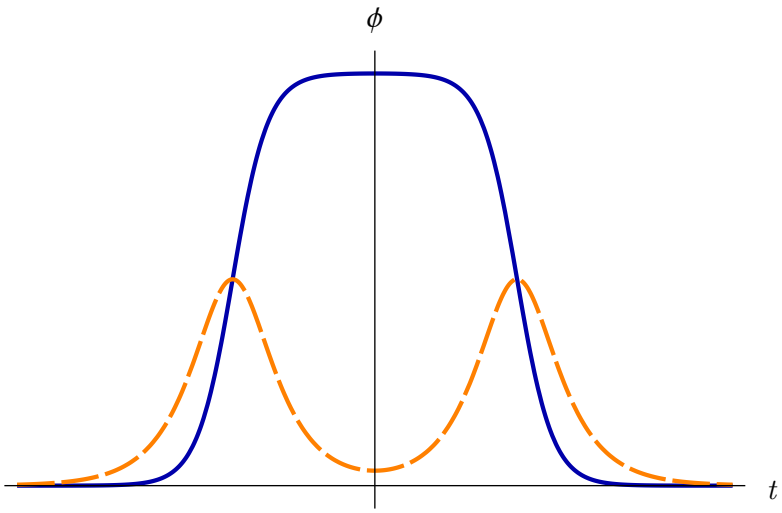

Figure 4.10: Complex saddle point field configuration of the non-degenerate double-well (blue curve is real part; orange, dashed curve imaginary part). It can be interpreted as an instanton/anti-instanton bound state, where the instanton interpolates between the absolute minimum of the potential and a complex turning point.

is reduced and the minima become degenerate, the binding potential between instanton and anti-instanton vanishes, the molecular gas makes way for a plasma of liberated instanton/anti-instantons and some physical effects (e.g., level-splitting) become suppressed by only a single instanton action.

In our conventions, the nonperturbative contribution to the ground state energy reads

$$E^{\text{np}} = 2^{-\frac{5(j_0+j)}{4\sqrt{\beta}}+3}\,\beta^{\frac{(j_0+j)}{2\sqrt{\beta}}-1}\,e^{-\frac{2\sqrt{2}}{3\beta}}\,\Gamma\!\left(\frac{j_0+j}{2\sqrt{\beta}}\right)\cos\!\left(\frac{j_0+j}{2\sqrt{\beta}}\,\pi\right)\times[1+\mathcal{O}(\beta)] \quad (4.37)$$

The cos in our expression is the continuation of $(-1)^p$ from [BY86] to noninteger p. The $e^{\cdots}$ is the standard instanton/anti-instanton suppression factor of the double well problem. The factor $1+\mathcal{O}(\beta)$ is a reminder that this expression is the leading term of yet another asymptotic series in the coupling. The factor $\Gamma(\cdot)$ comes from the integration of the size "modulus" or quasi-zero-mode.

In figure 4.11, we compare the different contributions to the amplitudes with reference values, again. Resummed perturbative values and derivatives of (4.37) are shown. The latter represent tree-level information of the saddle (including, however, the quasi-zero-mode integration). Calculational details

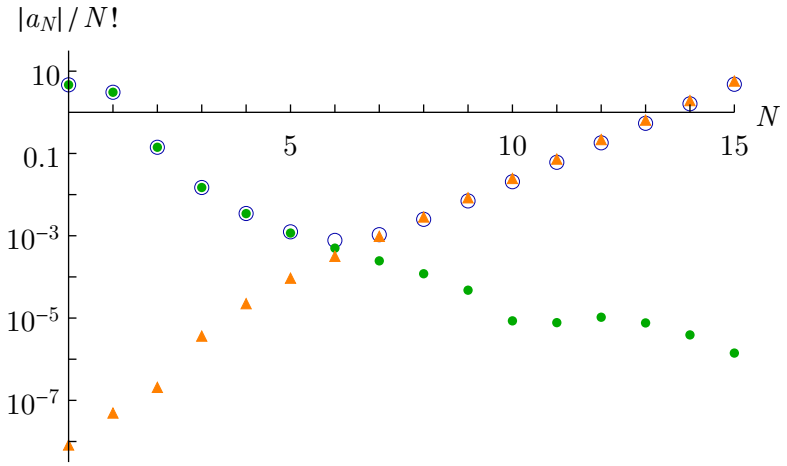

Figure 4.11: Comparison of contributions to the amplitudes of the quantum-mechanical non-degenerate double-well system with parameter choices $\beta = 1/20, j_0 = 3/\sqrt{80}$. Empty blue circles represent numerical reference values; green dots are resummed perturbative contributions; orange triangles are nonperturbative saddle contributions.

about the reference values and perturbation theory may be found in section 4.7.2.

It is obvious that perturbation theory gives very good answers at small coupling, where the deviations are exponentially small and approximately explained by the leading nonperturbative contribution. At larger multiplicity, the amplitudes are, again, dominated by the nonperturbative values. The observed deviations in this region are consistent with perturbative corrections to the saddle, $\mathcal{O}(\beta)$ suppressed.

We can, again, wonder, how the qualitative behavior of the derivatives of the nonperturbative contribution can be explained. Unlike in the previous case, this time it is the pole in the Γ function of (4.37), that determines the growth through the Darboux theorem. This pole at $j_0 + j = 0$ is related to the phase transition from the molecular gas to the plasma of instantons and anti-instantons. Just as we have done for the figure, one may, however, calculate the derivatives without any knowledge of this transition.

So in this quantum mechanical example, as well, tree level information of the saddle points of the path integral was enough to determine high multiplicity amplitudes. Like in the previous case, their physical value was dominated by the contribution of the nonperturbative saddle, alone. The simplicity of

this observation is promising for field theoretic calculations, as we will discuss next.

4.6 Outlook

In the first half of this chapter, we have elucidated the breakdown of perturbation theory due to the growing combinatorics in a field theory toy model. We have seen that the tree level approximation cannot be trusted even before perturbation theory breaks down. The critical multiplicity for the breakdown of perturbation theory is strongly reminiscent of the quantum collective effects studied in the previous chapters. It would be very interesting to gain more physical insight into the nature of this phenomenon for an actual field theory.

In the second half of the chapter, we have considered the physical values for the amplitudes directly. In an approach that resembled experimental mathematics, we have been able to predict high multiplicity amplitudes in all models under consideration to surprising accuracy. Our only input was tree-level information of all saddle points of the respective theories. In the non-Borel-summable models, our observation is even more striking. There, we have found the non-perturbative saddle point, alone, to dominate high-multiplicity amplitudes. We should stress that we were working in a "topologically trivial" sector each time. So standard perturbation theory gives a contribution, but is overwhelmed by the non-perturbative one.

We will now briefly outline, how these ideas might manifest themselves in field theory. It seems especially promising to consider field theoretic models, in which non-perturbative (possibly complex) saddle points make a real-valued contribution to physical quantities. Such saddles have been studied quite intensely, recently [DU12; BP+15; BD+15], in the context of resurgence. Our hope is that such non-perturbative saddles would, again, dominate high-multiplicity amplitudes.

The most direct application of our ideas might use the field theory of a real scalar with a non-degenerate double-well potential. In [Vol92], Voloshin observed that, as a function of a constant source, the energy has a branch cut. The cut starts, where the source renders the two vacua degenerate, because beyond that point, the original vacuum becomes meta-stable. Similar to our argument in 4.5.1, the position of this branch cut determines high-multiplicity amplitudes (for constant sources). It is not known, which saddle points need to be taken into account for the path integral in the true vacuum for the non-degenerate case[7]. We find it plausible that a complex saddle point similar

[7]There are very few field theories, for which such insights are available [Wit11].

to the one of 4.5.3 (in form of a complex bubble) exists and contributes. If such a solution can be constructed[8], one could calculate high derivatives of its contribution and compare to the prediction made by Voloshin[9]. If the amplitudes coincide (including prefactors), this might establish the role of the complex bubble.

We should note that our proposed method of calculating the saddle-point contribution for small, but arbitrary, source is related to the technique using "distorted instantons" of [LVV90]. At the same time, we need to stress that our calculations were in the topologically trivial sector, where there was no a-priori reason for the perturbative contribution to be sub-dominant.

In drawing a connection with our earlier investigations of black holes, we also want to mention gravitational scattering (see [Gid13] for a review and further references). The formation and evaporation of (micro) black holes in particle collisions is probably also a large-N scattering process and has recently been addressed in [DG+15]. Our observations about high-multiplicity scattering may also be relevant to these problems and other forms of UV-completion by classicalization [DG+11].

Independent of this specific application, we also want to draw attention to the fact that high-multiplicity amplitudes seem to be a great application for concepts of resurgence theory. They are a field of study, where non-perturbative contributions are not just important for the sake of having a complete understanding and cancelling exponentially suppressed imaginary parts. Instead, the non-perturbative saddles dominate these physical quantities.

4.7 Technicalities and Proofs

In this section, we have collected the more interesting techniques and proofs used to obtain the results of this chapter. Most of these methods represent generalizations of known techniques.

4.7.1 Quartic Integral

First, we will present the methods for the quartic integral (4.15). We will outline, how reference values for the cumulants were obtained. Then we will

[8] We have conducted some numerical experiments in this regard, with encouraging outcome.

[9] The process described by us is similar to, but distinct from, scattering within the false vacuum [Vol91].

turn to the perturbative coefficients for the cumulants and exhibit, how they were calculated and we will prove an exact form for the tree-level cumulants and an asymptotic one for the one-loop cumulants. We will also study, how perturbative coefficients at large loop-order behave.

Reference Cumulants

In calculating reference values for the cumulants of the quartic integral, we profit from the fact that at least the normalized moments have an expression in terms of special functions

$$\bar{\mu}_n = \sqrt{2}\,\Gamma(\tfrac{n+1}{2})\frac{(\frac{6}{\lambda})^{(n-1)/4}\,e^{-3\lambda/4}\;\mathrm{U}(\frac{n+1}{4},\frac{1}{2},\frac{3}{2\lambda})}{\mathrm{K}_{1/4}(\frac{3}{4\lambda})} \quad \text{for} \quad n\in 2\mathbb{N} \tag{4.38}$$

where K is the Bessel function and U the Tricomi confluent hypergeometric function. These can then be evaluated numerically to arbitrary precision. The odd moments naturally vanish. The reference cumulants can thus be obtained from their standard recursion relation

$$a_n = \bar{\mu}_n - \sum_{m=1}^{n-1}\binom{n-1}{m-1} a_m\,\bar{\mu}_{n-m} \tag{4.39}$$

Perturbative Coefficients

In order to calculate the perturbative coefficients of the cumulants, we used a recursion relation. The generating function W satisfies the Schwinger-Dyson equation

$$-\frac{1}{\mu}\frac{dW}{d\mu} = \left(\frac{dW}{dj}\right)^2 + \frac{d^2W}{dj^2} \tag{4.40}$$

Similar to [AH+01], we can obtain recursive stepping equations for the cumulant coefficients. After inserting the expansion (4.16) and comparing orders in j, we get

$$a_{2n}^{\text{tree}} = \frac{1}{2n-4}\sum_{m=1}^{n-2}\binom{2n}{2m+1} a_{2m+2}^{\text{tree}}\,a_{2n-2m}^{\text{tree}} \tag{4.41}$$

$$a_{2n}^{1-\text{loop}} = \frac{1}{n}\sum_{m=0}^{n-2}\binom{2n}{2m+1} a_{2m+2}^{1-\text{loop}}\,a_{2n-2m}^{\text{tree}} + \frac{1}{2n}a_{2n+2}^{\text{tree}} \tag{4.42}$$

For the tree coefficients with $n > 2$ and the 1-loop coefficients. These equations are used in the closed form derivations below.

The general form of the stepping equation for l-loop cumulant coefficients reads

$$a_{2n}^{(l)} = \frac{1}{2n+4l-4}\Bigg[2\sum_{m=0}^{n-2}\binom{2n}{2m+1}a_{2m+2}^{(l)}a_{2n-2m}^{\text{tree}} + \sum_{k=1}^{l-1}\sum_{m=0}^{n-1}\binom{2n}{2m+1}a_{2m+2}^{(l-k)}a_{2n-2m}^{(k)} + a_{2n+2}^{(l-1)}\Bigg] \tag{4.43}$$

Tree-Level Cumulants

The sequence of tree level cumulants is given by the closed form expression

$$a_{2n}^{\text{tree}} = (-1)^{n-1}\frac{(3n-3)!}{(n-1)!\,6^{n-1}} \tag{4.44}$$

This corresponds to the integer sequence OEIS A025035 up to alternating signs. Incidentally, these are the number of ways to group $3n-3$ objects in triples, but we do not know a combinatorial way to relate the tree graphs to triple-groupings.

This expression can easily be proven by induction. It obviously gives the correct numbers up to a_4^{tree}. Assuming that it holds up to a_{2n-2}^{tree}, we can calculate the sum on the right hand side of (4.41). Note that all factors that are powers of the form x^{n-1} trivially satisfy the stepping equations and are therefore dropped.

$$\frac{(2n)!}{2n-4}\sum_{m=1}^{n-2}\frac{(3m)!\,(3n-3m-3)!}{m!\,(2m+1)!\,(n-m-1)!\,(2n-2m-1)!} \tag{4.45}$$

This sum can be expressed as a generalized hypergeometric function.

$$= \frac{(2n)!}{2n-4}\,\frac{3}{4n-2}\,\frac{(3n-4)!}{(n-1)!\,(2n-3)!}\left({}_4F_3\left[\begin{matrix}\frac{1}{3},\frac{2}{3},\frac{1}{2}-n,1-n\\ \frac{3}{2},\frac{5}{3}-n,\frac{4}{3}-n\end{matrix};1\right]-2\right) \tag{4.46}$$

For these values of hypergeometric parameters, the Clausen formula applies and yields:

$$= \frac{(2n)!}{2n-4}\,\frac{3}{4n-2}\,\frac{(3n-4)!}{(n-1)!\,(2n-3)!}\left(\frac{(\frac{2}{3})_{n-1}\,(1)_{n-1}\,(\frac{4}{3})_{n-1}}{(2)_{n-1}\,(\frac{1}{3})_{n-1}\,(\frac{2}{3})_{n-1}}-2\right) \tag{4.47}$$

where $(n)_k$ is the Pochhammer symbol. This expression further simplifies to

$$= \frac{(3n-3)!}{(n-1)!}, \tag{4.48}$$

completing the induction.

Asymptotically for large n, the magnitude of tree level cumulants becomes

$$a_{2n}^{\text{tree}} \xrightarrow{n\to\infty} \frac{4}{3\sqrt{3\pi}}\,(2n-2)!\left(\frac{9}{8}\right)^n\left(\frac{1}{\sqrt{n}}+\mathcal{O}(n^{-3/2})\right) \tag{4.49}$$

This asymptotic form was previously obtained in [GV91] from the tree-level generating functional and in [Vol92] from the second Schwinger-Dyson equation using semi-analytic methods.

One-Loop Cumulants

Here we will show that the one-loop cumulants are asymptotically given by

$$a_{2n}^{1-\text{loop}} \sim (-1)^n \frac{(3n)!}{n!\,6^n}\,\frac{1}{\sqrt{n}} \tag{4.50}$$

This form self-consistently satisfies the stepping equation (4.42). Inserting the exact form of a_{2n}^{tree} and the asymptotics for $a_{2n}^{1-\text{loop}}$ into the stepping equation and dividing by the left hand side, we see that the a_{2n+2}^{tree} contribution is subleading and that the sum is dominated by m close to n. We therefore replace the summation index $m \to 2n-2-l$ and then take the limit $n \to \infty$, so that the right hand side becomes

$$\frac{8}{27}\sum_{l=0}^{\infty}\left(\frac{4}{3}\right)^l \frac{(3l+3)!}{(l+1)!\,(2l+3)!} = \frac{8}{27}\,{}_3F_2\left[\begin{matrix}1,\frac{4}{3},\frac{5}{3}\\ 2,\frac{5}{2}\end{matrix};1\right] = 1 \tag{4.51}$$

This confirms that the asymptotic form given above is at least proportional to the true asymptotics.

Cumulant Coefficients at High Loop

Here we will derive the approximations used for the perturbative coefficients of the cumulants at high loop order. The partition function $Z(j)$ is a diverging power series in λ, where each series coefficient is j dependent. When we expand the generating function of connected graphs as a power series in λ as well

$$W(j) = \sum_k w_k(j)\lambda^k \equiv \log Z(j) = \log\left(\sum_l z_l(j)\,\lambda^l\right) \tag{4.52}$$

each of its coefficients w_k is given as a linear combination of coefficients z_l with $l \le k$ (we suppress the j dependence here for notational convenience). One can imagine that if the series coefficients of Z grow fast enough, each w_k is dominated by z_k of the same order. This idea is formalized in a theorem due to Bender [Ben74; Ben75].

Assuming that the z_l satisfy the conditions of the theorem (this can be proven easily in our case), then the coefficients w_k are approximated by

$$w_k = \sum_{i=0}^{r} d_l \, \frac{z_{k-i}}{z_0} + \mathcal{O}\Big(\frac{z_{k-r-1}}{z_0}\Big) \tag{4.53}$$

for some $r \geq 0$, where the d_i are expansion coefficients of

$$D(j) = \sum_i d_i \lambda^i \equiv \frac{z_0(j)}{Z(j)} \tag{4.54}$$

In practice we will only use the first few d_i and equally few z_l for $l \sim k$.

For the system studied here, we are in the comfortable situation that a closed form expression is available for the z_l

$$\frac{z_l(j)}{z_0(j)} = \frac{(4l-1)!!}{l!} \left(\frac{-1}{24}\right)^l \exp(-\tfrac{j^2}{2}) \; {}_1F_1[2l+\tfrac{1}{2}; \tfrac{1}{2}; \tfrac{j^2}{2}] \tag{4.55}$$

as well as their series expansion in powers of j

$$\frac{z_l(j)}{z_0(j)} = \sum_n \bar{m}^{(l)}_{2n} \, j^{2n} \tag{4.56}$$

$$\bar{m}^{(l)}_{2n} = \frac{(4l-1)!!}{l!\, n!} (-\tfrac{1}{2})^n \Big(-\tfrac{1}{24}\Big)^k \; {}_2F_1[2l+\tfrac{1}{2}, -n; \tfrac{1}{2}; 1] \tag{4.57}$$

Note that this series in j actually converges and cannot be used in the theorem for the asymptotic coefficients of a logarithm.

After determining the first few d_i as polynomials in j,

$$d_0 = 1 \tag{4.58}$$

$$d_1 = \tfrac{1}{8} + \tfrac{1}{4} j^2 + \tfrac{1}{24} j^4 \tag{4.59}$$

$$d_2 = -\tfrac{29}{384} - \tfrac{29}{96} j^2 - \tfrac{7}{64} j^4 - \tfrac{1}{288} j^6 + \tfrac{1}{1152} j^8 \tag{4.60}$$

$$d_3 = \tfrac{107}{1024} + \tfrac{321}{512} j^2 + \tfrac{3839}{9216} j^4 + \tfrac{145}{2304} j^6 - \tfrac{11}{9216} j^8 - \tfrac{5}{13824} j^{10} + \tfrac{1}{82944} j^{12} \tag{4.61}$$

however, it becomes easy to extract the sought for cumulants by picking out appropriate (k, n) coefficients from (4.56). Note that in this process, moments with different numbers of external legs are involved in approximating a given cumulant.

Closed form expressions for successively better approximations to cumulant coefficients with l loops are obtained:

$$\Big(a^{(l)}_{2n}\Big)_{\text{lo approx}} \approx \frac{(-1)^{l+n}}{2^{n+2l-2}\, 3^{n+l-1}} \, \frac{(2n+2l-3)!!\,(4n+4l-5)!!}{(n+2l-2)!} \tag{4.62}$$

$$\left(a_{2n}^{(l)}\right)_{\text{nlo approx}} \approx \frac{(-1)^{l+n}}{2^{n+2l-2}\,3^{n+l-1}} \frac{(2n+2l-5)!!\,(4n+4l-9)!!}{(n+2l-2)!} \times \left((114-217n+136n^2-32n^3+2n^4)+(-229+288n-84n^2)l+(150-96n)l^2-32l^3\right) \quad (4.63)$$

For a given number of external legs n, these approximations become better as the loop order is increased. Thus these approximations are complementary to the exact and asymptotic forms obtained for tree and 1-loop contributions before.

If there is no closed-form expression for the coefficients of the moments, one can instead substitute the asymptotic coefficients of the moments from resurgence relations. We have verified that this method, that may prove useful in other cases, gives satisfactory results as well.

4.7.2 Double-Well Integral

In terms of techniques, we do not have much to add for the double-well integral (4.33). We quickly comment on the adaptations for the reference values and perturbative coefficients.

The numerical reference values are this time obtained by brute force. The integral (4.33) is calculated numerically to very high accuracy for a set of values for j and the derivatives of $W(j)$ are then obtained using finite-differences. The value of the distance dj is varied to ensure that no significant error is incurred in this step.

The perturbative coefficients of the cumulants are, again calculated using stepping equations. These are only slightly complicated with respect to (4.43) by the fact that odd coefficients are non-vanishing due to the cubic interaction and different initialization conditions

$$a_3^{\text{tree}} = \tau \qquad a_4^{\text{tree}} = -1 + 3\tau^2 \quad (4.64)$$

4.7.3 Quantum Mechanical Double-Well

Here we outline, how reference amplitudes and the perturbative coefficients were obtained for the quantum mechanical double-well system defined by the Hamiltonian (4.36).

Reference Values

The reference values for the amplitudes are obtained by brute force as finite-difference derivatives[10]. To this end, the Hamiltonian is diagonalized for different values of j using standard techniques.

The orthogonal basis of Hermite functions (centered around $x = 0$) is chosen. The well known recursion relations for Hermite polynomials are then used to express the Hamiltonian as a matrix in this basis. The result is a hermitian band matrix with entries specified by

$$h_{n,m} = \begin{cases} \frac{2n-1}{2}a^{-2} - \frac{2n-1}{2}a^2 + \frac{6n^2-6n+3}{4}\beta a^4 & m = n \\ \sqrt{\frac{n}{2}}(j_0 + j)a & m = n+1 \\ \frac{1}{2}\sqrt{n^2+n}\left(- a^{-2} - a^2 + (2n+1)\beta a^4\right) & m = n+2 \\ \frac{1}{4}\sqrt{n}\sqrt{n+1}\sqrt{n+2}\sqrt{n+3}\beta a^4 & m = n+4 \end{cases} \tag{4.65}$$

Where a is a scaling factor for the x-coordinate, introduced in order to improve the resulting accuracy at a given matrix-dimension. Empirically, good results were obtained when a was chosen to minimize the first discarded diagonal matrix entry.

The basis is truncated at sufficiently large dimension (typically 400, 600 or 800 rows were used and this number was varied to estimate the truncation error) and the Hamiltonian is diagonalized with high floating point accuracy using standard methods implemented in Mathematica.

Perturbative Coefficients

To determine the perturbative coefficients of amplitudes in the quantum mechanical double-well, the potential is expanded around its absolute minimum and the Hamiltonian can be written as

$$H = -\partial_{\tilde{x}}^2 + \tilde{x}^2 + \lambda q \tilde{x}^3 + \lambda^2 \tilde{x}^4 + \tilde{j}\tilde{x} \tag{4.66}$$

The relation between the parameters (and energy) of (4.36) and (4.66) is trivial to obtain.

The terms in the perturbative series were generated by the method outlined in [BW73], generalized to account for powers of the source $\tilde{j}$. When both, the energy $\tilde{E}$, as well as the ground state wave function ψ are expanded

[10] The step size Δj was varied to ensure a sufficiently small approximation error.

in positive powers of λ and $\tilde{j}$,

$$\psi(\tilde{x}) = e^{-\tilde{x}^2/2} \sum_{a,c,f} \alpha_{a,c,f}\, \tilde{j}^a \lambda^c \tilde{x}^f \tag{4.67}$$

$$\tilde{E} = 1 + \sum_{b,d} \epsilon_{b,d}\, \tilde{j}^b \lambda^d \tag{4.68}$$

the Schrödinger equation produces a recursion relation for the coefficients $\alpha_{a,c,f}$ of the wave function

$$\begin{aligned} 2f\alpha_{a,c,f} = -(f+1)(f+2)\alpha_{a,c,f+2} + q\alpha_{a,c-1,f-3} + \alpha_{a,c-2,f-4} + \\ \alpha_{a-1,c,f-1} + \sum_{\substack{(b,d)\in[0,a]\times[0,d] \\ \setminus\{(0,0),(a,c)\}}} 2\alpha_{b,d,2}\alpha_{a-b,c-d,f} \end{aligned} \tag{4.69}$$

and the coefficients for the energy $\epsilon_{b,d}$ are identified as

$$\epsilon_{b,d} = -2\alpha_{b,d,2} \tag{4.70}$$

Initialization conditions come from the convention for the normalization of the wave function $\psi(0) = 1$ or

$$\alpha_{b,d,0} = \delta_{b,0}\delta_{d,0} \tag{4.71}$$

and we also need

$$\alpha_{a,c,f} = 0 \quad \text{for } f > 3c + a \tag{4.72}$$

As an example, we show several of the q-dependent coefficients of the ground state energy $\epsilon_{b,d}$ in table 4.2.

$\epsilon_{b,d}$	$d=0$	1	2	3	4
$b=0$	1	0	$\frac{3}{4} - \frac{11}{16}q^2$	0	$-\frac{21}{16} + \frac{171}{32}q^2 - \frac{465}{256}q^4$
1	0	$-\frac{3}{4}q$	0	$\frac{31}{8}q - \frac{33}{16}q^3$	0
2	$-\frac{1}{4}$	0	$\frac{3}{4} - \frac{27}{32}q^2$	0	$-\frac{31}{8} + \frac{477}{32}q^2 - \frac{99}{16}q^4$
3	0	$-\frac{1}{8}q$	0	$\frac{33}{16}q - \frac{189}{128}q^3$	0
4	0	0	$\frac{1}{16} - \frac{9}{64}q^2$	0	$-\frac{33}{32} + \frac{729}{128}q^2 - \frac{6237}{2048}q^4$
5	0	0	0	$\frac{3}{16}q - \frac{27}{128}q^3$	0
6	0	0	0	0	$-\frac{1}{16} + \frac{63}{128}q^2 - \frac{189}{512}q^4$

Table 4.2: A few of the perturbative coefficients $\epsilon_{b,d}$ for the ground state energy (4.68) of the non-degenerate double well system.

Chapter 5

Conclusion

In this thesis, we have presented new results from several domains of high energy physics that will hopefully draw more attention to collective quantum effects in this realm. The conclusions reached here are closely in line with those of our respective publications.

With our focus on the graviton condensate picture of black holes, we have studied a Bosonic toy model that is also directly relevant in ultra-cold atoms. We have provided additional evidence of the phase transition in this system. Close to its critical point, interesting phenomena occur. Many excited states become light - maybe a precursor to the enormous entropy of actual black holes. We have also found quantum effects to be most significant near the quantum critical point. This result highlights, how many particle systems with weak two-body coupling, naively thought to behave more and more classical as the particle number is increased, may still be essentially quantum; a cornerstone of the graviton condensate picture of black holes. The quantumness, here, is encoded in higher-order long-range equal-time correlations - in contrast to more conventional spin chain systems, where correlations at the critical point have often been observed to be between nearest-neighbor sites. The presence of long range correlations may also be the key to understanding how black holes can lose information during the Hawking evaporation process. While our results do not allow us to draw detailed conclusions about actual black hole phenomenology, they give us renewed confidence that the long standing questions about black holes may still find a resolution in the realm of quantized Einstein effective theory, independently of the UV-completion of gravity.

We have also considered the question of fast information scrambling in black holes. Inspired by the known instability of three dimensional atomic Bose condensates, we have developed a picture for information scrambling in

the graviton condensate portrait. It is suggestive that the system would become entangled during the fast scrambling time. To strengthen the argument, we have performed real time simulations in our toy model at an analogous unstable point. After a quench across the phase transition, we have clearly identified entanglement creation on a time scale that scales as $\log N$, just the quantum break time we argued for.

While it is reassuring that we can even find hints of scrambling in the graviton condensate model, the proposed mechanism that posits instability and chaos as the root causes of scrambling transcends the concrete model. In this vein, we have pointed out the connection with matrix models of black holes, where classical chaos has recently been confirmed numerically.

Furthermore, we have derived the continuum limit of the Bethe equations for the attractive Lieb-Liniger model. An integral equation together with a constraint determine the large-N distribution of Bethe roots. Solutions to these equations have been presented for the weak and strong coupling phases, and confirmed by numerical calculations of the Bethe roots. At the phase transition, the functional form of the solution changes, although the distribution itself is continuous. The ground state energy that we have obtained from the continuum Bethe ansatz coincides with the mean-field result, as expected. It confirms that the phase transition is of second order.

We have highlighted that the continuum root distribution reveals an exact equivalence between the ground state of the Lieb-Liniger model and the 't Hooft large N_{color} limit of Yang-Mills theory quantized on a sphere. As it stands, the equivalence maps the Bethe root distribution to the density of boxes in the Yang tableaux of dominant representation in Yang-Mills. So far, we do not know, whether there is a useful dictionary between physical observables of both systems, or whether the equivalence is a mere mathematical coincidence. Further research is necessary to implement physical quantities in the continuum-Bethe formalism and potentially make a connection with Yang-Mills observables.

An obvious open problem is to determine the $1/N$ corrections in our formalism. While the leading order is equivalent to results from standard Bogoliubov calculations (see, e.g., the first excited state), the first $1/N$ corrections are much less trivial to obtain in a different way.

In the last part of this thesis, we have explored the behavior of high-multiplicity scattering amplitudes, which may play a role in the processes accessible at future particle colliders, but seem divergent in perturbation theory.

First we have studied the detailed nature of the breakdown of perturba-

tion theory for amplitudes with large particle number. In a tractable, Borel-summable, $0+0$ dimensional model, we have derived exact asymptotic forms for tree- and one-loop amplitudes as well as approximations for high-loop contributions. We have highlighted that the tree-level approximation ceases to be good even before perturbation theory breaks down. This is especially important to have in mind, when only tree level results are available and their accuracy needs to be assessed. We have found that Borel-Padé resummation is a practical tool to approximate the physical values of the amplitude from the coefficients of the diverging perturbation expansion.

Inspired by the Borel-plane structure of the high-multiplicity amplitudes, we have turned to the question of predicting the amplitudes nonperturbatively. In three different cases under consideration, we have been able to approximate the amplitude by combining leading-order information about all (also nonperturbative) saddle-points. For theories, in which nonperturbative saddles contribute to the path integral, we encountered a strikingly simple situation. We found the high-multiplicity amplitudes to be dominated by the contribution from the nonperturbative saddle, in spite of its usual exponential suppression.

Although it is far from clear, how general the latter results are and whether they directly translate to a field theory setting, they raise the hope, that approximations to high-multiplicity scattering amplitudes might be obtained by using the correct nonperturbative saddles in a similar fashion. In this way, resurgence theory and the systematic exploration of nonperturbative saddles find a natural application in high multiplicity amplitudes.

All in all, we have seen that collective quantum effects may play a very important role in high-energy physics. Although the black hole graviton condensate portrait is still speculative, we have shown that it and its associated collective effects yield a plausible qualitative explanation for otherwise mysterious phenomena, like scrambling. The way to understand and calculate high multiplicity amplitudes, also seems intimately interwoven with the existence of collective effects. Thus we hope that this thesis represents merely a first step. And that others will pick up the baton to more fully understand collective quantum effects in field theory and gravity.

Appendix

A Special Functions

For convenience and definiteness, we reproduce the definitions of special functions used in this thesis. The conventions follow [MT15].

- Elliptic function of the first kind

$$\mathrm{E}(x) = \int_0^1 \sqrt{1 - xu^2} \frac{du}{\sqrt{1 - u^2}} \tag{1}$$

- Elliptic function of the second kind

$$\mathrm{K}(x) = \int_0^1 \frac{1}{\sqrt{1 - xu^2}} \frac{du}{\sqrt{1 - u^2}} \tag{2}$$

- Elliptic function of the third kind

$$\Pi_1(x, y) = \int_0^1 \frac{1}{(1 - xu^2)\sqrt{1 - yu^2}} \frac{du}{\sqrt{1 - u^2}} \tag{3}$$

- Generalized hypergeometric function

$$ {}_pF_q\left[\begin{matrix} a_1, \ldots, a_p \\ b_1, \ldots, b_q \end{matrix} ; x \right] = \sum_{k=0}^{\infty} c_k \, x^k \tag{4}$$

  with $c_0 = 1$ and

$$\frac{c_{k+1}}{c_k} = \frac{(k + a_1) \cdots (k + a_p)}{(k + b_1) \cdots (k + b_q)(k + 1)} \tag{5}$$

  wherever this sum converges, and defined through analytic continuation otherwise.

Bibliography

[AA+12] G. Aad et al. "Observation of a new particle in the search for the Standard Model Higgs boson with the ATLAS detector at the LHC". *Phys. Lett.* B716 (2012), 1. DOI: 10.1016/j.physletb.2012.08.020. arXiv: 1207.7214 [hep-ex].

[AA+15] P. Ade et al. "Planck 2015 results. XIII. Cosmological parameters" (2015). arXiv: 1502.01589 [astro-ph.CO].

[AA+16a] M. Aaboud et al. "Search for resonances in diphoton events at $\sqrt{s}$=13 TeV with the ATLAS detector" (2016). arXiv: 1606.03833 [hep-ex].

[AA+16b] B. Abbot et al. "Tests of general relativity with GW150914" (2016). arXiv: 1602.03841 [gr-qc].

[AA+16c] B. Abbott et al. "Observation of Gravitational Waves from a Binary Black Hole Merger". *Phys. Rev. Lett.* 116 (2016), 061102. DOI: 10.1103/PhysRevLett.116.061102. arXiv: 1602.03837 [gr-qc].

[ABT11] C. Asplund, D. Berenstein, and D. Trancanelli. "Evidence for fast thermalization in the plane-wave matrix model". *Phys. Rev. Lett.* 107 (2011), 171602. DOI: 10.1103/PhysRevLett.107.171602. arXiv: 1104.5469 [hep-th].

[AD+16] A. Averin, G. Dvali, C. Gomez, and D. Lust. "Gravitational Black Hole Hair from Event Horizon Supertranslations" (2016). arXiv: 1601.03725 [hep-th].

[AH+01] E. N. Argyres, A. F. W. van Hameren, R. H. P. Kleiss, and C. G. Papadopoulos. "Zero-dimensional field theory". *Eur. Phys. J.* C19 (2001), 567. DOI: 10.1007/s100520100630. arXiv: hep-ph/0101346.

[AH12a] A. Altland and F. Haake. "Equilibration and macroscopic quantum fluctuations in the Dicke model". *New J. Phys.* 14 (2012), 073011. DOI: 10.1088/1367-2630/14/7/073011. arXiv: 1201.6514 [quant-ph].

[AH12b] A. Altland and F. Haake. "Quantum Chaos and Effective Thermalization". *Phys. Rev. Lett.* 108 (2012), 073601. DOI: 10.1103/PhysRevLett.108.073601. arXiv: 1110.1270 [nlin.CD].

[AM+13] A. Almheiri, D. Marolf, J. Polchinski, and J. Sully. "Black Holes: Complementarity or Firewalls?" *J. High Energy Phys.* 02 (2013), 062. DOI: 10.1007/JHEP02(2013)062. arXiv: 1207.3123 [hep-th].

[And67] P. W. Anderson. "Infrared Catastrophe in Fermi Gases with Local Scattering Potentials". *Phys. Rev. Lett.* 18 (1967), 1049. DOI: 10.1103/PhysRevLett.18.1049.

[AS64] M. Abramowitz and I. A. Stegun. *Handbook of mathematical functions: with formulas, graphs, and mathematical tables*. 55. Courier Corporation, 1964.

[ASV12] I. Aniceto, R. Schiappa, and M. Vonk. "The Resurgence of Instantons in String Theory". *Commun. Num. Theor. Phys.* 6 (2012), 339. DOI: 10.4310/CNTP.2012.v6.n2.a3. arXiv: 1106.5922 [hep-th].

[AU12] P. Argyres and M. Unsal. "A semiclassical realization of infrared renormalons". *Phys. Rev. Lett.* 109 (2012), 121601. DOI: 10.1103/PhysRevLett.109.121601. arXiv: 1204.1661 [hep-th].

[AV01] J. R. Anglin and A. Vardi. "Dynamics of a two-mode Bose-Einstein condensate beyond mean-field theory". *Phys. Rev.* A64 (2001), 013605. DOI: 10.1103/PhysRevA.64.013605. arXiv: physics/0105072.

[AW12] Z. Ambrozinski and J. Wosiek. "Resummation of not summable series" (2012). arXiv: 1106.5922 [quant-ph].

[AZ96] J. R. Anglin and W. H. Zurek. "Decoherence of quantum fields: Pointer states and predictability". *Phys. Rev.* D53 (1996), 7327. DOI: 10.1103/PhysRevD.53.7327. arXiv: quant-ph/9510021.

[BCS57] J. Bardeen, L. N. Cooper, and J. R. Schrieffer. "Theory of superconductivity". *Phys. Rev.* 108 (1957), 1175. DOI: 10.1103/PhysRev.108.1175.

[BD+15] A. Behtash, G. V. Dunne, T. Schaefer, T. Sulejmanpasic, and M. Unsal. "Toward Picard-Lefschetz Theory of Path Integrals, Complex Saddles and Resurgence" (2015). arXiv: 1510.03435 [hep-th].

[BDU13] G. Basar, G. V. Dunne, and M. Unsal. "Resurgence theory, ghost-instantons, and analytic continuation of path integrals". *J. High Energy Phys.* 10 (2013), 041. DOI: 10.1007/JHEP10(2013)041. arXiv: 1308.1108 [hep-th].

[BDZ08] I. Bloch, J. Dalibard, and W. Zwerger. "Many-body physics with ultracold gases". *Rev. Mod. Phys.* 80 (2008), 885. DOI: 10.1103/RevModPhys.80.885. arXiv: 0704.3011.

[Bek73] J. D. Bekenstein. "Black holes and entropy". *Phys. Rev.* D7 (1973), 2333. DOI: 10.1103/PhysRevD.7.2333.

[Ben74] E. A. Bender. "Asymptotic methods in enumeration". *SIAM Rev.* 16 (1974), 485.

[Ben75] E. A. Bender. "An asymptotic expansion for the coefficients of some formal power series". *J. London Math. Soc.* 2 (1975), 451.

[Ben99] M. Beneke. "Renormalons". *Phys. Rept.* 317 (1999), 1. DOI: 10.1016/S0370-1573(98)00130-6. arXiv: hep-ph/9807443.

[Ber87] M. V. Berry. "Quantum chaology (The Bakerian Lecture, 1987)". *Proc. R. Soc. London A* 413 (1987), 183. DOI: 10.1098/rspa.1987.0109.

[Bet31] H. Bethe. "Zur Theorie der Metalle. I. Eigenwerte und Eigenfunktionen der linearen Atomkette". *Z. Phys.* 71 (1931), 205. DOI: 10.1007/BF01341708.

[BF+97] T. Banks, W. Fischler, S. H. Shenker, and L. Susskind. "M theory as a matrix model: A Conjecture". *Phys. Rev.* D55 (1997), 5112. DOI: 10.1103/PhysRevD.55.5112. arXiv: hep-th/9610043.

[BF+98a] T. Banks, W. Fischler, I. R. Klebanov, and L. Susskind. "Schwarzschild black holes from matrix theory". *Phys. Rev. Lett.* 80 (1998), 226. DOI: 10.1103/PhysRevLett.80.226. arXiv: hep-th/9709091.

[BF+98b] T. Banks, W. Fischler, I. R. Klebanov, and L. Susskind. "Schwarzschild black holes in matrix theory. 2." *J. High Energy Phys.* 01 (1998), 008. DOI: 10.1088/1126-6708/1998/01/008. arXiv: hep-th/9711005.

[BH64] D. R. Brill and J. B. Hartle. "Method of the Self-Consistent Field in General Relativity and its Application to the Gravitational Geon". *Phys. Rev.* 135 (1964), B271. DOI: 10.1103/PhysRev.135.B271.

[BH91] M. V. Berry and C. J. Howls. "Hyperasymptotics for Integrals with Saddles". *Proc. R. Soc. London A*. Vol. 434. 1892. The Royal Society. 1991, 657.

[BM+13] F. Berkhahn, S. Muller, F. Niedermann, and R. Schneider. "Microscopic Picture of Non-Relativistic Classicalons". *J. Cosmol. Astropart. Phys.* 1308 (2013), 028. DOI: 10.1088/1475-7516/2013/08/028. arXiv: 1302.6581 [hep-th].

[BM11] J. L. F. Barbon and J. M. Magan. "Chaotic Fast Scrambling At Black Holes". *Phys. Rev.* D84 (2011), 106012. DOI: 10.1103/PhysRevD.84.106012. arXiv: 1105.2581 [hep-th].

[BM12] J. L. F. Barbon and J. M. Magan. "Fast Scramblers, Horizons and Expander Graphs". *J. High Energy Phys.* 08 (2012), 016. DOI: 10.1007/JHEP08(2012)016. arXiv: 1204.6435 [hep-th].

[Bog80] E. B. Bogomolny. "Calculation of instanton-anti-instanton contributions in quantum mechanics". *Phys. Lett.* B91 (1980), 431. DOI: 10.1016/0370-2693(80)91014-X.

[Bou13] R. Bousso. "Complementarity Is Not Enough". *Phys. Rev.* D87 (2013), 124023. DOI: 10.1103/PhysRevD.87.124023. arXiv: 1207.5192 [hep-th].

[BP+15] A. Behtash, E. Poppitz, T. Sulejmanpasic, and M. Ünsal. "The curious incident of multi-instantons and the necessity of Lefschetz thimbles". *J. High Energy Phys.* 11 (2015), 175. DOI: 10.1007/JHEP11(2015)175. arXiv: 1507.04063 [hep-th].

[BSP84] T. Banks, L. Susskind, and M. E. Peskin. "Difficulties for the Evolution of Pure States Into Mixed States". *Nucl. Phys.* B244 (1984), 125. DOI: 10.1016/0550-3213(84)90184-6.

[BW73] C. M. Bender and T. T. Wu. "Anharmonic oscillator. 2: A Study of perturbation theory in large order". *Phys. Rev.* D7 (1973), 1620. DOI: 10.1103/PhysRevD.7.1620.

[BY86] I. I. Balitsky and A. V. Yung. "Instanton Molecular Vacuum in $N = 1$ Supersymmetric Quantum Mechanics". *Nucl. Phys.* B274 (1986), 475. DOI: 10.1016/0550-3213(86)90295-6.

[BZ78] G. P. Berman and G. M. Zaslavsky. "Condition of stochasticity in quantum nonlinear systems". *Physica A* 91 (1978), 450. DOI: 10.1016/0378-4371(78)90190-5.

[CC+00] S. L. Cornish, N. R. Claussen, J. L. Roberts, E. A. Cornell, and C. E. Wieman. "Stable ^{85}Rb Bose-Einstein Condensates with Widely Tunable Interactions". *Phys. Rev. Lett.* 85 (2000), 1795. DOI: 10.1103/PhysRevLett.85.1795. arXiv: cond-mat/0004290.

[CC07a] P. Calabrese and J.-S. Caux. "Dynamics of the attractive 1D Bose gas: analytical treatment from integrability". *J. Stat. Mech. Theor. Exp.* 8 (2007), 32. DOI: 10.1088/1742-5468/2007/08/P08032. arXiv: 0707.4115 [cond-mat].

[CC07b] P. Calabrese and J.-S. Caux. "Correlation Functions of the One-Dimensional Attractive Bose Gas". *Phys. Rev. Lett.* 98 (2007), 150403. DOI: 10.1103/PhysRevLett.98.150403. arXiv: cond-mat/0612192.

[CCR00] L. D. Carr, C. W. Clark, and W. P. Reinhardt. "Stationary solutions of the one-dimensional nonlinear Schrödinger equation. II. Case of attractive nonlinearity". *Phys. Rev.* A62 (2000), 063611. DOI: 10.1103/PhysRevA.62.063611. arXiv: cond-mat/9911178.

[CD96] Y. Castin and R. Dum. "Bose-Einstein Condensates in Time Dependent Traps". *Phys. Rev. Lett.* 77 (1996), 5315. DOI: 10.1103/PhysRevLett.77.5315.

[CGZ07] M. Cozzini, P. Giorda, and P. Zanardi. "Quantum phase transitions and quantum fidelity in free fermion graphs". *Phys. Rev.* B75 (2007), 014439. DOI: 10.1103/PhysRevB.75.014439. arXiv: quant-ph/0608059.

[Cha+12] S. Chatrchyan et al. "Observation of a new boson at a mass of 125 GeV with the CMS experiment at the LHC". *Phys. Lett.* B716 (2012), 30. DOI: 10.1016/j.physletb.2012.08.021. arXiv: 1207.7235 [hep-ex].

[CKÜ15] A. Cherman, P. Koroteev, and M. Ünsal. "Resurgence and Holomorphy: From Weak to Strong Coupling". *J. Math. Phys.* 56 (2015), 053505. DOI: 10.1063/1.4921155. arXiv: 1410.0388 [hep-th].

[CL14] P. Calabrese and P. Le Doussal. "Interaction quench in a Lieb-Liniger model and the KPZ equation with flat initial conditions". *J. Stat. Mech. Theor. Exp.* 5 (2014), 05004. DOI: 10.1088/1742-5468/2014/05/P05004. arXiv: 1402.1278 [cond-mat.dis-nn].

[CLP78] P. Cvitanovic, B. E. Lautrup, and R. B. Pearson. "The Number and Weights of Feynman Diagrams". *Phys. Rev.* D18 (1978), 1939. DOI: 10.1103/PhysRevD.18.1939.

[CM11] J.-S. Caux and J. Mossel. "Remarks on the notion of quantum integrability". *J. Stat. Mech.* 1102 (2011), P02023. DOI: 10.1088/1742-5468/2011/02/P02023. arXiv: 1012.3587 [cond-mat.str-el].

[Col77] S. R. Coleman. "The Fate of the False Vacuum. 1. Semiclassical Theory". *Phys. Rev.* D15 (1977), 2929. DOI: 10.1103/PhysRevD.15.2929.

[Col88] S. Coleman. *Aspects of Symmetry: Selected Erice Lectures*. Cambridge University Press, 1988.

[Cor90] J. M. Cornwall. "On the High-energy Behavior of Weakly Coupled Gauge Theories". *Phys. Lett.* B243 (1990), 271. DOI: 10.1016/0370-2693(90)90850-6.

[CP13] F. Colomo and A. G. Pronko. "Third-order phase transition in random tilings". *Phys. Rev.* E88 (2013), 042125. DOI: 10.1103/PhysRevE.88.042125. arXiv: 1306.6207 [math-ph].

[Dar] G. Darboux. "Mémoire sur lapproximation des fonctions de très-grands nombres, et sur une classe étendue de développements en série". *J. Math. Pures* 4 (), 5. URL: http://portail.mathdoc.fr/JMPA/afficher_notice.php?id=JMPA_1878_3_4_A1_0.

[DC87] P. D. Drummond and S. J. Carter. "Quantum-field theory of squeezing in solitons". *J. Opt. Soc. Am. B* 4 (1987), 1565. DOI: 10.1364/JOSAB.4.001565.

[DF+13] G. Dvali, D. Flassig, C. Gomez, A. Pritzel, and N. Wintergerst. "Scrambling in the Black Hole Portrait". *Phys. Rev.* D88 (2013), 124041. DOI: 10.1103/PhysRevD.88.124041. arXiv: 1307.3458 [hep-th].

[DF+15] G. Dvali, A. Franca, C. Gomez, and N. Wintergerst. "Nambu-Goldstone Effective Theory of Information at Quantum Criticality". *Phys. Rev.* D92 (2015), 125002. DOI: 10.1103/PhysRevD.92.125002. arXiv: 1507.02948 [hep-th].

[DG+11] G. Dvali, G. F. Giudice, C. Gomez, and A. Kehagias. "UV-Completion by Classicalization". *J. High Energy Phys.* 08 (2011), 108. DOI: 10.1007/JHEP08(2011)108. arXiv: 1010.1415 [hep- ph].

[DG+15] G. Dvali, C. Gomez, R. S. Isermann, D. Lüst, and S. Stieberger. "Black hole formation and classicalization in ultra-Planckian 2N scattering". *Nucl. Phys.* B893 (2015), 187. DOI: 10.1016/j.nuclphysb.2015.02.004. arXiv: 1409.7405 [hep-th].

[DG12a] G. Dvali and C. Gomez. "Black Hole Macro - Quantumness" (2012). arXiv: 1212.0765 [hep-th].

[DG12b] G. Dvali and C. Gomez. "Landau-Ginzburg limit of black holes quantum portrait: Self-similarity and critical exponent". *Phys. Lett.* B716 (2012), 240. DOI: 10.1016/j.physletb.2012.08.019. arXiv: 1203.3372 [hep-th].

[DG13a] G. Dvali and C. Gomez. "Black Hole's 1/N Hair". *Phys. Lett.* B719 (2013), 419. DOI: 10.1016/j.physletb.2013.01.020. arXiv: 1203.6575 [hep-th].

[DG13b] G. Dvali and C. Gomez. "Black Hole's Quantum N-Portrait". *Fortsch. Phys.* 61 (2013), 742. DOI: 10.1002/prop.201300001. arXiv: 1112.3359 [hep-th].

[DG14] G. Dvali and C. Gomez. "Black Holes as Critical Point of Quantum Phase Transition". *Eur. Phys. J.* C74 (2014), 2752. DOI: 10.1140/epjc/s10052-014-2752-3. arXiv: 1207.4059 [hep-th].

[DG16] G. Dvali and A. Gussmann. "Skyrmion Black Hole Hair: Conservation of Baryon Number by Black Holes and Observable Manifestations" (2016). arXiv: 1605.00543 [hep-th].

[DI99] P. Deligne and N. Institute for Advanced Study (Princeton. *Quantum fields and strings: a course for mathematicians.* Quantum Fields and Strings: A Course for Mathematicians. American Mathematical Society, 1999. ISBN: 9780821811986.

[Din73] R. B. Dingle. *Asymptotic Expansions: Their Derivation and Interpretation.* Academic Press London, 1973. ISBN: 9780122165504.

[DK93] M. R. Douglas and V. A. Kazakov. "Large N phase transition in continuum QCD in two-dimensions". *Phys. Lett.* B319 (1993), 219. DOI: 10.1016/0370-2693(93)90806-S. arXiv: hep-th/9305047.

[DK94] J.-M. Daul and V. A. Kazakov. "Wilson loop for large N Yang-Mills theory on a two-dimensional sphere". *Phys. Lett.* B335 (1994), 371. DOI: 10.1016/0370-2693(94)90366-2. arXiv: hep-th/9310165.

[Don94] J. F. Donoghue. "General relativity as an effective field theory: The leading quantum corrections". *Phys. Rev.* D50 (1994), 3874. DOI: 10.1103/PhysRevD.50.3874. arXiv: gr-qc/9405057.

[Dor14] D. Dorigoni. "An Introduction to Resurgence, Trans-Series and Alien Calculus" (2014). arXiv: 1411.3585 [hep-th].

[DS+93] P. D. Drummond, R. M. Shelby, S. R. Friberg, and Y. Yamamoto. "Quantum solitons in optical fibres". *Nature* 365 (1993), 307. DOI: 10.1038/365307a0.

[DS01] R. A. Duine and H. T. Stoof. "Explosion of a Collapsing Bose-Einstein Condensate". *Phys. Rev. Lett.* 86 (2001), 2204. DOI: 10.1103/PhysRevLett.86.2204. arXiv: cond-mat/0007320.

[DU12] G. V. Dunne and M. Unsal. "Resurgence and Trans-series in Quantum Field Theory: The CP(N-1) Model". *J. High Energy Phys.* 11 (2012), 170. DOI: 10.1007/JHEP11(2012)170. arXiv: 1210.2423 [hep-th].

[DU14] G. V. Dunne and M. Unsal. "Uniform WKB, Multi-instantons, and Resurgent Trans-Series". *Phys. Rev.* D89 (2014), 105009. DOI: 10.1103/PhysRevD.89.105009. arXiv: 1401.5202 [hep-th].

[Dys52] F. J. Dyson. "Divergence of perturbation theory in quantum electrodynamics". *Phys. Rev.* 85 (1952), 631. DOI: 10.1103/PhysRev.85.631.

[DZ83] J.-M. Drouffe and J.-B. Zuber. "Strong coupling and mean field methods in lattice gauge theories". *Phys. Rep.* 102 (1983), 1.

[Eca81] J. Ecalle. *Les Fonctions Résurgentes*. Vol. I - III. Publ. Math. Orsay, 1981. URL: http://www.math.u-psud.fr/~ecalle/publi.html.

[Ehr27] P. Ehrenfest. "Bemerkung über die angenäherte Gültigkeit der klassischen Mechanik innerhalb der Quantenmechanik". *Z. Phys.* 45 (1927), 455–457. DOI: 10.1007/BF01329203.

[Ein16] A. Einstein. "Näherungsweise Integration der Feldgleichungen der Gravitation". *Sitzungsber. Preuss. Akad. Wiss. Berlin (Math. Phys.)* (1916), 688.

[FD+11] V. L. Fish, S. S. Doeleman, C. Beaudoin, R. Blundell, D. E. Bolin, G. C. Bower, R. Chamberlin, et al. "1.3 mm Wavelength VLBI of Sagittarius A*: Detection of Time-variable Emission on Event Horizon Scales". *Astrophys. J.* 727 (2011), L36. DOI: 10.1088/2041-8205/727/2/L36. arXiv: 1011.2472.

[Fes58] H. Feshbach. "Unified theory of nuclear reactions". *Annals Phys.* 5 (1958), 357. DOI: 10.1016/0003-4916(58)90007-1.

[FFP15] D. Flassig, A. Franca, and A. Pritzel. "Large-N ground state of the Lieb-Liniger model and Yang-Mills theory on a two-sphere" (2015). arXiv: 1508.01515 [cond-mat.quant-gas].

[Fla16] D. Flassig. "Resurgence of High-Multiplicity Amplitudes" (in preparation).

[FMS11] P. J. Forrester, S. N. Majumdar, and G. Schehr. "Non-intersecting Brownian walkers and Yang-Mills theory on the sphere". *Nucl. Phys.* B844 (2011), 500. DOI: 10.1016/j.nuclphysb.2011.12.009. arXiv: 1009.2362 [math-ph].

[FPW13] D. Flassig, A. Pritzel, and N. Wintergerst. "Black holes and quantumness on macroscopic scales". *Phys. Rev.* D87 (2013), 084007. DOI: 10.1103/PhysRevD.87.084007. arXiv: 1212.3344.

[FW15] V. F. Foit and N. Wintergerst. "Self-similar Evaporation and Collapse in the Quantum Portrait of Black Holes". *Phys. Rev.* D92 (2015), 064043. DOI: 10.1103/PhysRevD.92.064043. arXiv: 1504.04384 [hep-th].

[Gau71] M. Gaudin. "Boundary Energy of a Bose Gas in One Dimension". *Phys. Rev.* A4 (1971), 386. DOI: 10.1103/PhysRevA.4.386.

[GH+06] G. Gabrielse, D. Hanneke, T. Kinoshita, M. Nio, and B. C. Odom. "New Determination of the Fine Structure Constant from the Electron g Value and QED". *Phys. Rev. Lett.* 97 (2006). [Erratum: Phys. Rev. Lett.99,039902(2007)], 030802. DOI: 10.1103/PhysRevLett.97.030802.

[GH+15] L. Gruending, S. Hofmann, S. Müller, and T. Rug. "Probing the Constituent Structure of Black Holes". *J. High Energy Phys.* 05 (2015), 047. DOI: 10.1007/JHEP05(2015)047. arXiv: 1407.1051 [hep-th].

[GHS16] G. Gur-Ari, M. Hanada, and S. H. Shenker. "Chaos in Classical D0-Brane Mechanics". *J. High Energy Phys.* 02 (2016), 091. DOI: 10.1007/JHEP02(2016)091. arXiv: 1512.00019 [hep-th].

[Gid13] S. B. Giddings. "The gravitational S-matrix: Erice lectures". *Subnucl. Ser.* 48 (2013), 93. DOI: 10.1142/9789814522489_0005. arXiv: 1105.2036 [hep-th].

[Gid14] S. B. Giddings. "Possible observational windows for quantum effects from black holes". *Phys. Rev.* D90 (2014), 124033. DOI: 10.1103/PhysRevD.90.124033. arXiv: 1406.7001 [hep-th].

[Gid16] S. B. Giddings. "Gravitational wave tests of quantum modifications to black hole structure – with post-GW150914 update" (2016). arXiv: 1602.03622 [gr-qc].

[GL50] V. L. Ginzburg and L. D. Landau. "On the Theory of superconductivity". *Zh. Eksp. Teor. Fiz.* 20 (1950), 1064.

[GMN16] A. Gorsky, A. Milekhin, and S. Nechaev. "Douglas-Kazakov on the road to superfluidity: from random walks to black holes" (2016). arXiv: 1604.06381 [hep-th].

[Gol90] H. Goldberg. "Breakdown of perturbation theory at tree level in theories with scalars". *Phys. Lett.* B246 (1990), 445. DOI: 10.1016/0370-2693(90)90628-J.

[GS04] A. A. Gerasimov and S. L. Shatashvili. "Towards integrability of topological strings. I. Three-forms on Calabi-Yau manifolds". *J. High Energy Phys.* 11 (2004), 074. DOI: 10.1088/1126-6708/2004/11/074. arXiv: hep-th/0409238.

[Gut91] M. Gutzwiller. *Chaos in Classical and Quantum Mechanics*. Interdisciplinary Applied Mathematics. Springer New York, 1991. ISBN: 9780387971735.

[GV91] H. Goldberg and M. T. Vaughn. "Tree and nontree multiparticle amplitudes". *Phys. Rev. Lett.* 66 (1991), 1267. DOI: 10.1103/PhysRevLett.66.1267.

[Haw05] S. W. Hawking. "Information loss in black holes". *Phys. Rev.* D72 (2005), 084013. DOI: 10.1103/PhysRevD.72.084013. arXiv: hep-th/0507171.

[Haw74] S. W. Hawking. "Black hole explosions". *Nature* 248 (1974), 30. DOI: 10.1038/248030a0.

[Haw75] S. W. Hawking. "Particle Creation by Black Holes". *Commun. Math. Phys.* 43 (1975), 199. DOI: 10.1007/BF02345020.

[Haw76] S. W. Hawking. "Breakdown of Predictability in Gravitational Collapse". *Phys. Rev.* D14 (1976), 2460. DOI: 10.1103/PhysRevD.14.2460.

[HG+09] E. Haller, M. Gustavsson, M. J. Mark, J. G. Danzl, R. Hart, G. Pupillo, and H.-C. Nägerl. "Realization of an excited, strongly correlated quantum gas phase". *Science* 325 (2009), 1224. DOI: 10.1126/science.1175850.

[HH13] D. Harlow and P. Hayden. "Quantum Computation vs. Firewalls". *J. High Energy Phys.* 06 (2013), 085. DOI: 10.1007/JHEP06(2013)085. arXiv: 1301.4504 [hep-th].

[Hig64] P. Higgs. "Broken Symmetries and the Masses of Gauge Bosons". *Phys. Rev. Lett.* 13 (1964), 508. DOI: 10.1103/PhysRevLett.13.508.

[HJ15] M. Honda and D. P. Jatkar. "Interpolating function and Stokes Phenomena". *Nucl. Phys.* B900 (2015), 533. DOI: 10.1016/j.nuclphysb.2015.09.024. arXiv: 1504.02276 [hep-th].

[HOC14] C. Herzog, M. Olshanii, and Y. Castin. "Une transition liquide-gaz pour des bosons en interaction attractive à une dimension". *C. R. Phys.* 15 (2014), 285. DOI: 10.1016/j.crhy.2013.12.004. arXiv: 1311.3857 [cond-mat.quant-gas].

[Hoo85] G. 't Hooft. "On the Quantum Structure of a Black Hole". *Nucl. Phys.* B256 (1985), 727. DOI: 10.1016/0550-3213(85)90418-3.

[Hoo93] G. 't Hooft. "Dimensional reduction in quantum gravity". *Salamfest 1993:0284-296*. 1993, 0284–296. arXiv: gr-qc/9310026.

[How97] C. J. Howls. "Hyperasymptotics for Multidimensional Integrals, Exact Remainder Terms and the Global Connection Problem". *Proc. R. Soc. London A* 453 (1997), 2271. DOI: 10.1098/rspa.1997.0122.

[HP07] P. Hayden and J. Preskill. "Black holes as mirrors: Quantum information in random subsystems". *J. High Energy Phys.* 09 (2007), 120. DOI: 10.1088/1126-6708/2007/09/120. arXiv: 0708.4025 [hep-th].

[HPS16] S. W. Hawking, M. J. Perry, and A. Strominger. "Soft Hair on Black Holes" (2016). arXiv: 1601.00921 [hep-th].

[HR16] S. Hofmann and T. Rug. "A Quantum Bound-State Description of Black Holes". *Nucl. Phys.* B902 (2016), 302. DOI: 10.1016/j.nuclphysb.2015.11.008. arXiv: 1403.3224 [hep-th].

[HT73] A. Hasegawa and F. Tappert. "Transmission of stationary nonlinear optical pulses in dispersive dielectric fibers. I. Anomalous dispersion". *Appl. Phys. Lett.* 23 (1973), 142. DOI: 10.1063/1.1654836.

[HV01] L. Henderson and V. Vedral. "Classical, quantum and total correlations". *J. Phys. A* 34 (2001), 6899. DOI: 10.1088/0305-4470/34/35/315. arXiv: quant-ph/0105028.

[IM+98] N. Itzhaki, J. M. Maldacena, J. Sonnenschein, and S. Yankielowicz. "Supergravity and the large N limit of theories with sixteen supercharges". *Phys. Rev.* D58 (1998), 046004. DOI: 10.1103/PhysRevD.58.046004. arXiv: hep-th/9802042.

[JK15] J. Jaeckel and V. V. Khoze. "Upper limit on the scale of new physics phenomena from rising cross sections in high multiplicity Higgs and vector boson events". *Phys. Rev.* D91 (2015), 093007. DOI: 10.1103/PhysRevD.91.093007. arXiv: 1411.5633 [hep-ph].

[KBI93] V. E. Korepin, N. M. Bogoliubov, and A. G. Izergin. *Quantum Inverse Scattering Method and Correlation Functions*. Cambridge University Press, 1993. ISBN: 9780511628832. DOI: 10.1017/CBO9780511628832.

[Kho14] V. V. Khoze. "Multiparticle Higgs and Vector Boson Amplitudes at Threshold". *J. High Energy Phys.* 07 (2014), 008. DOI: 10.1007/JHEP07(2014)008. arXiv: 1404.4876 [hep-ph].

[KS+02] L. Khaykovich et al. "Formation of a Matter-Wave Bright Soliton". *Science* 296 (2002), 1290. DOI: 10.1126/science.1071021. arXiv: cond-mat/0205378.

[KS+11] E. Komatsu et al. "Seven-Year Wilkinson Microwave Anisotropy Probe (WMAP) Observations: Cosmological Interpretation". *Astrophys. J. Suppl.* 192 (2011), 18. DOI: 10.1088/0067-0049/192/2/18. arXiv: 1001.4538 [astro-ph.CO].

[KS+13] M. Kormos, A. Shashi, Y.-Z. Chou, J.-S. Caux, and A. Imambekov. "Interaction quenches in the one-dimensional Bose gas". *Phys. Rev.* B88 (2013), 205131. DOI: 10.1103/PhysRevB.88.205131. arXiv: 1305.7202 [cond-mat.stat-mech].

[KS+16] V. Khachatryan et al. "Search for narrow resonances decaying to dijets in proton-proton collisions at $\sqrt{(s)} = 13$ TeV". *Phys. Rev. Lett.* 116 (2016), 071801. DOI: 10.1103/PhysRevLett.116.071801. arXiv: 1512.01224 [hep-ex].

[KSU03] R. Kanamoto, H. Saito, and M. Ueda. "Quantum phase transition in one-dimensional Bose-Einstein condensates with attractive interactions". *Phys. Rev.* A67 (2003), 013608. DOI: 10.1103/PhysRevA.67.013608. arXiv: cond-mat/0210229.

[KSU06] R. Kanamoto, H. Saito, and M. Ueda. "Critical fluctuations in a soliton formation of attractive Bose-Einstein condensates". *Phys. Rev.* A73 (2006), 033611. DOI: 10.1103/PhysRevA.73.033611. arXiv: cond-mat/0511684.

[KW89] D. E. Knuth and H. S. Wilf. "A short proof of Darboux's lemma". *Appl. Math. Lett.* 2.2 (1989), 139. DOI: 10.1016/0893-9659(89)90007-4.

[Lau83] R. B. Laughlin. "Anomalous quantum Hall effect: An Incompressible quantum fluid with fractionally charged excitations". *Phys. Rev. Lett.* 50 (1983), 1395. DOI: 10.1103/PhysRevLett.50.1395.

[LB90] W. A. Lin and L. E. Ballentine. "Quantum tunneling and chaos in a driven anharmonic oscillator". *Phys. Rev. Lett.* 65 (1990), 2927. DOI: 10.1103/PhysRevLett.65.2927.

[Lee95] H.-W. Lee. "Theory and application of the quantum phase-space distribution functions". *Phys. Rep.* 259 (1995), 147. DOI: 10.1016/0370-1573(95)00007-4.

[Lip77] L. N. Lipatov. "Divergence of the Perturbation Theory Series and the Quasiclassical Theory". *Sov. Phys. JETP* 45 (1977). [Zh. Eksp. Teor. Fiz.72,411(1977)], 216.

[LL63] E. H. Lieb and W. Liniger. "Exact analysis of an interacting Bose gas. 1. The General solution and the ground state". *Phys. Rev.* 130 (1963), 1605. DOI: 10.1103/PhysRev.130.1605.

[LRT97] M. V. Libanov, V. A. Rubakov, and S. V. Troitsky. "Multiparticle processes and semiclassical analysis in bosonic field theories". *Phys. Part. Nucl.* 28 (1997), 217. DOI: 10.1134/1.953038.

[LS+13] N. Lashkari, D. Stanford, M. Hastings, T. Osborne, and P. Hayden. "Towards the Fast Scrambling Conjecture". *J. High Energy Phys.* 04 (2013), 022. DOI: 10.1007/JHEP04(2013)022. arXiv: 1111.6580 [hep-th].

[LSY00] E. H. Lieb, R. Seiringer, and J. Yngvason. "Bosons in a trap: A rigorous derivation of the Gross-Pitaevskii energy functional". *Phys. Rev.* A61 (2000), 043602. DOI: 10.1103/PhysRevA.61.043602. arXiv: math-ph/9908027.

[LVV90] L. D. McLerran, A. I. Vainshtein, and M. B. Voloshin. "Strong Instanton Induced Amplitudes in a Weakly Coupled Theory". *Phys. Rev.* D42 (1990), 180. DOI: 10.1103/PhysRevD.42.180.

[Lyn85] J. Lyness. "The Euler Maclaurin expansion for the Cauchy principal value integral". *Numer. Math.* 46 (1985), 611.

[Mal03] J. M. Maldacena. "Eternal black holes in anti-de Sitter". *J. High Energy Phys.* 04 (2003), 021. DOI: 10.1088/1126-6708/2003/04/021. arXiv: hep-th/0106112.

[Mal99] J. M. Maldacena. "The Large N limit of superconformal field theories and supergravity". *Int. J. Theor. Phys.* 38 (1999), 1113. DOI: 10.1023/A:1026654312961. arXiv: hep-th/9711200.

[Mat05] S. D. Mathur. "The Fuzzball proposal for black holes: An Elementary review". *Fortsch. Phys.* 53 (2005), 793. DOI: 10.1002/prop.200410203. arXiv: hep-th/0502050.

[MC81] V. F. Mukhanov and G. V. Chibisov. "Quantum Fluctuation and Nonsingular Universe. (In Russian)". *JETP Lett.* 33 (1981). [Pisma Zh. Eksp. Teor. Fiz.33,549(1981)], 532.

[McG64] J. B. McGuire. "Study of Exactly Soluble One-Dimensional N-Body Problems". *J. Math. Phys.* 5 (1964), 622. DOI: 10.1063/1.1704156.

[Mig75] A. A. Migdal. "Recursion Equations in Gauge Theories". *Sov. Phys. JETP* 42 (1975). [Zh. Eksp. Teor. Fiz.69,810(1975)], 413.

[MO33] W. Meissner and R. Ochsenfeld. "Ein neuer effekt bei eintritt der supraleitfähigkeit". *Naturwissenschaften* 21 (1933), 787.

[Mot97] L. Motl. "Proposals on nonperturbative superstring interactions" (1997). arXiv: hep-th/9701025.

[MS13] J. Maldacena and L. Susskind. "Cool horizons for entangled black holes". *Fortsch. Phys.* 61 (2013), 781. DOI: 10.1002/prop.201300020. arXiv: 1306.0533 [hep-th].

[MS14] S. N. Majumdar and G. Schehr. "Top eigenvalue of a random matrix: large deviations and third order phase transition". *J. Stat. Mech. Theor. Exp.* 1 (2014), 01012. DOI: 10.1088/1742-5468/2014/01/P01012. arXiv: 1311.0580 [cond-mat.stat-mech].

[MSS15] J. Maldacena, S. H. Shenker, and D. Stanford. "A bound on chaos" (2015). arXiv: 1503.01409 [hep-th].

[MT15] O. Marichev and M. Trott. *functions.wolfram.com*. Wolfram Research, Inc. 2015. URL: http://functions.wolfram.com/.

[NS09] N. A. Nekrasov and S. L. Shatashvili. "Quantum integrability and supersymmetric vacua". *Prog. Theor. Phys. Suppl.* 177 (2009), 105. DOI: 10.1143/PTPS.177.105. arXiv: 0901.4748 [hep-th].

[OL07] N. Oelkers and J. Links. "Ground-state properties of the attractive one-dimensional Bose-Hubbard model". *Phys. Rev.* B75 (2007), 115119. DOI: 10.1103/PhysRevB.75.115119. arXiv: cond-mat/0611510.

[Ols98] M. Olshanii. "Atomic Scattering in the Presence of an External Confinement and a Gas of Impenetrable Bosons". *Phys. Rev. Lett.* 81 (1998), 938. DOI: 10.1103/PhysRevLett.81.938. arXiv: cond-mat/9804130.

[ON02] T. J. Osborne and M. A. Nielsen. "Entanglement in a simple quantum phase transition". *Phys. Rev.* A66 (2002), 032110. DOI: 10.1103/PhysRevA.66.032110. arXiv: quant-ph/0202162.

[Onn11] H. K. Onnes. *Commun. Phys. Lab. Univ. Leiden* 120b (1911).

[Onn14] H. K. Onnes. *Commun. Phys. Lab. Univ. Leiden* 140 (1914).

[OZ02] H. Ollivier and W. H. Zurek. "Quantum Discord: A Measure of the Quantumness of Correlations". *Phys. Rev. Lett.* 88 (2002), 017901. DOI: 10.1103/PhysRevLett.88.017901. arXiv: quant-ph/0105072.

[Pag93a] D. N. Page. "Average entropy of a subsystem". *Phys. Rev. Lett.* 71 (1993), 1291. DOI: 10.1103/PhysRevLett.71.1291. arXiv: gr-qc/9305007.

[Pag93b] D. N. Page. "Information in black hole radiation". *Phys. Rev. Lett.* 71 (1993), 3743. DOI: 10.1103/PhysRevLett.71.3743. arXiv: hep-th/9306083.

[Pan15] M. Panchenko. "The Lieb-Liniger model at the critical point as toy model for Black Holes" (2015). arXiv: 1510.04535 [hep-th].

[PDC13] M. Panfil, J. De Nardis, and J.-S. Caux. "Metastable Criticality and the Super Tonks-Girardeau Gas". *Phys. Rev. Lett.* 110 (2013), 125302. DOI: 10.1103/PhysRevLett.110.125302. arXiv: 1211.3866 [cond-mat.quant-gas].

[Pip91] A. C. Pipkin. *A Course on Integral Equations*. Texts in Applied Mathematics 9. Springer-Verlag, New York, Berlin, Heidelberg, 1991. ISBN: 9780-387-97557-3.

[PM+97] V. M. Pérez-Garca, H. Michinel, J. I. Cirac, M. Lewenstein, and P. Zoller. "Dynamics of Bose-Einstein condensates: Variational solutions of the Gross-Pitaevskii equations". *Phys. Rev.* A56 (1997), 1424. DOI: 10.1103/PhysRevA.56.1424.

[Pol15] J. Polchinski. "Chaos in the black hole S-matrix" (2015). arXiv: 1505.08108 [hep-th].

[PR14] K. Papadodimas and S. Raju. "State-Dependent Bulk-Boundary Maps and Black Hole Complementarity". *Phys. Rev.* D89 (2014), 086010. DOI: 10.1103/PhysRevD.89.086010. arXiv: 1310.6335 [hep-th].

[Pre92] J. Preskill. "Do black holes destroy information?" *International Symposium on Black holes, Membranes, Wormholes and Superstrings Woodlands, Texas, January 16-18, 1992.* 1992. arXiv: hep-th/9209058.

[Pri14] A. Pritzel. "Non-perturbative Effects in field theory and gravity". PhD thesis. Munich U., 2014. URL: http://edoc.ub.uni-muenchen.de/17715/.

[PS03] L. Pitaevski and S. Stringari. *Bose-Einstein Condensation.* Intl. Series of Monographs on Physics 116. Clarendon Press, Oxford, 2003. ISBN: 019-850719-4.

[PV+06] D. Perez-Garcia, F. Verstraete, M. M. Wolf, and J. I. Cirac. "Matrix Product State Representations" (2006). arXiv: quant-ph/0608197.

[PW+04] B. Paredes et al. "Tonks–Girardeau gas of ultracold atoms in an optical lattice". *Nature* 429 (2004), 277. DOI: 10.1038/nature02530.

[RST92] V. A. Rubakov, D. T. Son, and P. G. Tinyakov. "Classical boundary value problem for instanton transitions at high-energies". *Phys. Lett.* B287 (1992), 342. DOI: 10.1016/0370-2693(92)90994-F.

[Rub95] V. A. Rubakov. "Nonperturbative aspects of multiparticle production". *2nd Rencontres du Vietnam: Consisting of 2 parallel conferences: Astrophysics Meeting: From the Sun and Beyond / Particle Physics Meeting: Physics at the Frontiers of the Standard Model Ho Chi Minh City, Vietnam, October 21-28, 1995.* 1995. arXiv: hep-ph/9511236.

[Rus90] B. E. Rusakov. "Loop averages and partition functions in U(N) gauge theory on two-dimensional manifolds". *Mod. Phys. Lett.* A5 (1990), 693. DOI: 10.1142/S0217732390000780.

[RW57] T. Regge and J. A. Wheeler. "Stability of a Schwarzschild singularity". *Phys. Rev.* 108 (1957), 1063. DOI: 10.1103/PhysRev.108.1063.

[Sau07] D. Sauzin. "Resurgent functions and splitting problems" (2007). arXiv: 0706.0137 [math.DS].

[SB+92] G. F. Smoot et al. "Structure in the COBE differential microwave radiometer first year maps". *Astrophys. J.* 396 (1992), L1. DOI: 10.1086/186504.

[Sch16] K. Schwarzschild. "Über das Gravitationsfeld eines Massenpunktes nach der Einsteinschen Theorie". *Sitzungsber. Preuss. Akad. Wiss. Berlin (Math. Phys.)* (1916), 189.

[SDD07] A. G. Sykes, P. D. Drummond, and M. J. Davis. "Excitation spectrum of bosons in a finite one-dimensional circular waveguide via the Bethe ansatz". *Phys. Rev.* A76 (2007), 063620. DOI: 10.1103/PhysRevA.76.063620. arXiv: 0707.2422 [cond-mat].

[SG+99] C. A. Sackett, J. M. Gerton, M. Welling, and R. G. Hulet. "Measurements of Collective Collapse in a Bose-Einstein Condensate with Attractive Interactions". *Phys. Rev. Lett.* 82 (1999), 876. DOI: 10.1103/PhysRevLett.82.876.

[She90] S. H. Shenker. "The Strength of nonperturbative effects in string theory". *Cargese Study Institute: Random Surfaces, Quantum Gravity and Strings Cargese, France, May 27-June 2, 1990.* 1990, 191. URL: http://alice.cern.ch/format/showfull?sysnb=0123660.

[Son96] D. T. Son. "Semiclassical approach for multiparticle production in scalar theories". *Nucl. Phys.* B477 (1996), 378. DOI: 10.1016/0550-3213(96)00386-0. arXiv: hep-ph/9505338.

[SP+02] K. E. Strecker, G. B. Partridge, A. G. Truscott, and R. G. Hulet. "Formation and propagation of matter-wave soliton trains". *Nature* 417 (2002), 150. DOI: 10.1038/nature747. arXiv: cond-mat/0204532.

[SPS04] K. Sengupta, S. Powell, and S. Sachdev. "Quench dynamics across quantum critical points". *Phys. Rev.* A69 (2004), 053616. DOI: 10.1103/PhysRevA.69.053616. eprint: cond-mat/0311355.

[SS+05] K. Sakmann, A. I. Streltsov, O. E. Alon, and L. S. Cederbaum. "Exact ground state of finite Bose-Einstein condensates on a ring". *Phys. Rev.* A72 (2005), 033613. DOI: 10.1103/PhysRevA.72.033613. arXiv: cond-mat/0505323.

[SS07] C. Sulem and P. Sulem. *The Nonlinear Schrödinger Equation: Self-Focusing and Wave Collapse*. Applied Mathematical Sciences. Springer New York, 2007. ISBN: 9780387227689.

[SS08] Y. Sekino and L. Susskind. "Fast Scramblers". *J. High Energy Phys.* 10 (2008), 065. DOI: 10.1088/1126-6708/2008/10/065. arXiv: 0808.2096 [hep-th].

[SS14] S. H. Shenker and D. Stanford. "Black holes and the butterfly effect". *J. High Energy Phys.* 03 (2014), 067. DOI: 10.1007/JHEP03(2014)067. arXiv: 1306.0622 [hep-th].

[Sto99] H. T. C. Stoof. "Coherent versus incoherent dynamics during Bose-Einstein condensation in atomic gases". *J. Low Temp. Phys.* 114 (1999), 11. arXiv: cond-mat/9805393.

[STU93] L. Susskind, L. Thorlacius, and J. Uglum. "The Stretched horizon and black hole complementarity". *Phys. Rev.* D48 (1993), 3743. DOI: 10.1103/PhysRevD.48.3743. arXiv: hep-th/9306069.

[Sus93] L. Susskind. "Some speculations about black hole entropy in string theory" (1993). arXiv: hep-th/9309145.

[Sus95] L. Susskind. "The World as a hologram". *J. Math. Phys.* 36 (1995), 6377. DOI: 10.1063/1.531249. arXiv: hep-th/9409089.

[SV96] A. Strominger and C. Vafa. "Microscopic origin of the Bekenstein-Hawking entropy". *Phys. Lett.* B379 (1996), 99. DOI: 10.1016/0370-2693(96)00345-0. arXiv: hep-th/9601029.

[Tha81] H. B. Thacker. "Exact integrability in quantum field theory and statistical systems". *Rev. Mod. Phys.* 53 (1981), 253. DOI: 10.1103/RevModPhys.53.253.

[TSG82] D. C. Tsui, H. L. Stormer, and A. C. Gossard. "Two-dimensional magnetotransport in the extreme quantum limit". *Phys. Rev. Lett.* 48 (1982), 1559. DOI: 10.1103/PhysRevLett.48.1559.

[TVS93] E. Tiesinga, B. J. Verhaar, and H. T. C. Stoof. "Threshold and resonance phenomena in ultracold ground-state collisions". *Phys. Rev.* A47 (1993), 4114. DOI: 10.1103/PhysRevA.47.4114.

[Ven13] G. Veneziano. "Quantum hair and the string-black hole correspondence". *Class. Quant. Grav.* 30 (2013), 092001. DOI: 10.1088/0264-9381/30/9/092001. arXiv: 1212.2606 [hep-th].

[Vis15] M. Visser. "Thermality of the Hawking flux". *J. High Energy Phys.* 07 (2015), 009. DOI: 10.1007/JHEP07(2015)009. arXiv: 1409.7754 [gr-qc].

[VL+03] G. Vidal, J. I. Latorre, E. Rico, and A. Kitaev. "Entanglement in Quantum Critical Phenomena". *Phys. Rev. Lett.* 90 (2003), 227902. DOI: 10.1103/PhysRevLett.90.227902. arXiv: quant-ph/0211074.

[Vol91] M. B. Voloshin. "An Illustrative model for nonperturbative scattering in theories with weak coupling". *Nucl. Phys.* B363 (1991), 425. DOI: 10.1016/0550-3213(91)80028-K.

[Vol92] M. B. Voloshin. "Multiparticle amplitudes at zero energy and momentum in scalar theory". *Nucl. Phys.* B383 (1992), 233. DOI: 10.1016/0550-3213(92)90678-5.

[Vol93] M. B. Voloshin. "Summing one loop graphs at multiparticle threshold". *Phys. Rev.* D47 (1993), 357. DOI: 10.1103/PhysRevD.47.R357. arXiv: hep-ph/9209240.

[Vol94] M. B. Voloshin. "Nonperturbative methods". *27th International Conference on High-energy Physics (ICHEP 94) Glasgow, Scotland, July 20-27, 1994*. 1994. arXiv: hep-ph/9409344.

[VT+97] J. M. Vogels, C. C. Tsai, R. S. Freeland, S. J. J. M. F. Kokkelmans, B. J. Verhaar, and D. J. Heinzen. "Prediction of Feshbach resonances in collisions of ultracold rubidium atoms". *Phys. Rev.* A56 (1997), R1067. DOI: 10.1103/PhysRevA.56.R1067.

[VV13] E. Verlinde and H. Verlinde. "Passing through the Firewall" (2013). arXiv: 1306.0515 [hep-th].

[Wal01] R. M. Wald. "The thermodynamics of black holes". *Living Rev. Rel.* 4 (2001), 6. DOI: 10.12942/lrr-2001-6. arXiv: gr-qc/9912119.

[Wei67] S. Weinberg. "A Model of Leptons". *Phys. Rev. Lett.* 19 (1967), 1264. DOI: 10.1103/PhysRevLett.19.1264.

[Wig32] E. P. Wigner. "On the quantum correction for thermodynamic equilibrium". *Phys. Rev.* 40 (1932), 749. DOI: 10.1103/PhysRev.40.749.

[Win14] N. Wintergerst. "Faces of gravity: from classical cosmology to Quantum Black Holes." PhD thesis. LMU Munich, 2014. URL: https://edoc.ub.uni-muenchen.de/17407/.

[Wit11] E. Witten. "Analytic Continuation Of Chern-Simons Theory". *AMS/IP Stud. Adv. Math.* 50 (2011), 347. arXiv: 1001.2933 [hep-th].

[Wit91] E. Witten. "On quantum gauge theories in two-dimensions". *Commun. Math. Phys.* 141 (1991), 153. DOI: 10.1007/BF02100009.

[Wit95] E. Witten. "String theory dynamics in various dimensions". *Nucl. Phys.* B443 (1995), 85. DOI: 10.1016/0550-3213(95)00158-O. arXiv: hep-th/9503124.

[Yan07] M.-F. Yang. "Ground-state fidelity in one-dimensional gapless models". *Phys. Rev.* B76 (2007), 180403. DOI: 10.1103/PhysRevB.76.180403. arXiv: 0707.4574 [quant-ph].

[YY69] C.-N. Yang and C. Yang. "Thermodynamics of a One-Dimensional System of Bosons with Repulsive Delta-Function Interaction". *J. Math. Phys.* 10 (1969), 1115. DOI: 10.1063/1.1664947.

[Zak91] V. I. Zakharov. "High-energy production of scalar bosons in weak coupling theories". *Phys. Rev. Lett.* 67 (1991), 3650. DOI: 10.1103/PhysRevLett.67.3650.

[Zin81] J. Zinn-Justin. "Multi - Instanton Contributions in Quantum Mechanics". *Nucl. Phys.* B192 (1981), 125. DOI: 10.1016/0550-3213(81)90197-8.

[ZJ04] J. Zinn-Justin and U. D. Jentschura. "Multi-instantons and exact results I: Conjectures, WKB expansions, and instanton interactions". *Annals Phys.* 313 (2004), 197–267. DOI: 10.1016/j.aop.2004.04.004. arXiv: quant-ph/0501136.

[ZP06] P. Zanardi and N. Paunkovi. "Ground state overlap and quantum phase transitions". *Phys. Rev.* E74 (2006), 031123. DOI: 10.1103/PhysRevE.74.031123. arXiv: quant-ph/0512249.

[Zur03] W. H. Zurek. "Decoherence, einselection, and the quantum origins of the classical". *Rev. Mod. Phys.* 75 (2003), 715. DOI: 10.1103/RevModPhys.75.715.

Acknowledgements

I would like to extend my deep gratitude to my advisor Gia Dvali for the opportunity to work with him and in his group. His dedication to and deep insight in physics and his pursuit of an intuitive understanding have been an inspiring example. I also want to thank him, as a mentor, for the encouragement and guidance that allowed me to explore so many fascinating facets of physics.

I am much obliged to my collaborators Andre Franca, Cesar Gomez, Alexander Pritzel, and Nico Wintergerst for countless hours of fruitful discussions that have strongly shaped my understanding of physics.

I also want to thank Stefan Hofmann for agreeing to co-examine this thesis and for his advice and motivation.

I am grateful to all my friends and colleagues, for the amazing time we had, discussing physics and otherwise, especially Alex Pritzel, Alex Gussmann, Andre Franca, Andrei Khmelnitski, Claudius Krause, Cristiano Germani, Lasma Alberte, Leila Mirzagholi, Lena Funcke, Lukas Gründing, Mischa Panchenko, Nico Wintergerst, Oscar Cata, Sarah Folkerts, Sebastian Zell, Tehseen Rug.

A special thanks goes to Alex P., Andre and Tehseen who read parts of this work and gave valuable comments.

I want to thank Gabi Bodenmüller and Herta Wiesbeck-Yonis for their administrative support.

Finally, I am forever grateful to my family, my parents Uschi and Willy, my brother Fabian and grandmother Gerti Seebacher who were always there for me - and who are, in large part responsible that I ever chose to do physics.

I want to save the last lines to thank Elisa Vietz for all her patience (especially in the last frantic weeks) and her perpetual inspiration and support.